CZECH TECHNICAL UNIVERSITY IN PRAGUE

FACULTY OF NUCLEAR SCIENCES AND PHYSICAL ENGINEERING

———— DISSERTATION THESIS ————

Neutron Imaging at Very Low Power Research Reactors

Commented set of scientific papers

Prague 2024   **Jana Matoušková**

Bibliografický záznam

Bibliographic Entry

Abstrakt

Disertační práce je zpracovaná formou komentovaného souboru odborných článků a zabývá se možnostmi využití neutronového zobrazování na výzkumných reaktorech velmi nízkého výkonu. Tyto možnosti byly demonstrovány vývojem zařízení pro neutronové zobrazování na školním reaktoru VR-1 s výkonem pouhých 100 W. Práce popisuje úplný vývoj zařízení pro neutronové zobrazování od návrhu, konstrukce, bezpečnostního hodnocení, výpočtů, až po testování jednotlivých částí zařízení (detekční systém, neutronový svazek a stínění) a uvedení do provozu. Při vývoji zařízení pro neutronové zobrazování na reaktoru s takto nízkým výkonem bylo nutné překonat spoustu výzev spojených nejen s omezeným výkonem, ale i specifickým provozem reaktoru velmi nízkého výkonu. Přesto se v průběhu doktorského studia podařilo úspěšně vybudovat a uvést do standardního provozu zařízení nejen pro neutronovou radiografii, ale i neutronovou počítačovou tomografii. Navíc se jedná o první zařízení pro neutronovou tomografii provozované na výzkumném reaktoru s takto nízkým výkonem na světě. Přestože jedním z cílů práce bylo zahrnout neutronové zobrazování do standardní výuky na reaktoru VR-1, výsledky vývoje ukázali využitelnost zařízení i v multidisciplinárním výzkumu například v oblasti zachování kulturního dědictví. S využitím nově vybudovaného zařízení pro neutronové zobrazování byly úspěšně analyzovány interní struktury votivní soch z centrální Asie. Znalosti a zkušenosti z vývoje zařízení pro neutronové zobrazování z reaktoru VR-1 byly dále využity k úpravě detekčního systému pro neutronové zobrazování na reaktoru RA-6 v Argentině.

Abstract

The dissertation thesis is compiled as a commented set of scientific papers and deals with the possibilities of using neutron imaging in very low-power research reactors. These possibilities have been demonstrated by the development of a neutron imaging facility at the Training reactor VR-1 with a power of only 100 W. The thesis describes the complete development of a neutron imaging facility from design, construction, safety assessment, and calculations, to testing individual parts of the facility (detection system, neutron beam and shielding) and commissioning. During the development of a neutron imaging facility at such a low-power reactor, it was necessary to overcome many challenges related not only to the limited power but also to the specific operation of a very low-power research reactor. Nevertheless, during the PhD studies, it was possible to successfully build and commission the facility not only for neutron radiography but also for neutron computed tomography. In addition, it is the first neutron tomography facility operated at such a low-power research reactor in the world. Although one of the goals of the thesis was to include neutron imaging in standard teaching at the VR-1 reactor, the results also showed the potential for multidisciplinary research, such as cultural heritage preservation. Using the newly developed neutron imaging facility, the internal structures of votive statues from Central Asia were successfully analysed. Later, the knowledge and experience from the development of a neutron imaging facility at the VR-1 reactor was used to upgrade the detection system for neutron imaging at the RA-6 reactor in Argentina.

Acknowledgement.

Contents

List of Symbols and Acronyms

List of Symbols

$\mathring{A}$	Ångström, wavelength unit (-)
b	barn, microscopic cross-section unit (-)
$°C$	degree Celsius, temperature unit (-)
D	diameter of the diaphragm (cm)
eV	electron Volt, energy unit (-)
f	fission reaction (-)
h	hour, time unit (-)
I	intensity of neutron beam ($1/\text{m}^2 \text{ s}^1$)
L	length of beamline (cm)
L/D	collimation ratio (-)
m	metre, length unit (-)
n	neutron (-)
N	atomic density ($1/\text{cm}^3$)
n/cm^2s	neutron flux unit (-)
n/cm^2	neutron fluence unit (-)
p	proton (-)
P_θ	projection of the two-dimensional slice (-)
Q_θ	filtered projection (-)
s	second, time unit (-)
$S(u,v)$	Fourier transform of the slice (-)
Sv/h	dose equivalent (-)
$\$$	dolar, reactivity unit (-)
T	transmission (-)
W	watt, power unit (-)

α	alpha radiation (-)
γ	gamma radiation (-)
δ	angular increment (-)
Θ	projection angle (-)
μ	attenuation coefficient (-)
π	pi, mathematical constant (-)
σ	microscopic cross-section (cm^2)
σ_{α}	microscopic cross-section for α producing reaction (cm^2)
σ_{γ}	microscopic cross-section for radiative capture (cm^2)
σ_{e}	microscopic cross-section for elastic scattering (cm^2)
σ_{f}	microscopic cross-section for fission (cm^2)
σ_{i}	microscopic cross-section for inelastic scattering (cm^2)
σ_{n}	microscopic cross-section for neutron-producing reaction (cm^2)
σ_{p}	microscopic cross-section for proton producing reaction (cm^2)
σ_{tot}	total microscopic cross-section (cm^2)
Σ_{tot}	total macroscopic cross-section (1/cm)
ϕ	neutron flux (n/cm^{2}s)
ϕ_{th}	thermal neutron flux (n/cm^{2}s)
ω	spatial frequency (-)

List of Acronyms

2D	two-dimensional
3D	three-dimensional
CCD	charged-coupled device (camera)
CMOS	complementary metal–oxide–semiconductor (camera)
CNEN	National Nuclear Energy Commission
CPU	Central processing unit
CT	computed tomography
CTU	Czech Technical University in Prague
D-D	deuterium – deuterium neutron generator
D-T	deuterium – tritium neutron generator
di	dark image
ESF	edge spread function
FoV	field of view
IAEA	International Atomic Energy Agency
INL	Idaho National Laboratory
ISNR	International Society for Neutron Radiography
LSF	line spread function
M	number of projections
MLZ	Heinz Maier-Leibnitz Zentrum
MTF	modulation transfer function
NAA	neutron activation analysis
NICOS	Networked Instrument Control System
NIFFLER	Neutron Imaging Facility for Learning and Research
NSIL	Nuclear Science and Instrumentation Laboratory
ob	open beam image
PE	polyethylene
PLA	polylactic acid
RRDB	research reactor database
SNR	signal-to-noise ratio
STORNI	Smart Tomography and Radiography Neutron Instrument
WoS	web of science

List of Tables and Figures

List of Tables

Main text

Annex A.1

Annex A.2

Annex A.5

List of Figures

Main text

Annex A.1

Annex A.2

Introduction

Neutron imaging is a nuclear analytical technique used to investigate internal structures and material composition of optically opaque objects. Like other nuclear analytical techniques, neutron imaging requires a sufficient source of radiation, in this case, a source of neutrons. For this reason, neutron imaging has been mostly performed at high power neutron sources, such as high-power research reactors or spallation sources. However, new detection systems, based on combination of CCD or CMOS cameras with scintillator screens, have brought new possibilities for neutron imaging at low-power neutron sources, like very low-power research reactors. However, the use of neutron imaging at very low power neutron sources is associated with several challenges. The main challenge is related to low power of the source (reactor) which is connected to the low neutron flux at the sample. This challenge can be partly solved by optimisation of the neutron beam and long exposure times. Another challenge, which is connected to low power research reactors is their specific mode of operation. Unlike high-power reactors, low-power reactors are operated on a daily shift basis, and it is mostly impossible to carry out multiple activities simultaneously. On the other hand, the advantage of low power nuclear research reactors is that they could provide more options for the education of students and basic investigations, due to their lower operational costs, in multidisciplinary research.

The dissertation thesis is compiled in the form of a commented set of five publications that were published in international journals with impact factor and are indexed in the international databases Web of Science and Scopus. The main goal of the dissertation thesis was to study the possibilities of using neutron imaging at very low-power research reactors. This topic has only been explored at a few low-power research reactors worldwide, specifically, five research reactors with a power of less than 30 kW. These are the ARGONAUTA reactor (200 W), the UTR KINKI reactor (1 W), the AGN-201K reactor (10 W), the SLOWPOKE-2 reactor (20 kW) and the AKR-2 reactor (2 W). Except for the SLOWPOKE-2 reactor, which has slightly higher power than the other reactors, all reactors are able to perform only neutron radiography, not neutron tomography. All these very low-power research reactors use their neutron imaging facilities mainly for education, with minimal use in various research disciplines.

The possibilities of using neutron imaging at very low-power research reactors were in this thesis demonstrated by the development of a neutron imaging facility at the Training reactor VR-1 with a reactor power of only 100 W. The development of the NIFFLER – "Neutron Imaging Facility for Learning and Research" at the VR-1 reactor was divided into several steps. First, the individual parts of the facility were designed, and the safety assessment was carried out. Then, the individual parts were constructed and tested at the reactor and necessary modifications were performed. And after sufficient number of measurements, the facility was commissioned and put into permanent operation. The development of the NIFFLER facility was focused on all necessary parts, such as the detection system, the neutron beam, the shielding, and the tomography setup. Despite the very low power of the reactor, it was possible to successfully build and commission the facility not only for neutron radiography but also for neutron computed tomography. With that, the VR-1 reactor is the first reactor with such a low power to operated neutron tomography facility worldwide.

After the development of the facility, the activities were focused on testing different applications of neutron imaging. The main emphasis was on the incorporation of neutron imaging into education at the Department of Nuclear Reactors. Neutron imaging was successfully incorporated into standard education for Master students. However, the results of neutron imaging experiments at the VR-1 reactor showed the potential for multidisciplinary research; for example, the applications of neutron imaging in cultural heritage preservation were tested. Measurements of internal structures of Asian votive statues were performed, as a first step in collaboration with the National Gallery Prague.

Later, the knowledge and experience from the development of a NIFFLER neutron imaging facility at the VR-1 reactor was used for the upgrade of other facilities, mainly their detection systems. An example of this was an upgrade of detection system for neutron imaging at the RA-6 reactors. This system was designed as a long-distance periscope, to fulfil specific shielding requirements at the RA-6 reactor in San Carlos de Bariloche, Argentina. The upgrade of this facility was the first step in the knowledge transfer from the development of the neutron imaging facility at the Training reactor VR-1 to other research reactors worldwide.

Chapter 1

Status of Neutron Imaging

Neutron imaging as a non-destructive imaging technique has been used since the 1930s [1]. However, this method was significantly developed in the 1960s [1], with the use of research reactors as a sufficient neutron source, which allowed an increase in image quality. By the mid-1980s [1], initially analogue images were digitised and stored on computers, which allowed advanced image processing techniques for quantitative analysis. Currently, digital neutron imaging is a well-developed, standardised, and even commercially used technique with several main trends in which the development is heading. This thesis is only focused on research activities in neutron imaging and does not include commercial activities.

One of the modern trends goes towards high-resolution and smaller samples. This trend focuses on imaging small samples with very high resolution in micrometres. This is achieved with particular detection systems using very thin gadolinium scintillator screens and high numerical aperture magnifying lenses or Wolter optics [2, 3]. This requires a high or at least medium-power neutron source.

Another modern trend goes towards advanced neutron imaging techniques. These techniques focus on the particle-wave dualism of neutrons. Instead of measuring the direct attenuation of the neutron beam, they exploit the wave properties of the neutron. These techniques include Bragg-Edge Imaging [4, 5], phase contrast and dark field imaging [6, 7], diffractive imaging [8], neutron grating interferometry [9], and imaging with polarised neutrons [10, 11]. These techniques require a high-power neutron source; nearly all these advanced methods even require specific neutron energies – cold neutrons.

The last modern trend of neutron imaging goes towards downscaling neutron imaging facilities from high-power neutron sources to low-power neutron sources such as low and very low-power research reactors. This trend is focused on possibilities of utilisation of neutron imaging at low-power neutron sources, especially in the field of education and training but also

multidisciplinary research. The development of digital detection systems consisting of cooled scientific CCD (charged-coupled device) or CMOS (complementary metal-oxide semiconductor) cameras for long exposure times in combination with scintillation screens contributed to the expansion of this trend, which allowed tests of the possibility of neutron imaging at low-power neutron sources. Even so, there are still only a few low and very low-power neutron sources that use this method.

Since the main topic of the dissertation thesis is neutron imaging at very low-power research reactors, this is the latest trend of downscaling neutron imaging from high-power neutron sources to low-power neutron sources, especially low-power research reactors, which is expanded in the following chapters.

1.1   Neutron Imaging at Low-Power Neutron Sources

Neutron imaging is mainly performed at two types of neutron sources: reactor neutron sources – research reactors, and spallation neutron sources – accelerators. The advantages of research reactors are primarily the constant intensity of neutrons and the high neutron intensity. Conversely, the main disadvantage is high operational costs [12].

According to the International Atomic Energy Agency (IAEA) Research Reactor Database (RRDB), in December 2023, 68 research reactors [13] that are in operation or temporarily shut down declare the use of neutron imaging. Declaration of use/possibility of use of neutron imaging at these research reactors does not have to necessarily mean regular use of this method. In 2019, in collaboration with the IAEA, the International Society for Neutron Radiography (ISNR) published the International Survey on Neutron Imaging Facilities Worldwide, listing regularly used neutron imaging facilities [14]. However, this document is from 2019, and unfortunately, some information is no longer up to date as several facilities were permanently shut down and new facilities were built or underwent significant reconstruction. The ISNR website lists examples of the world's most well-known neutron imaging facilities. (See Tab. 1 [15])

Most of the high-quality neutron imaging facilities are operated at high-power neutron sources, with research reactors with reactor power in dozens of MW and spallation sources with power around 1 MW, even though there are several examples of high-quality neutron imaging facilities operated at medium or low-power neutron sources, primarily research reactors, for example, a digital computed neutron tomography system at 250 kW test reactor at the Idaho National Laboratory (INL), Idaho Falls, United States of America [16] or a neutron imaging facility at 250 kW TRIGA Mark-II reactor at Vienna University of Technology, Vienna, Austria [17].

The main challenge of performing neutron imaging at low-power neutron sources is, of course, connected to the low power/low neutron flux. However, it is the main but not the only challenge connected with neutron imaging at low-power research reactors. The second serious challenge concerns a specific mode of operation of low-power research reactors. High-power reactors are

in operation 24/7 during a cycle of several weeks, and several activities can be performed simultaneously. On the other hand, low-power reactors are usually operated on a daily-shift basis and, in most cases, cannot be used for several activities simultaneously. Therefore, a special reactor time must be dedicated to neutron imaging.

Tab. 1 – *Most well-known neutron imaging facilities [15]*

Facility	Country	Neutron source	Power
DINGO [18]	Australia	Reactor OPAL	15 MW
NEXT [19]	France	Reactor ILL High Flux	58.3 MW
ANTARES [20] NECTAR [21]	Germany	Reactor FRM II	20 MW
RAD [22] NORMA [23]	Hungary	Reactor BRR	10 MW
TNRF [24] CNRF [24]	Japan	Reactor JRR	20 MW
RADEN [25]	Japan	Spallation source	< 1 MW
NEUTRA [26] ICON [26] BOA [26] POLDI [26]	Switzerland	Spallation source	0.8 MW
ERNI [27]	USA	Spallation source	0.08 MW
CG1D [28] SNAP [29]	USA	Reactor HFIR	85 MW
BT2 [30] CNII [31]	USA	Reactor NIST	20 MW

Some references, for example, the IAEA research reactor utilisation matrix from the IAEA document called Applications of research reactors [32], state only limited capability for neutron imaging at research reactors with reactor power of less than 1 MW and no capability at research reactors with reactor power of less than 100 kW. Nevertheless, a few neutron imaging facilities are still operated at very low-power neutron sources. With a focus on research reactors with reactor power under 30 kW, with Training reactor VR-1 omitted, there are five research reactors that tested the possibility of using neutron imaging or that operate neutron imaging facilities. These are the ARGONAUTA reactor at National Nuclear Energy Commission (CNEN), Rio de Janeiro, Brazil [33], the UTR KINKI reactor at Kinki University, Osaka, Japan, the AGN-201K reactor at Kyung Hee University, Yongin, Korea [34], the SLOWPOKE-2

reactor at Royal Military College, Kingston, Canada [35] and the AKR-2 reactor at Technical University Dresden, Germany [36]. (See Tab. 2 [13]) Except for the SLOWPOKE-2 reactor, which has slightly higher power than the other reactors, all reactors can perform only neutron radiography, not neutron tomography measurements.

Tab. 2 – *Very low-power research reactors with neutron imaging facilities [13]*

Reactor	Country	Power (kW)
ARGONAUTA	Brazil	0.2
URT KINKI	Japan	0.001
AGN-201K	Korea	0.01
SLOWPOKE-2	Canada	20
AKR-2	Germany	0.002

1.2 Use of Neutron Imaging at Low-Power Research Reactors

The range of potential applications of neutron imaging is primarily limited by the intensity of the neutron beam, which depends on the intensity of the neutron source or reactor power. Most of the above-mentioned research reactors are operated by universities. Therefore, they use their neutron imaging facilities mainly for education and training, focusing on providing hands-on neutron radiography experiments for university students. That is something that large-scale facilities operated at high-power neutron sources cannot deliver because they are usually overbooked with research experiments. However, despite the low neutron intensity, some of these reactors found other uses for their neutron imaging facilities in various research areas.

The research reactors SLOWPOKE-2 and ARGONAUTA decided to focus their neutron imaging research on material science and engineering. The research at the SLOWPOKE-2 reactor is focused on the inspection of water ingress into the flight control surfaces of the CF-18 Hornet [35]. With the reactor power of 20 kW, they could perform both neutron radiography and computed neutron tomography of water movements in CF-18 Hornet rudders [35]. On the other hand, the research at reactor ARGONAUTA is focused on visualising crust in metallic piping through real-time neutron radiography [37]. Neutron radiography was used to visualise crust in the interior of metallic piping of small diameter [37]. Unlike the previous two reactors, the research reactor AKR-2 tested the possibility of using neutron imaging in energy research. The experiments focused on neutron radiography of hydrogen storage devices for two configurations, filled with hydrogen to one-fifth of maximum capacity and completely drained [36]. Based on the studies in the references, for now, education and training remain the primary use of neutron imaging at low-power neutron sources. However, it is also apparent that low-power neutron sources can be used for neutron imaging for other applications in various research areas, e.g., already-tested material science and engineering or energy research and other not-yet-tested areas, such as cultural heritage preservation.

Chapter 2

Dissertation Thesis Objectives

The dissertation thesis is focused on studying neutron imaging at very low-power research reactors. Neutron imaging as a nuclear analytical technique is mainly performed at high-power neutron sources such as high or medium-power research reactors or spallation sources. However, the situation started slowly changing in the last few years with the development of digital imaging systems. This brought new chances for utilising neutron imaging at low-power neutron sources, such as low-power research reactors. Even though a few very low-power research reactors tested the possibility of using neutron radiography, it is still challenging to build and operate neutron imaging facilities at such low-power neutron sources because of their low neutron intensity and specific mode of operation.

The Training reactor VR-1 is a very low-power research reactor operated by the Faculty of Nuclear Sciences and Physical Engineering of the Czech Technical University in Prague, with a reactor power of 100 W. In this context, the objectives of the dissertation thesis are:

1) Development of a neutron imaging facility at very low-power research reactors. The development of a neutron imaging facility includes design, construction and safety assessment of the neutron imaging facility and measurements and calculations.

2) Commissioning of the neutron imaging facility at the Training reactor VR-1. The commissioning includes testing the neutron imaging facility at the Training reactor VR-1 and standard operation of the developed neutron imaging facility at the VR-1 reactor.

3) Proposals for incorporating the developed neutron imaging facility into education at the Department of Nuclear Reactors, such as nuclear engineering courses, as well as short-term courses for other engineering and other multidisciplinary fields, for example, natural or social sciences, humanities and others.

Chapter 3

Neutron Imaging

Neutron imaging is a non-destructive analytical technique used to investigate internal structures and material composition of optically opaque objects. Neutron imaging belongs to the group of analytical imaging methods based on the beam attenuation in the investigated sample [1]. This group of methods includes gamma imaging, proton imaging and x-ray imaging, which is most well-known by the general public. The imaging principle is similar for all methods, the radiation intensity is attenuated by passing through the investigated object by an amount that depends on the thickness of the object and its material composition [1]. However, the difference is in the way of interaction of the incident particle with the matter.

3.1   Imaging Principle

A neutron is an uncharged fundamental particle with many unique attributes that provide a variety of contrast mechanisms, enabling many imaging techniques [38]. Due to their electric neutrality, neutrons interact mainly by strong interaction with atomic nuclei and are highly penetrating and well-able to investigate the interior of large assemblies non-destructively. Neutron-matter interactions include:

- Neutron scattering (n, n) or (n, n')

- Radiative capture (n, γ)

- Production of charged particles (n, α), (n, p)

- Fission reaction (n, f)

- Neutron producing reaction (n, 2n), (n, 3n)

The probability that one of the interactions mentioned above occurs is described by a microscopic cross-section σ (m^2) [39]. Each type of interaction is described by its own cross-section, and the probability of all interactions is called total microscopic cross-section σ_{tot} [39]. The above-mentioned neutron-matter interactions can be divided into two groups – absorption

reactions [radiative capture (σ_γ), production of charged particles fission-reaction (σ_α, σ_p), fission reaction (σ_f) and neutron producing reaction (σ_n)] and scattering reactions (σ_s). The scattering reactions can be further divided into coherent and incoherent scattering. In a coherent scattering process, neutron waves scattered by different nuclei combine to produce an interference pattern that depends on the relative locations of the atoms in the material [1]. Coherent scattering only happens on crystal lattices. In an incoherent scattering process, there is a randomisation of the strength of the scattering cross-section, which results in a component of the neutron scattering that depends only on the scattering from individual atoms and does not give rise to an interference pattern [1]. Both coherent and incoherent scattering can scatter elastically (σ_e) and inelastically (σ_i) [39]. Based on total microscopic cross section σ_{tot}, a total macroscopic cross section Σ_{tot} (1/cm) can be defined as:

$$\Sigma_{tot} = N \cdot \sigma_{tot} \tag{1}$$

where N (1/cm^3) is atomic density [39]. In contrast to neutrons, X-rays interact only by electromagnetic interaction (photo effect, Compton scattering, production of electron-positron pairs) [1]. Therefore, the probability of X-ray interaction with the material depends on the number of protons of the elements (and thus on their atomic number) of which the object is composed. The dependency of mass attenuation coefficient on the atomic number for X-rays, gamma and fast and thermal neutrons is shown in Fig. 1 [40].
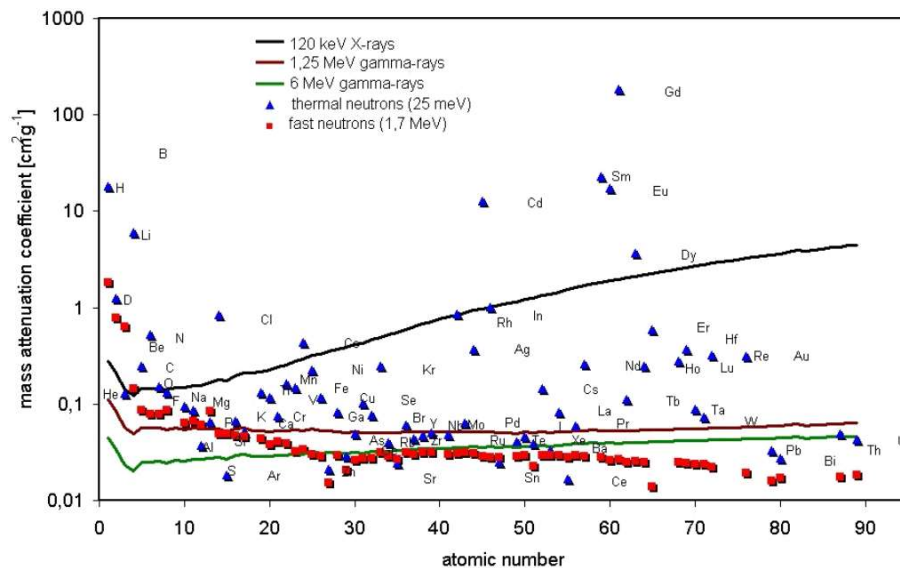
Fig. 1 – *Dependency of mass attenuation coefficient on atomic number*

Another important aspect of neutron-matter interaction is neutron energy, as the microscopic cross section is energy dependent. It is possible to divide the neutron energy spectrum into a few parts with similar characteristics (See Tab. 3 [41]). Neutrons from the source are usually produced in fast energy ranges, the specific energy range depends on the source type, generally in MeV. However, thermal or cold neutrons are most often used for neutron imaging due to their favourable detection reactions and their contrast behaviour [1]. In the range of thermal

and cold neutrons, there is a high probability (microscopic cross section) of neutron-matter interaction in the form of absorption, which is the ideal attenuation process for neutron imaging. Therefore, neutrons from the source are mostly moderated to required thermal or cold energies. Fast neutrons are not frequently used for neutron imaging, but it is still possible to use them [42]. Unlike for thermal and cold neutrons, the probability of the neutron-matter interaction for fast neutrons in the form of absorption is nearly not existent. In contrast, the probability of the neutron-matter interaction in the form of scattering is much higher - nearly all the interactions [42].

Tab. 3 – *Neutron classification at various energy ranges for neutron imaging [41]*

Neutron classification	Energy range	Wavelength (Å)
Ultra Cold	< 0.12 meV	> 26.1
Cold	0.12 meV – 12 meV	26.1 – 2.6
Thermal	12 meV – 100 meV	2.6 – 0.9
Epithermal	100 meV – 1 eV	0.9 – 0.28
Intermediate	1 eV –0.8 MeV	
Fast	> 0.8 MeV	

For neutron imaging, neutrons interact with matter and thereby are removed from the incident beam either by absorption or by a change in direction (scattering) as they interact with the investigated material [1]. The ideal attenuation process for neutron imaging is absorption because it completely removes neutrons from the beam. The scattering also causes an attenuation process, but scattered neutrons do not have to be removed from the beam. They may still hit the detector in a place different from the original path, thus creating a background of scattered neutrons that produce background noise and blurring [38]. The beam attenuation is described by the basic law of radiation attenuation in a matter (Lambert's law):

$$I\left(x\right) = I_0 \cdot e^{-\int \Sigma_{tot}\, dx} \tag{2}$$

where I_0 $(1/\text{m}^2\,\text{s}^1)$ is the intensity of neutrons incident on the sample, x (m) is the thickness of the object, and Σ_{tot} is the total macroscopic cross-section, also called linear attenuation coefficient [1]. The attenuated neutron beam is detected by a detection system which is located perpendicular to the beam propagation direction. This creates a grayscale image that contains all the information about the thickness and material composition of the sample. One of the fundamental quantities used in neutron radiography is the transmission of T, which is defined by following equation:

$$T = \frac{I}{I_0} \tag{3}$$

Where I is the intensity of the neutrons that passed through the sample, and I_0 is the intensity of the neutrons incident on the sample [1]. Unfortunately, reality is more complicated, and this formula has certain limitations. It breaks down in situations involving relatively thick objects,

objects consisting of highly absorbing or highly scattering materials. Due to the energy dependence of the probability of neutron-matter interaction, multiple scattering effects and changes in the radiation energy need to be considered [1].

3.2   Neutron Imaging Instrumentation

Neutron imaging facilities require several important parts – neutron source, collimator/diaphragm and detection system. Neutron sources for neutron imaging can be divided into two main groups: reactor sources and non-reactor sources [43]. Non-reactor sources include accelerator-based (spallation) sources and neutron generators. The main criteria for selecting a suitable neutron source for neutron imaging are the intensity and energy of neutrons, the intensity and energy of the associated gamma radiation, price, dimensions, etc. For the comparison of physical parameters of neutron sources for neutron imaging, see Tab. 4 [44].

Tab. 4 – *Comparison of main parameters of neutron sources for neutron imaging*

Source type	Neutron intensity	Initial neutron energy* (MeV)
Research reactor	10^9 - 10^{15} n/cm^{2}s	2
Spallation source	10^8 - 10^{16} n/s	2
D-D generator	10^6 - 10^8 n/s	2.5
D-T generator	10^8 - 10^{11} n/s	14

* This is the energy value where the energy spectrum reaches its maximum.

The collimator with a diaphragm is another essential part of the neutron imaging system. The diaphragm creates the smallest diameter of the collimator. Once neutrons are produced and slowed down (if required), they must be formed into a beam [1]. Unlike electrons, because of their neutral charge, neutrons cannot be focused. The most straightforward approach uses the diaphragm (pinhole) and collimator, which allows for creating a quasi-parallel neutron beam and removing neutrons moving other than quasi-parallel. An essential parameter of the neutron imaging facility, which affects the spatial resolution of the resulting image, is the collimation ratio L/D, where L is the length between the smallest diameter of the collimator or diaphragm and the sample, and D is the smallest diameter of the collimator [1]. Higher L/D ratio produces better image resolution.

Then, it is possible to modify the neutron beam using flight tubes or neutron guides [45]. Both neutron guides and flight tubes are used to transport neutrons from the source or moderator to the detection position with minimal loss. Neutron guides are made of highly reflective materials for neutrons. So, they can transport neutrons over large distances with high efficiency [45]. This works only for thermal and cold neutrons. Unfortunately, due to high reflection angles, neutron guides create divergent beams and, therefore, alone are not an optimal choice for neutron imaging. On the other hand, flight tubes are tubes with walls lined with a neutron opaque material with a high cross section for absorption, which allows removing

neutrons moving other than approximately parallel to the collimator axis. However, a neutron guide can be used for neutron imaging in combination with another pinhole and flight tube [45]. The additional pinhole and the consecutive distance of the flight tube limit the divergence of the beam and overcome the restrictions of a neutron guide alone.

To create an image, it is necessary to detect the neutron beam passing through the investigated object. As neutrons do not have an electrical charge, they cannot be detected directly. It is necessary to use materials that convert the incident neutron to charged particles or electromagnetic radiation [1]. Such a material is called a converter and forms the basis of every neutron detector. A suitable isotope for a neutron converter is an isotope with a large cross-section for neutron absorption and a small cross-section for reaction with gamma radiation and charged particles [38]. Suitable conversion materials for thermal and cold neutrons are ^{6}Li and ^{10}B with (n, α) reaction, ^{3}He with (n, p) reaction, ^{157}Gd with (n, γ) reaction and ^{235}U with (n, f) reaction. (See Tab. 5 [38])

Tab. 5 – *Microscopic cross sections and type of reaction for conversion materials*

Isotope	Reaction	Absorption cross section* σ_a (b)
^{3}He	^{3}He (n, p) ^{3}H	5333
^{6}Li	^{6}Li (n, α) ^{3}H	940
^{10}B	^{10}B (n, α) ^{7}Li	3835
^{157}Gd	^{157}Gd (n, γ) ^{158}Gd	259000
^{235}U	^{235}U (n, f)	681

*Cross section values are given for thermal neutrons.

There are a few different types of detection systems that have been developed for neutron imaging, for example, photographic film detectors with convertor foils, imaging plates [46], flat panels based on amorphous silicon, track-etch-foils or CCD cameras with scintillator screen and CMOS cameras with scintillator screen [1].

Modern digital neutron imaging facilities use mostly CMOS or CCD cameras and scintillator screens [47, 48]. Both CMOS and CDD cameras capture light and convert it to digital images. The difference between them is in the way of signal collection. While CMOS sensors have a readout matrix connected to each pixel via a transistor, which can address each pixel directly, CCD sensors shift charge pixel-wise across the whole chip sequentially to a single readout amplifier. CCD sensors are usually more expensive, slower (because of the sequential charge readout) and more energy-consuming than CMOS sensors [49]. On the other hand, CCD sensors provide slightly higher sensitivity and less noise. CMOS or CCD sensors are used in combination with scintillator screens. Scintillators are materials that exhibit luminescence after irradiation, which means they produce photons in the visible range of the electromagnetic spectrum proportional to the intensity of the incident neutrons, which are then captured by an electronic detection system (CCD or CMOS camera) [49]. The main parameters of the scintillator screen

are light output, detection efficiency, conversion efficiency, emission spectrum and spatial resolution. A comparison of the main parameters of some scintillator screens is given in Tab. 6 [50]. Some of the parameters of scintillator screens depend on beam properties, detection system (sensor), thickness of the absorber layer and luminescent material. Values in the table may vary due to the measurement environment [50].

Tab. 6 – *Comparison of main parameters of some scintillator screens [50]*

Scintillator type	Thickness (µm)	Resolution (µm)	Relative light output*
^{6}LiF/ZnS: (Cu) or (Ag)	~ 50 - 400	~ 50 - 400	100 %
^{10}B$_2$O$_3$/ZnS: (Cu) or (Ag)	~ 50 - 400	~ 50 - 400	~ 50 %
Gd$_2$O$_2$S: (Tb)	~ 10 - 40	~ 10 - 40	~ 6 %
Gd$_2$O$_2$S: (Tb) enriched ^{157}Gd	~ 5	~ 5	~ 6 %

*Relative light output depends on the used absorber but also the thickness of the absorber layer. Values of light output in table 5 are listed for 100 µm for ^{6}LiF/ZnS and ^{10}B$_2$O$_3$/ZnS, 20 µm for Gd$_2$O$_2$S and 5 µm for Gd$_2$O$_2$S with enriched ^{157}Gd.

From Tab. 6, it is evident that some scintillator screens are available with different emission spectra. An example of the emission spectra of the scintillator is given in Fig. 2 [50]. ^{6}Li-based and ^{10}B$_2$O$_3$ scintillators are usually available in two variants: Cu-activated scintillators that emit green light with a peak wavelength of ~520 nm and Ag-activated ones that emit blue light ~450 nm [51]. In comparison, Gd-based scintillators are mostly available in the variant of Tb-activated scintillators that emit green light with a peak wavelength of ~549 nm [50]. When choosing an optimum scintillator screen, the properties of the detection system (camera) need to be considered. The green-emitting type scintillators match standard CCD and CMOS camera systems very well [50].
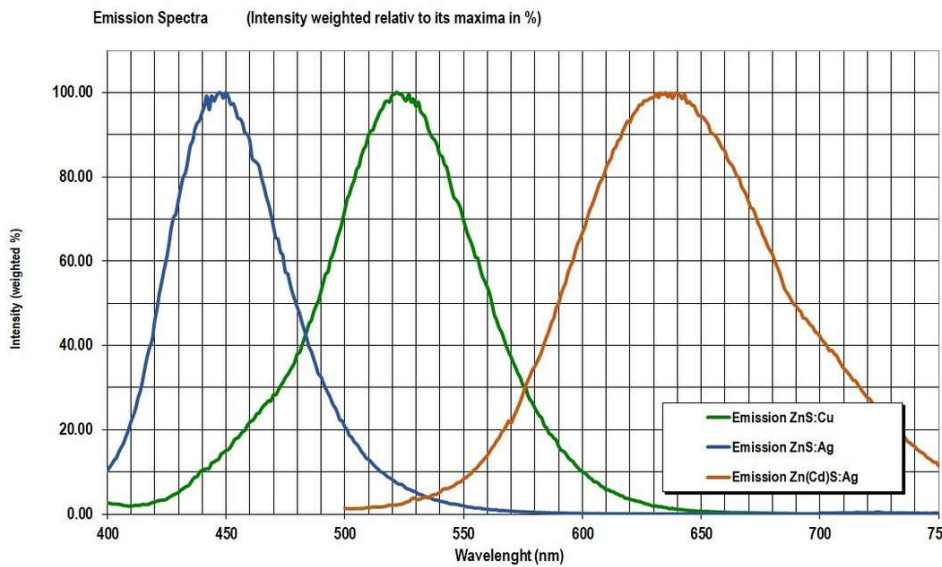
Fig. 2 – *An example of emission spectra of scintillator screen [50]*

3.3   Neutron Radiography and Neutron Computed Tomography

Neutron imaging includes two basic methods: Neutron radiography, i.e., two-dimensional (2D) imaging and neutron computed tomography (CT), i.e. three-dimensional (3D) imaging. Neutron radiography produces a 2D attenuation map of neutron radiation that has penetrated a 3D object. On the other hand, neutron computed tomography uses a large number of 2D neutron radiographs recorded under different angles to reconstruct a 3D image [1].

The basic principle of tomography is the reconstruction of information in the third dimension by solving the integral through the path of the neutron through the displayed object [52]. In practice, a series of 2D projections is made while the sample rotates around its vertical (or horizontal) axis in small steps. In the case of the parallel beam, which is used for neutron imaging, the reconstruction is done in layers reconstructed from single lines. In contrast, in a cone beam, which is used for X-ray imaging, the operation must be done in 3D from the start.

There are several mathematical methods used for image reconstruction. One of them is the Radon transformation method. The principle of projection and Radon transformation method [52] is that a number of neutrons hit each detector element; their intensity is given by Lambert's law [52]:

$$I(x) = I_0 \cdot \exp\left(-\int_{path} \mu(x, y) \cdot ds\right) \tag{4}$$

where I_0 is the intensity of neutrons incident on the sample and the linear attenuation coefficient $\mu(x,y)$ at position (x,y). Integration is performed along with the straight beam paths through the plane [52]. The projection of the two-dimensional slice as a one-dimensional function of the variable t perpendicular to the rays is:

$$P_\theta(t) = \int_{ray} \mu(x, y) \cdot ds \tag{5}$$

A new coordinate system (t,s) is defined that expresses the rotated sample system (t,s) with respect to the fixed detector system (x,y) [52]. The transformation of the (x,y) system into the (t,s) system is defined as:

$$t = x \cdot \cos(\theta) + y \cdot \sin(\theta) \tag{6}$$

Then projection $P_\theta(t)$ is equal to:

$$P_\theta(t) = \int_{-\infty}^{+\infty} \int_{-\infty}^{+\infty} \delta\left(x \cdot \cos(\theta) + y \cdot \sin(\theta) - t\right) \cdot \mu(x, y) dx dy \tag{7}$$

This is defined as a Radon transformation [52].

The projection of the two-dimensional slice must then be converted from the spatial domain to the frequency domain using the Fourier transform. The one-dimensional Fourier-Transform of the projection $P_\theta(\omega)$ is:

$$P_\theta(\omega) = \int_{-\infty}^{+\infty} P_\theta(t) \cdot e^{-2\pi i \omega t} dt \tag{8}$$

and the two-dimensional Fourier-Transform $S(u,v)$ of the slice to be reconstructed is:

$$S(u, v) = \int_{-\infty}^{+\infty} \int_{-\infty}^{+\infty} \mu(x, y) \cdot e^{-2\pi i(ux+vy)} dxdy \tag{9}$$

Equations 8 and 9 combined deliver the Fourier Slice Theorem:

$$P_\theta(t) = S(\omega cos\theta, \omega sin\theta) \equiv S(\omega, \theta) \tag{10}$$

The principle of Fourier Slice Theorem is schematically illustrated in Fig. 3 [52]:
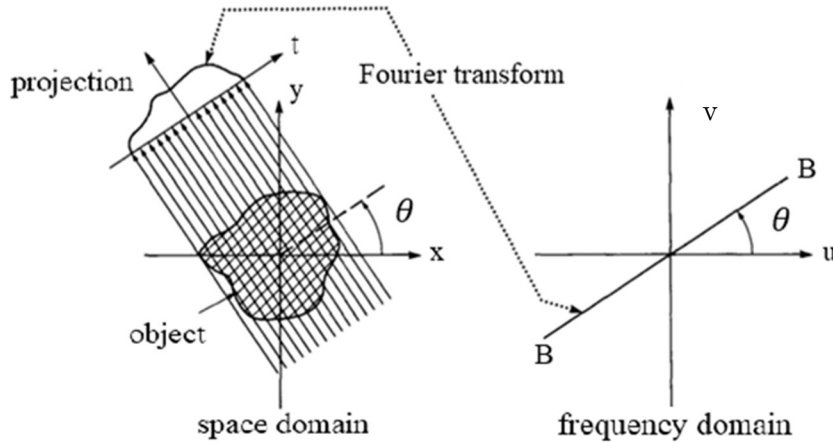
Fig. 3 – *Projection transformation principle*

In theory, it would be possible to fill the entire Fourier space by measuring an infinite number of projections and then to obtain the distribution $\mu(x,y)$ by a two-dimensional Fourier Back transform of $S(u,v)$ [52]. In reality, the number of projections is limited, and the function $S(u,v)$ is known only at a few points on radial lines, as shown in Fig. 4 [52]:
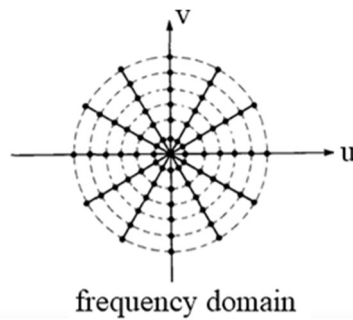
Fig. 4 – *Measured value in the frequency domain*

The points on radial lines must be interpolated using a quadratic mesh. With increasing radial distance, the density of measured values decreases, and interpolation uncertainty increases, and the reconstructed image appears smoothed or smeared [52]. A simple reconstruction can be performed by simply summing up the two-dimensional Fourier Transforms of the single lines. Each of the projections delivers only a single line, not the information for a "cake slice" of width $2\pi/\omega//k$ as it should. However, the lines are weighted with a ramp filter of height $2\pi/\omega//k$,

so that the new wedge has the same "mass "as the cake slice, which represents filtered data in the frequency domain [52]. The scheme of a ramp filter is shown in Fig. 5 [52]:

a) b) c)
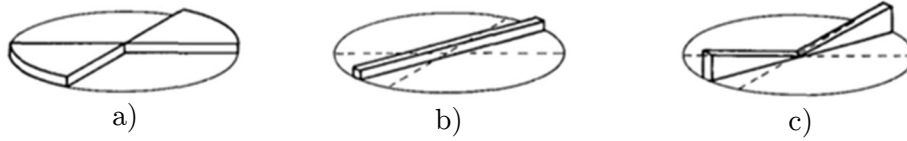
Fig. 5 – *Required, real and filtered data representation in the frequency domain.*

Then the distribution $\mu(x,y)$ by a two-dimensional Fourier Filtered Back transform of $S(u,v)$ equals:

$$\mu(x, y) = \int_0^\pi \int_0^{+\infty} S(\omega, \theta)e^{2\pi i\omega} |\omega|d\omega d\theta \tag{11}$$

Now the one-dimensional Fourier Transform $P_\theta(\omega)$ of the projection at angle can be substituted for the two-dimensional Fourier Transform $S(\omega, \theta)$:

$$\mu(x, y) = \int_0^\pi Q_\theta(x cos\theta + y sin\theta)d\theta \tag{12}$$

With:

$$Q_\theta(t) = \int_0^{+\infty} P_\theta(\omega)e^{2\pi i\omega t}|\omega|d\omega \tag{13}$$

where $Q_\theta(t)$ is called "filtered projection" [52]. These filtered projections are "back-projected" onto the reconstruction field. Each filtered projection $Q_\theta(t)$ contributes the same value to all points of the reconstruction field along the original ray. Thus, the filtered back projection is being "smeared" along the original ray path across the reconstruction field [52].

The number of projections should be in the same order as the number of rays in one projection [52]. For M projections with N rays over 180°, the angular increment δ between two consecutive projections is given in Fourier space as:

$$\delta = \frac{\pi}{M} \tag{14}$$

For distance T between two neighbouring rays, the maximum spatial frequency ω_{max} in the projection, given by Nyquist's Theorem, as:

$$\omega_{max} = \frac{1}{2T} \tag{15}$$

For N values for each projection in the spatial domain, there are also N values for each measured line in the frequency domain so that the distance ε between two consecutive measured values on a radial line (or diameter) in the frequency domain is given as [52]:

$$\varepsilon = \frac{2\omega_{max}}{N} = \frac{1}{TN} \tag{16}$$

For the worst azimuthal resolution in the frequency domain to match the radial resolution, the following must be demanded:

$$\frac{1}{2T}\frac{\pi}{M} \approx \frac{1}{TN} \tag{17}$$

From equation 17, it means [52]:

$$\frac{Number\ of\ projections}{Number\ of\ rays} = \frac{M}{N} \approx \frac{\pi}{2} \tag{18}$$

Unfortunately, this is the mathematically ideal case, but in practice, much fewer projections are used before the limit of the resolution is reached (or at least approximated) due to other sources of unsharpness in the system.

3.4 Data Analysis and Resolution Measurement

Neutron imaging experiments usually produce a large amount of data that must be processed to obtain the required information i.e., attenuation coefficient, resolution, pixel size etc. The resulting images are intensity values of the neutrons transmitted through a sample. The first steps in data processing are verification and optimisation of measured data [53]. An example is adjusting an image's brightness and contrast, focusing on narrow grey level intervals for better visual resolution of local details, white spot reduction or noise reduction to remove noise caused mainly by gamma radiation [54]. White spots are local charge clouds generated on the camera chip caused by a direct hit of a gamma photon from the sample or elsewhere. Another processing operation is the normalisation of the image. Normalization is a data correction process for beam inhomogeneity, thermal noise, and offset. For image normalisation and thus calculation of transmission, two extra images must be taken. An open beam image (ob), an image without a sample, is taken because the neutron beam and the detection system are inhomogeneous. A dark image (di), an image with a closed beam shutter, contains thermal noise and offset of the camera [55]. The information acquired by neutron imaging (after normalisation process) is the transmission of neutrons (T) through a sample. Then, the transmission after the normalisation process is:

$$T = \frac{data - di}{ob - di} \tag{19}$$

Based on Lambert's law (equation 2), an attenuation coefficient of different materials can be determined from the transmission. Other image processing steps depend on the type of experiment, e.g., for computed tomography data processing includes CT reconstruction, noise reduction, segmentation, visualisation, etc. [53].

The parameter that affects the quality of the image is a signal-to-noise ratio. The signal-to-noise ratio measures the noise strength in your signal [56]. Noise is unwanted information in a signal that is present in neutron imaging measurements. There are a few factors that influence the strength of noise – neutron flux, pixel size, exposure time, scintillator type, and efficiency. The main types of noise are spatially uncorrelated noise, which is a noise in each pixel independent of the pixel neighbourhood; structured noise, which is noise that depends on the values of the pixel neighbourhood and is thus spatially correlated; and event noise, which is a random activation function that triggers the event of each pixel with some probability [56]. Mostly, the noise consists of a combination of all three types. In general, noise is driven by

a random distribution. The most common random distribution is the Gaussian noise. All other distributions asymptotically converge towards the Gaussian distribution thanks to the central limit theorem [56]. The Poisson noise is the main noise model for event counting processes, i.e. neutron flux and generated photon flux, electronic readout noise, etc. Poisson noise is the square root of the detected particles. [57] The Poisson noise distribution is asymmetric for a few particles, while it takes a Gaussian shape when many particles are counted [56]. The pixel size, neutron flux, exposure time and detection efficiency all influence the number of detected neutrons or photons and, thus, the inherent Poisson noise. In addition, there is an electronic readout noise, thermal noise (charge/thermal electrons generated in the silicon by temperature) and noise in the number of detected photons due to the depth of the detection process on the screen. The signal-to-noise ratio can be improved by increasing the number of neutrons per pixel. This can be achieved by increasing neutron flux, exposure time, pixel size or detector material or thickness. While the pixel effective size, exposure time and neutron flux all influence the Poisson noise, the detector material and thickness influence the detection efficiency and the number of photons emitted towards the detector, depending on the depth of interaction.

Signal to noise ratio (SNR) is defined as:

$$SNR = \frac{mean(f)}{stddev(f)} \tag{20}$$

To determine the quality of the detection system, there are two quantities – effective pixel size and image resolution. Effective pixel size measures the distance between two adjacent pixels [58]. The lens's magnification and the camera's pixel size determine the detector system's effective pixel size [55]. The effective pixel size is obtained by measuring the number of pixels in a sample of a well-known size and then dividing the metric distance by the number of pixels. On the other hand, the resolution measures the ability of an optical system to resolve two features in an observed scene [58]. The resolution depends on various components of the neutron imaging instrument (filters, pinhole, scintillator, lens, camera). There are two main methods to measure resolution – using test patterns or an absorbing edge [59]. The most straightforward and fastest way to determine resolution is to use test patterns, e.g., line patterns or a Siemens star. Although the resolution can be determined visually from the test patterns, there are analytical approaches to find more precise resolution values from the Siemens star or line patterns [59]. For example, a method to find the resolution is to extract line profiles over the different line patterns, e.g., using an average profile. Another method to determine resolution is to use a sharp edge of highly absorbing material. This method is based on extracting the intensity profile across a high-contrast sharp edge, such as a thin gadolinium sheet [59]. The edge images from the high-contrast edge device can be evaluated by determining the line spread function or the modulation transfer function (MTF). The line spread function (LSF) is defined as a derivation of the edge spread function (ESF) – the intensity profile along the edge. The Fourier transformation of the LSF gives the corresponding MTF. While the LSF is measured in real space using a metric distance, the MTF is measured in reciprocal space

using frequencies as units [59]. Resolution is usually given as 10% MTF visible. The resolution performance of the imaging system is also limited by the Nyquist frequency limit. Nyquist frequency is the limit of the detection system given by pixel size - one line pair bright/dark in two pixels.

3.5   Applications of Neutron Imaging

Neutron imaging, the same as X-ray imaging, has a wide variety of applications. The advantage of neutrons against X-rays is the ability to image elements with low atomic numbers and penetrate many elements with high atomic numbers [60]. Neutrons can also deliver a contrast between many neighbouring elements in the periodic system or isotopes of the same element [1]. For this reason, neutron imaging has been established as a complementary non-destructive investigation method to X-ray imaging.

The range of potential applications of neutron imaging is primarily limited by the intensity of the neutron beam, which is proportional to the power of the neutron source [32]. The following text covers different applications of neutron imaging and examples from different facilities worldwide. The applications of neutron imaging were divided into several main categories, which include energy research, material science and engineering research, cultural heritage research and biomedical and biological research [1]. The following list of neutron imaging applications is based on a study of the references and does not include all ever-tested possibilities or options.

Material Science and Engineering

Material science and engineering, i.e., mechanical engineering, nuclear engineering, civil engineering, etc., represent the largest group of neutron imaging applications. Examples of application include many different types of samples such as industrial samples like motors, turbines, etc. [61], irradiated nuclear fuel [16] and also different phenomena such as visualisation of strains [62], residual stress [63], determination of crystalline phases, structure variations [63, 64], hydrogen embrittlement of materials [65], particulate materials and porous media, visualisation of fluid mechanics [66], multi-phase flow in heat pipes etc. Neutron imaging in material science and engineering uses classic imaging methods, e.g., radiography, tomography, or stroboscopic imaging, and also advanced imaging methods, e.g., energy selective imaging, phase contrast imaging [64], etc. These advanced methods provide different contrast mechanisms which reveal material properties that cannot be obtained by standard imaging techniques [4].

Energy Research

Neutron imaging in energy research is used in two main research activities – battery research [67] and hydrogen economy research [68]. Unlike x-rays, neutrons provide high sensitivity and contrast for light elements such as hydrogen and lithium [67]. High attenuation of neutrons by both these elements enables direct observations of lithium-ion batteries and energy production

and storage devices based on hydrogen. Neutron imaging in battery research is mainly focused on better understanding the performance, degradation, and failure of lithium-ion batteries in lithium redistribution, electrolyte consumption, and gas formation [67]. On the other hand, hydrogen economy research uses neutron imaging, for example, for efficient flow field design, gas diffusion layer characteristics, characterisation of two-phase flow phenomena and membrane durability for fuel cells [69] and materials for hydrogen storage devices [68]. A new trend in using neutron imaging for energy research is to use advanced imaging methods such as energy-resolved imaging or imaging with polarised neutrons.

Cultural Heritage Preservation

Many museums and scientific centres use X-ray imaging to study cultural heritage objects. However, X-ray imaging is unsuitable for metal objects filled with organic matter or fossils embedded in ferrous rock. Therefore, the main research areas in cultural heritage preservation where neutron imaging can be used are – archaeology, palaeontology and culturology. An example of the application of neutron imaging in archaeology is neutron imaging of archaeological bronzes [70], Roman bronze sculptures and other metallic samples [71] and metallurgic examinations on medieval swords [5]. An example of the application of neutron imaging in palaeontology is neutron computed tomography with thermal and cold neutrons of fossils embedded in rock [5], exploring hominin and non-hominin primate dental fossil remains with neutron microtomography [72] and new views of plant fossils from Antarctica: a comparison of X-ray and neutron imaging techniques [73]. Advanced methods such as Energy Selective or Bragg Edge Imaging can be used to achieve detailed results.

Biomedical and Biological Research

Another possibility of using neutron imaging is in biomedical and biological research. There are two main research areas - measurements of biological tissues and plant physiology. Measurements of biological samples using neutrons are useful for phenomena such as bone-implant interface, cardiac or respiratory deformations and tumour identification [1]. As neutron imaging poses a radiological hazard, it is not performed on living human subjects, only on small animals [74]. As for plant physiology, studies of water uptake in plants or trees were historically performed in invasive or destructive ways. Neutron imaging provides the non-destructive option of water observation in plants and soils and root development under different soil conditions [75]. This technique is also useful for observation of water movement in seeds, roots in soil and wood. Based on that, it is possible to better understand the activity of living plants, their development, and their adaptation to environmental changes.

Education and Training

Neutron imaging is also used in education and training to allow students or young professionals to perform hands-on experiments. The primary providers of education in neutron imaging are universities. They can provide their students with theoretical knowledge of neutron imaging

methods and, in some cases, provide access to experimental instruments to perform measurements, data analysis and other hands-on activities. Although not many universities provide complete semester courses focused on neutron imaging, some at least include neutron imaging in other courses, such as neutron applications, etc. or provide a possibility to perform individual research in the form of bachelor or master theses. Providers of training in neutron imaging can be research institutes operating imaging instruments or, for example, the International Atomic Energy Agency that launched e-learning courses [76] and provides training workshops in neutron imaging [77].

Chapter 4

Training Reactor VR-1

The Training reactor VR-1 is a very low-power research reactor operated by the Czech Technical University in Prague. The VR-1 reactor is a state-of-the-art experimental instrumentation for the education of students in the field of nuclear engineering from the Czech Republic and abroad [78]. Research and development activities at the reactor are mainly focused on current challenges in nuclear energy development, particularly on the safe operation of nuclear installations, theoretical and experimental reactor physics, nuclear safety, and nuclear fuel cycle. Apart from traditional nuclear technology research, the VR-1 reactor is also active in using neutron applications in research, which enables various multidisciplinary research studies that put together nuclear sciences and technology and natural sciences, social sciences, and humanities [78]. A photo of the Training reactor VR-1 is shown in Fig. 6 [79], and a photo of the reactor core in Fig. 7 [79].
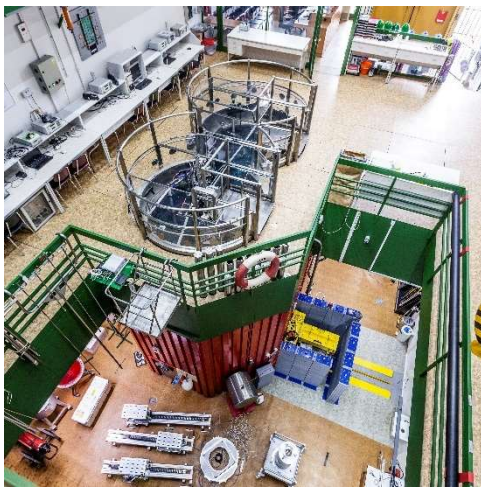
Fig. 6 – *The Training reactor VR-1*
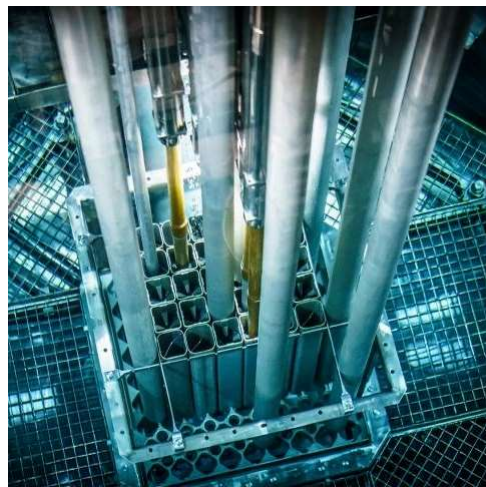
Fig. 7 – *The VR-1 reactor core*

The VR-1 reactor is a pool-type, light water reactor based on low-enriched uranium with 19.7% of 235U [78]. The reactor uses IRT-4M-type concentric fuel elements. The nominal thermal power of the reactor is 100 W, which can be increased up to 500 W up to 70 h annually [78]. Thermal neutron flux in the core at the power of 100 W corresponds to $5 \cdot 10^9 \, \mathrm{n/cm^2 s^1}$. The reactor is operated at atmospheric pressure at a temperature of about 20 °C. A neutron moderator is demineralised light water, which is also used as a neutron reflector, biological shielding and a coolant [79]. The experimental equipment of the VR-1 reactor consists of several vertical irradiation tubes, one radial horizontal beam port, one tangential horizontal beam port, shutter and measuring boxes for experiments on a radial beam port, instrumentation for detection of delayed neutrons, instrumentation for bubble boiling simulation, instrumentation for the study of temperature reactivity effects, instrumentation for fast reactivity changes, etc., [79].

4.1 Utilisation of Neutron Imaging at the Training Reactor VR-1

The Training reactor VR-1 was particularly designed for the education of students and the training of professionals, and it has performed twenty-five years of typical low-power research with one far dominant utilisation - education and training. During the last decade, the reactor has been step-by-step converted from a single-purpose training reactor to a multipurpose reactor with a strong focus on research. The first extension step was dedicated to state-of-the-art research in neutron activation analysis [80]. The second extension step should focus on the possibility of using neutron imaging. The first step in testing the possibility of using neutron imaging at the VR-1 reactor was research within the framework of student theses from 2013-2016. The theses namely were "Use of Research Reactors for Neutron Radiography and Tomography" [81], "Neutron Imaging at Research Reactors in the Czech Republic" [82] and "The Neutron Imaging at Training Reactor VR-1" [83]. The research was focused on testing neutron imaging at the VR-1 reactor using photographic films with convertors and image plates in various configurations of the radial beamline [84]. Although the results of the measurements were strongly influenced by gamma radiation, these activities still showed a potential for using neutron imaging at low-power neutron sources like the VR-1 reactor. However, based on the results, the capability for neutron imaging should be considerably limited, with the main application in education and training.

Chapter 5

Neutron Imaging at the Training Reactor VR-1

The dissertation thesis is focused on the development and utilisation of neutron imaging at low and very low-power research reactors. The main goal of the thesis was to design, develop and test possibilities of operation for a neutron imaging facility at the Training reactor VR-1. The development of a new neutron imaging facility at the VR-1 reactor was a step-by-step process, with the main steps being design, construction, safety evaluation, calculations and experimental evaluation and testing.

5.1   Development of Neutron Imaging Facility at the VR-1 Reactor

The newly developed neutron imaging facility was called NIFFLER – "Neutron Imaging Facility for Learning and Research". Development of neutron imaging at the VR-1 reactor was divided into two main topics - individual parts of the facility and time steps. The development of a neutron imaging facility at the VR-1 reactor is described in detail in following chapters based on individual parts of the facility. The first part is focused on the capabilities of neutron imaging at the reactor. Then, the most important part is focused on the individual parts, which included:

1. Detection system
2. Beamline
3. Shielding
4. Tomography setup

The development was also divided into several time steps, which are briefly described in the following paragraph and included:

1. Design
2. Safety evaluation
3. Construction
4. Testing
5. Commissioning
6. Permanent operation

The design was focused on individual parts of the facility, i.e., the detection system, beamline modifications, shielding modification and tomography setup. An important step after the design was safety evaluation. Since the designed facility was to be operated on a nuclear reactor, a safety assessment had to be conducted before its testing. It was necessary to assess the effect on safety, security, and safeguards. Safety includes nuclear safety, radiation protection and emergency preparedness, and security includes physical and cyber security. The developed facility does not affect any security (neither physical nor cyber security) and safeguards issues, so these topics are not discussed further in the text. The effect on safety, i.e., nuclear safety and radiation protection, is described further. Then, the individual components of the design facility were manufactured. All parts of the facility were prepared at CTU. The next step focused on testing the developed facility and its modification. The aim was to optimise the facility for the capabilities of the VR-1 reactor. After conducting enough tests, the facility was commissioned and later put into permanent operation at the VR-1 reactor.

Although it was expected that the potential for neutron imaging at such a low-power neutron source would be very limited, the results proved that there is a significant potential not only for neutron radiography but also, surprisingly, for neutron computed tomography. The results from the VR-1 reactor could provide important insight for neutron imaging for other low-power neutron sources worldwide.

Capabilities of Neutron Imaging at the VR-1 reactor

From the point of view of the topic addressed in the thesis, the following VR-1 reactor equipment had to be considered for the development of a neutron imaging facility. The reactor is equipped with two horizontal beamlines – radial and tangential. The radial beamline is 25 cm in diameter with possible reduction to 9 cm and 190 cm in length. The front of the beamline touches the reactor core. During the standard operation of the reactor, the radial beamline is closed and filled with shielding plugs. The tangential beamline is 10 cm in diameter and 180 cm in length. Shielding plugs are placed in the biological shielding of the reactor. The rest of the internal volume of the tube of the tangential beamline (except for the shielding plugs) can be filled with a material, e.g., water or heavy water. For the development of a neutron imaging facility at the VR-1 reactor, a radial beamline was chosen for several reasons. The first reason is easier access, while the radial beamline is a part of the reactor construction, the tangential

beamline is a removable component not permanently placed in the reactor vessel. To use the tangential beamline in the reactor, the tube of the beamline must first be placed in the reactor through an opening in the biological shielding of the reactor after removing the permanently placed shielding plugs. A second reason why the radial beamline was chosen for the purposes of neutron imaging was very low reactor power. Since the VR-1 reactor has a reactor power of only 100 W, it was necessary to extract as many neutrons as possible from the reactor core. The radial beamline, unlike the tangential beamline, has a direct view of the reactor core, which results in higher neutron flux outside the reactor. A disadvantage of the radial beamline is that it provides a higher gamma background. Nevertheless, the radial beamline is the best option for the purposes of neutron imaging at the VR-1 reactor. The cross section of the VR-1 with radial and tangential beamlines is shown in Fig. 8.
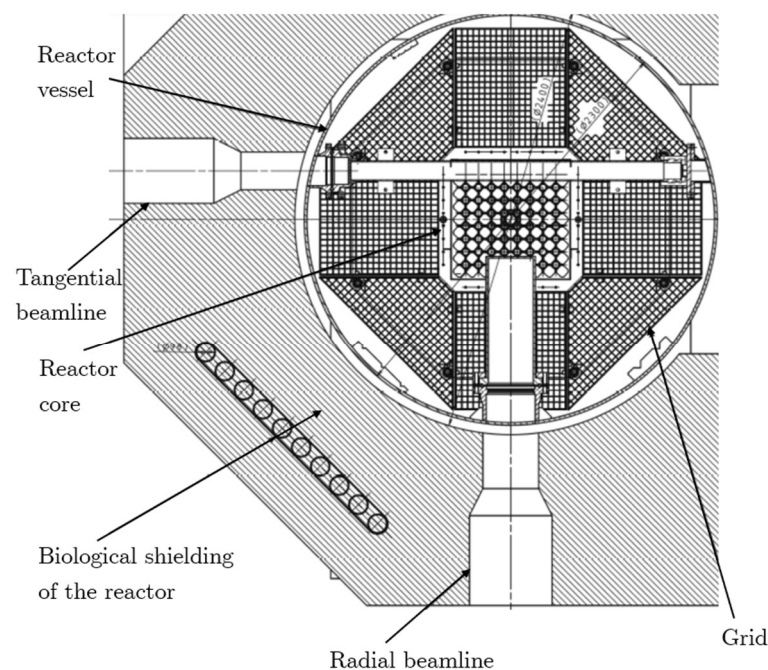
Fig. 8 – *The diagram of the VR-1 reactor with radial and tangential channels.*

Beamline Modifications

The crucial part of the development of the neutron imaging facility at the VR-1 reactor was devoted to the radial beam adjustments. All modifications, calculations and measurements were exclusively done by the author. Since the original diameter of the radial beamline at the reactor VR-1 25 cm is too large and resulted in a low collimation ratio (L/D = 10), a reduction of the diameter to 9 cm was used.

Before any modification of the radial beamline has been made, a fundamental parameter for neutron imaging – thermal neutron flux had to be determined. The verification of thermal neutron flux was performed at several positions in the reactor core and radial beamline using both measurements and calculations. In the beginning, the thermal neutron flux was verified in the reactor core. The measurement of the thermal neutron flux was performed using neutron

activation analysis (NAA) of gold foils. Since the measurements were focused on thermal neutron flux, sets of gold foils with and without cadmium covers were placed in different positions of the reactor core, both vertically and horizontally. For comparison, a calculations of thermal neutron flux were also performed using Monte Carlo calculation code SERPENT, version 2.1.31 [85] with a nuclear data library ENDF/B-VII.0 [86]. The input file to the SERPENT calculation code was prepared using the serpentaz2 tool. The serpentaz2 tool is a standardised tool developed at the Department of Nuclear Reactors for the preparation of verified input files to the SERPENT code with an already prepared model of the VR-1 reactor, usually used for core calculations at the reactor. The calculation of thermal neutron flux at the reactor core was performed in the same positions as the measurements. The thermal neutron flux in the reactor core at the reactor power of 100 W was $1 - 5 \cdot 10^9 \, \text{neutrons/cm}^{-2}\text{s}^{-1}$ depending on the position in the core. The deviation between the calculations and neutron activation analysis measurements were around 10%.

However, the determination of the thermal neutron flux in the considered position of the sample was more important. The considered sample position is at the end of the radial beamline, which is 190 cm from the reactor core. The measurement of the thermal neutron flux was again performed using neutron activation analysis of gold foils. While in the reactor core, cadmium covers were placed on both sides of the gold foils, in the radial beamline, the covers were placed only on one side, since in the reactor core, an isotropic flux is measured, while in the radial beamline, a directed flux is measured. For comparison, calculations were again performed. In this case, a necessary modification of the reactor model in the serpentaz2 tool, mainly modification of the radial beamline, had to be made. The starting configuration of the radial beamline of the reactor for neutron imaging was opened radial beamline with diameter reduced to 9 cm using a hollow aluminium plug containing water with a central channel. Fig. 9 shows a model of the radial beamline at the reactor VR-1 with reduced diameter. This configuration corresponds to L/D = 20. The results of neutron activation analysis measurements and SERPENT calculation for this configuration are given in Tab. 3 of [87] which is included in Annex A.1.
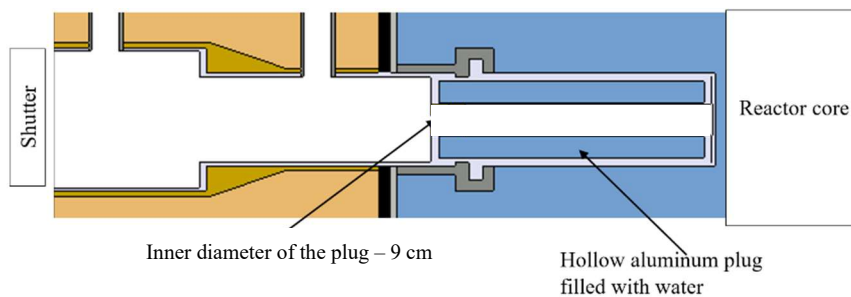
Fig. 9 – *Model of the radial beamline at the reactor VR-1 with reduced diameter*

Then, the first modification of the radial beamline was performed. This modification focused on improving beam divergence and increasing the collimation ratio L/D. This was achieved by placing a pinhole limiting the neutron beam diameter to 2 cm. Technical details of this

modification are described in [87] and [88], which are included in Annex A.1, respectively Annex A.2. This configuration corresponds to L/D = 50. Fig. 10 shows a model of the radial beamline at the reactor VR-1 with a pinhole.
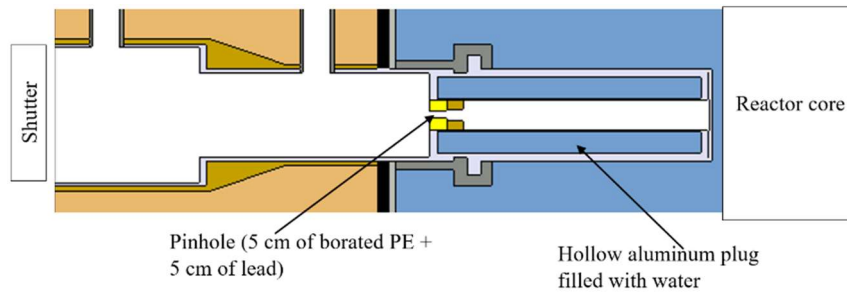
Fig. 10 – *Model of the radial beamline at the reactor VR-1 with a pinhole*

Also, for the first modification, the thermal neutron flux was calculated using the SERPENT code at the sample position. The comparison of calculated thermal neutron flux for different beamline diameters (different L/D) is given in Table 1. of [88], which is included in Annex A.2. Neutron radiography measurements for both configurations (L/D = 20 and L/D = 50) are given in Figure 6 and Figure 7 of [87], which is included in Anex A.1 and a comparison of these modifications is given in Figure 5 of [88], which is included in Annex A.2. The results of neutron radiography measurements showed that although the neutron flux in the sample position decreases due to the insertion of the pinhole (i.e., reducing the diameter of the beam), images with a similar neutron fluence due to sufficient increase in exposure time, are sharper with higher collimation ratio L/D. Further increase in the L/D ratio would not make sense because it would lead to a more pronounced reduction of the thermal neutron flux at the sample position and decreased image quality or significantly prolonged exposure times. In the case of a low-power neutron sources, like a VR-1 reactor, a balance between sufficient neutron flux at sample position and collimation ratio L/D is crucial and should be found.

After the calculations, it was found that the energy spectrum of the neutron beam coming from the reactor is wide, mostly thermal neutrons with a remaining share of epithermal and fast neutrons. This is caused by the fact that the radial beamline is located close to the reactor core with only 1 cm of water (moderator) between the core and the tube of the beamline. In order to increase the thermal neutron flux at the sample position, another modification of the radial beamline was carried out, namely placing an additional moderator inside the radial beam tube next to the reactor core. Several materials (light water, heavy water, paraffin, and polyethylene) with several different thicknesses (1-5 cm) were considered for this purpose. Another calculation using SERPENT code was performed. The results of thermal neutron flux of all moderator configurations are given in Tab. 7. The reduced table of selected moderator materials is shown in Table 2 of [88], which is included in Annex A.2. From Tab. 7, it is evident that the 4 cm of additional moderator in form of paraffin provide the largest increase in thermal neutron flux at the sample position.

Tab. 7 – *Calculated thermal neutron flux of radial beamline with additional moderators*

Material	Thickness (cm)	Thermal neutron flux ϕ_{th} (n/cm^{2}s)
no moderator	-	$3.5 \cdot 10^4$
water	2	$3.9 \cdot 10^4$
paraffin	2	$3.7 \cdot 10^4$
heavy water	2	$3.6 \cdot 10^4$
polyethylene	2	$4.2 \cdot 10^4$
water	3	$4 \cdot 10^4$
paraffin	3	$4.1 \cdot 10^4$
heavy water	3	$3.5 \cdot 10^4$
polyethylene	3	$4.3 \cdot 10^4$
water	4	$4.2 \cdot 10^4$
paraffin	4	$5 \cdot 10^4$
heavy water	4	$3.8 \cdot 10^4$
polyethylene	4	$4.8 \cdot 10^4$
water	5	$3.6 \cdot 10^4$
paraffin	5	$3.8 \cdot 10^4$
heavy water	5	$3.7 \cdot 10^4$
polyethylene	5	$4.2 \cdot 10^4$

The final configuration of the radial beamline of the VR-1 reactor is given in Fig. 11 and also Figure 4 of [88]. This configuration includes 4 cm of additional moderator in form of paraffin and a pinhole with 2 cm in diameter. By adjusting the beamline by inserting an additional moderator, it was possible to increase the thermal neutron flux at the position of the sample from $3.5 \cdot 10^4$ to $5 \cdot 10^4$ n/cm^{2}s, which is almost 1.5 times more. This was later experimentally verified using two types of measurements - neutron activation analysis and neutron imaging. In case of NAA, thermal neutron flux at the sample position was measured. In case of neutron imaging, the difference in light output was measured. In both cases, the measurement results confirmed an increase in the thermal neutron flux at the position due to using an additional moderator.
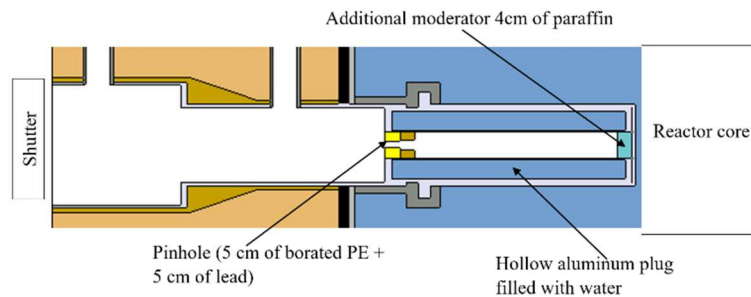
Fig. 11 – *Model of the radial beamline at the reactor VR-1 in the final configuration*

Neutron radiography measurements for different additional moderator configurations are given in Figure 6 and Figure 7 of [88], which is included in Annex A.2. In the final configuration, the verification of thermal neutron flux using both NAA and calculation code SERPENT was performed. Tab. 8 gives the comparison for the values.

Tab. 8 – *Thermal neutron flux at the sample position in the final beamline configuration*

Verification	Thermal neutron flux ϕ_{th}
NAA measurement	$4.5 \cdot 10^4$ n/cm^{2}s
SERPENT calculation	$5 \cdot 10^4$ n/cm^{2}s

Additional filters, neutron guides and flight tubes provide another possibility to adjust the neutron beam. In the case of the very low power reactor VR-1, it didn't make sense to use any filters. This is due to the fact that the use of any filter would lead to a reduction of the thermal neutron flux at the sample position which is already low. Also, neither a neutron guide nor a flight tube is useful in this case since the collimation ratio L/D is only 50, and the distance between the pinhole and the detection system is relatively short, only one meter, and the whole beamline is placed in the biological shielding of the reactor.

The final configuration of the beamline and the detection system were later used to determine fundamental neutron imaging parameters – signal-to-noise ratio, effective pixel size and resolution. The signal-to-noise ratio for neutron radiography at 100 W reactor power, the 10 minutes exposure time and thermal neutron fluence at the sample $3 \cdot 10^7$ n/cm^2 equals to 15.7. The effective pixel size depends on the field of view (FoV) of the detection system and the used binning. The detection system enables two different FoV, 6x6 cm^2 and 10x10 cm^2. The native camera pixel array is 3027 x 2048 and pixel size 2.4 um. In case of the FoV 6x6 cm^2 and binning 1x1, the effective pixel size equals 19.5 µm, and in the case of FoV 10x10 cm^2 and binning 1x1, the effective pixel size equals 32.5 µm. Binning means combining the signal from several adjacent pixels into an output for a single pixel. For 2x2 binning, an array of 4 pixels becomes a single larger pixel, reducing the overall number of pixels that need to be read out and also reducing the resolution available. For most of the neutron imaging measurements at the VR-1 reactor binning 2x2 was used. In case of the FoV 6x6 cm^2 and binning 2x2, the effective pixel size equals 39 µm, and in the case of FoV 10x10 cm^2 and binning 2x2, the effective pixel size equals 65 µm. The resolution off the system was determined with the measurement using the gadolinium edge method as a 10% of MTF and equals to 350 µm.

Since the VR-1 is a nuclear reactor and part of the neutron imaging facility is installed in the radial beamline of the reactor, it was necessary to evaluate its influence on nuclear safety. Modifications of radial beamline influence the reactivity of the reactor in 0.2 \$. This reactivity change is within operation limits of the reactor and is routinely compensated by the change in the control rod position. Thus, the nuclear safety of the reactor is not affected in any way.

Detection System

An affordable detection system was designed for the needs of testing neutron imaging at low-power neutron sources. The detection system was designed by the Heinz Maier Leibnitz Zentrum (MLZ) of the Technical University of Munich [48]. This detection system was constructed, adjusted and tested by the author.

The detection system is based on a CMOS camera in combination with a scintillator screen. The detector consists of a light tight aluminium outer casing (detector box), which inside contains several components. The detector box consists of two individual parts: the camera box and mirror box. For this reason, the detection system enables two fields of view, 6x6 cm^2 and 10x10 cm^2. Depending on the required field of view, the mirror box can be replaced. Then the main parts of the detection system are the scintillator screen and cooled CMOS camera with lens and additional components such as an external cooling, lead shielding in front and behind the camera and a mirror. Even though, the camera is air cooled, with a Peltier cooler on the chip, due to small detector box and long measurement times, for example for neutron tomography, it requires external cooling which consists of copper pipes and a brass ring for water cooling. The camera and scintillator type, their technical details, and important parameters of the detection system, like the field of view and effective pixel size, are given in [87] which is included in Annex A.1. Based on the information given in Tab. 6, a ^{6}Li-based, Cu-activated scintillator screen that emits green light, was chosen for the first measurements. As part of the development of the detection system, other scintillation screens were also tested, for example, ^{10}B-based screens. Neutron radiography results with these screens hardly showed an image due to low thermal neutron flux at the sample position and low light output of the screen. Based on the results from the VR-1 reactor, ^{6}Li-based scintillator screens seem to be the most suitable scintillator screens for neutron imaging at low power sources, primarily due to the high light output per captured neutron.

Later, the original detector box was renovated. The first detector system consisted of an aluminium housing. The original detector box was later redesigned to a 3D-printed housing made from standard PLA filament. Figure 5 of [89], included in Annex A.4, shows the compact 3D printed detector design with few parts for both the camera and mirror box. The new detector box was first tested at the TRIGA Mark II reactor at the Vienna University of Technology. The test radiography of a printed circuit board with a CPU socket is shown in Figure 6 of [89]. This detector box was also later tested at the VR-1 reactor. The advantage of a 3D printed detector box, against the original aluminium box, is that it consists of fewer parts, which are easier to manufacture and adjust. Only a 3D printer with a standard PLA filament is needed for the detector box preparation. The plastic detector housing also avoids gamma spots originating from neutron capture in an aluminium detector housing.

Part of the dissertation was not only the development of the neutron imaging facility at the VR-1 reactor but also its testing, or the testing of the detection system on other neutron

sources. The developed detection system was tested at two research reactors, e.g., the TRIGA Mark-II reactor at the Vienna University of Technology and the LVR-15 reactor at CVR Rez. Testing the developed detection system for neutron imaging at other neutron sources should have revealed the capabilities of the detection system and compared results from different source powers, beam parameters, etc. (see Tab. 9.)

Tab. 9 – *Research reactors used for testing the developed detection system*

Facility	Reactor Power	Power Ratio*	L/D	Thermal neutron flux at sample position
VR-1	100 W	-	50	$5 \cdot 10^4 \ n/cm^2 s$
TRIGA Mark-II	250 kW	2.5E3	80	$1 \cdot 10^7 \ n/cm^2 s$
LVR-15	10 MW	1E5	30	$2 \cdot 10^8 \ n/cm^2 s$

*The power ratio is the ratio of the reactor power of either the TRIGA Mark-II or the LVR-15 reactor to the reactor power of the VR-1 reactor.

A comparison of neutron radiography measurements of the 2.5" hard drive from the VR-1 reactor, the TRIGA Mark II reactor and the LVR-15 reactor is given in Fig. 12.
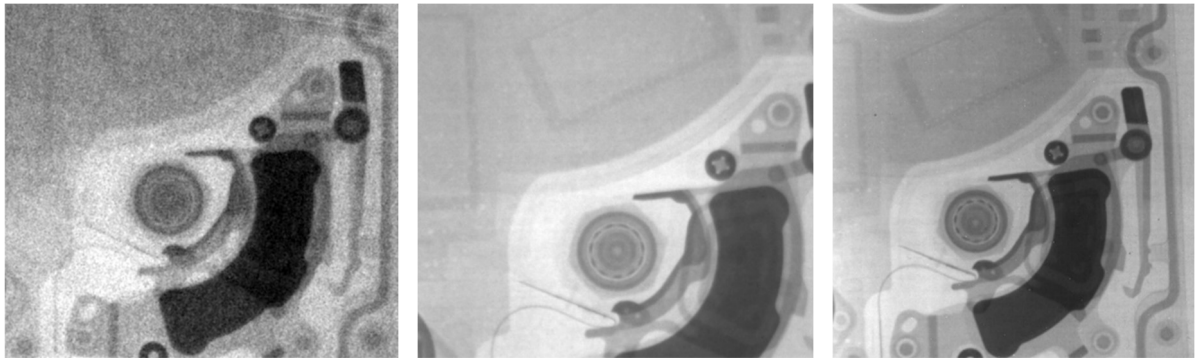
Fig. 12 – *Comparison of neutron radiography of 2.5" hard drive from a) the VR-1 reactor b) the TRIGA Mark II reactor c) the LVR-15 reactor*

At the VR-1 reactor, the exposure time was set to 10 minutes with neutron fluence at sample $3 \cdot 10^7 \ n/cm^2$, while at the TRIGA Mark II reactor, the exposure time was 20 s with neutron fluence at sample $1 \cdot 10^8 \ n/cm^2$ and the LVR-15 reactor the exposure time was 10 s with neutron fluence at sample $2 \cdot 10^9 \ n/cm^2$. All reactors use thermal neutrons for neutron imaging. The results confirm that with increasing neutron source power, i.e., increasing neutron flux at the sample, the quality of the image significantly improves. The results from the TRIGA Mark II reactor and the LVR-15 reactor are very similar. However, the reactor power of the LVR-15 reactor is considerably higher. This is caused by the fact that although the LVR-15 reactor has a higher neutron flux at the sample position, the beam is barely collimated, and the collimation ratio L/D is significantly lower than at the TRIGA Mark II reactor. Although the L/D ratio is relatively low in both cases (lower than 100), the results from both reactors are relatively sharp. This is because a thin sample placed directly on the scintillation screen was used for

measurements. The results from the VR-1 reactor are of the least quality with the most noise. Still, it is possible to distinguish the components of a 2.5" hard disk. The resolution was not measured at the TRIGA Mark II reactor and the LVR-15 reactor.

As for the external shielding, depending on the reactor power, sufficient shielding, i.e., lead bricks, borated rubber, or borated polyethylene, had to be added to protect the camera. In the case of the VR-1 reactor and the TRIGA Mark II reactor, a few lead bricks and borated rubber in front of the detector were sufficient. In the case of the LVR-15 reactor, due to high reactor power, an extra layer of shielding in the form of lead bricks and borated polyethylene blocks had to be added from all sides of the detector.

Even though the developed detection system is quite affordable, the results from the TRIGA Mark II reactor and the LVR-15 reactor showed its high quality even for high-power neutron sources like medium and high-power research reactors. Combined with a collimated neutron beam, with a collimation ratio L/D of at least 100, the detection system could provide resolution in dozens of micrometres.

Later, neutron imaging measurements with the developed detection system were performed to test the possibilities using D-D and D-T portable generators as neutron sources. Since neutron imaging using D-T and D-D generators as a neutron source is not the main topic of this dissertation thesis, this topic is just briefly introduced. The first measurements in the field of the use of neutron generators as a source for neutron imaging were performed at the International Atomic Energy Agency, Nuclear Science and Instrumentation Laboratory (NSIL) in Seibersdorf. Due to some limitations, the generators at NSIL are shielded up close with polyethylene and a combination of water canisters and concrete blocks, respectively. Since the CTU is equipped with D-D and D-T neutron generators, comparison measurements have been performed without close-up shielding. The measurements were performed in various configurations. The D-T generator, owned by the CTU, produces fast neutrons with the maximum of the energy spectrum at 14 MeV with source intensity around $5 \cdot 10^8$ n/s into 4π. Fast neutrons from the source can be used for neutron radiography. For the first configuration, the ^{6}Li-based scintillator, sensitive to thermal neutrons, had to be replaced with a fast neutron-sensitive scintillator screen, and a 6 mm thick lead sheet had to be placed between the detector and the D-T generator because X-ray radiation is also produced in the generator during the interaction. For the second configuration, the ^{6}Li-based scintillator screen was returned to the detection system, a 6 mm lead sheet remained, and 2 cm of moderator in the form of polyethylene was added. In other configurations, different thicknesses and sizes of the moderator were tested. Similar configurations were then tested for the D-D generator. Because the power/neutron intensity of the generators is very low, in the case of a D-D generator significantly lower than that of a D-T generator, the possibilities of using neutron imaging are very limited. All results were very noisy, with limited image quality.

The comparison of measurements from the IAEA NSIL and the CTU showed the major influence of close-up shielding around the setup on the results, due to the large amount of scattered neutrons from the shielding. The best setup using a D-D or a D-T portable generator as a neutron source would be an open space room with the generator and the detector standing freely without directly surrounding shielding.

Shielding Modifications

For the needs of neutron imaging, it was also necessary to modify the shielding around the radial channel of the VR-1 reactor. As experiments with open radial beamlines are considered non-standard at the reactor, additional shielding had to be installed. All modifications and measurements were exclusively done by the CTU neutron imaging group.

First, a wall of heavy concrete in combination with plates of borated polyethylene was built behind the detection system. Later, a beam stopper from a combination of lead bricks and borated polyethylene blocks was added to increase the shielding behind the detection system. The final state of the additional shielding for the detection system is shown in Figure 3 of [87], which is included in Annex A.1. The whole shielding of the neutron imaging facility at the VR-1 reactor is shown in Fig. 13.
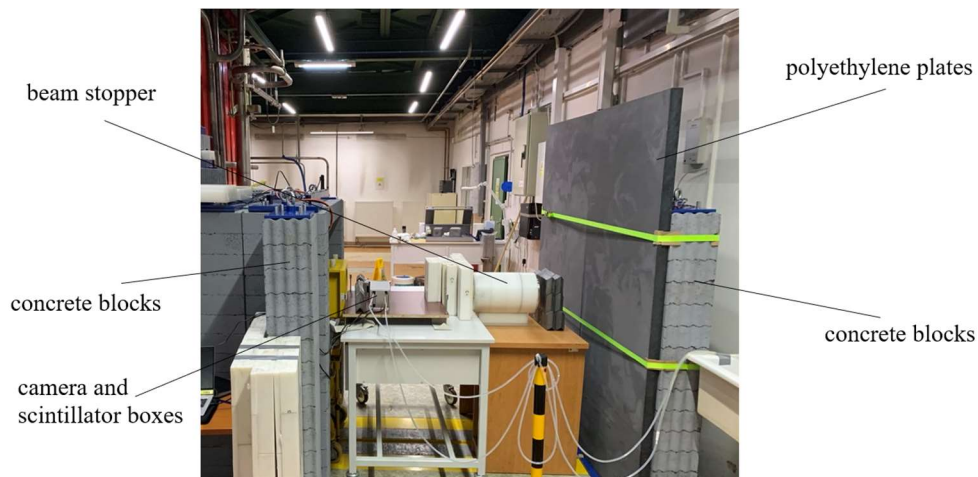
Fig. 13 – *Shielding of the neutron imaging facility at the VR-1 reactor*

The installed shielding had to be evaluated to fulfil radiation protection requirements at the reactor as well as national limits. The radiation situation around the newly developed neutron imaging facility was comprehensively measured using detectors for both gamma and neutron radiation. In the final configuration of the radial beamline, with reactor power 100 W and external shielding added, the radiation situation was measured in the centre of the beam behind the shielding, the dose equivalent of gamma equals 0.5 μSv/h, and the dose equivalent of neutrons equals 10 μSv/h. The working position in which the computer with control software is placed, is located at least 5 m from the detection system. The radiation situation in this position is at the level of a slightly increased background. These values fulfil both the internal radiation protection limits at the reactor and the national radiation protection limits.

Tomography Setup

Another part of the development of a neutron imaging facility at the VR-1 reactor was the design and development of the setup for neutron computed tomography. The tomography setup was designed by the Heinz Maier Leibnitz Zentrum (MLZ) of the Technical University of Munich, but it was assembled, adjusted for the NIFFLER facility, and tested by the author.

At first, a simple and affordable setup was built to test the possibility of performing neutron tomography at a reactor with such a low power. This setup was based on a rotation stage, a translation/linear stage and a controller. The controller consists of a Raspberry Pi computer and a Gertbot stepper motor controller. The Gertbot stepper motor controller had to be later replaced with a Waveshare HAT stepper motor controller because the Gertbot was discontinued. Other parts of the setup remained the same. The controller is designed to control the tomography sequence, which consists of tomography measurements, a series of radiographies recorded under different angles for tomography and measurements of the open beam and dark field images, controlled by a Python script on the Raspberry Pi. Later, the controller for the tomography sequence was improved, instead of using a Python script, the new control system is based on the Networked Instrument Control System (NICOS) developed at MLZ [90, 91]. Communication to the hardware was implemented using Entangle [92], an implementation of TANGO [93] developed at MLZ. Detailed information on the first neutron tomography measurements is given in [87], which is included in Annex A.1.

5.2 Applications of Neutron Imaging at the VR-1 Reactor

The Training reactor VR-1 is a state-of-the-art facility for education and training. For this reason, the neutron imaging facility at the VR-1 reactor was developed mainly for these purposes. Later, the results of the measurements showed the potential for using neutron imaging not only for education but also for research in various fields.

Education

The top quality of academic education in any nuclear discipline can only be completed with state-of-the-art experimental facilities, experimental education, and hands-on activities. Research reactors, in general, are suitable for students at all academic levels, not only in nuclear engineering but also in various non-nuclear engineering studies, nuclear analytical techniques and neutron applications, such as power engineering, electrical engineering, natural sciences, medical sciences, physical sciences, as well as students studying archaeology, anthropology, cultural heritage preservation, life sciences and environmental monitoring, biology, medicine, chemistry, forensics, etc. Experimental education at low-power research reactors for these students can significantly increase the quality of theoretical academic education and extend the practical hands-on experience for students.

The Training reactor VR-1, which was particularly designed for the education of students and the training of professionals, has more than thirty years of tradition of education in nuclear

engineering, particularly in experimental reactor physics and reactor kinetics and dynamics. In the last decade, experimental education at the reactor was extended to neutron activation analysis, and recently, with the regular operation of the NIFFLER imaging facility, also education in neutron imaging.

After its final development and testing, the neutron imaging facility at the VR-1 reactor was included in education at the Department of Nuclear Reactors. Since 2022, neutron imaging has been included in the educational program in the form of individual experiments of 2–3 hours. The main goal of these experiments is to show the basic principles of neutron radiography and demonstrate its capabilities in several nuclear and power engineering disciplines, such as material structure investigation. These demonstration experiments are part of two master courses at the Czech Technical University in Prague, Faculty of Nuclear Sciences and Physical Engineering, Department of Nuclear Reactors, called Advanced experimental neutron physics and Research reactors. In addition, individual research-oriented education is organised at the reactor. This individual education based on students' research is carried out in the frame of their thesis (bachelor, master, or doctoral thesis) or participation in research projects.

In the future, a detailed full-semester course in Neutron Imaging will be introduced for students at the Department of Nuclear Reactors, Faculty of Nuclear Sciences and Physical Engineering, Czech Technical University in Prague. The course is aimed at students in master's and doctoral study programmes. The Neutron Imaging course syllabus is shown in Tab. 10. During the course, the detailed theoretical background of neutron imaging methods, instrumentation, measurements, data processing, and imaging capabilities in various disciplines will be explained during the theoretical lectures during and hands on exercises the whole semester.

Tab. 10 – *Neutron Imaging course annotation and syllabus*

Annotation
The course is focused on neutron imaging methods, instrumentation, and applications. The first lecture provides an introduction to the basics of neutron imaging, physical background, basic principle, and important parameters. The second part is devoted to the specifics of neutron radiography and neutron tomography and their comparison with other imaging methods. The third part of the lectures is focused on the instrumentation for neutron imaging, the necessary parts of neutron imaging instruments, their importance, requirements, and main parameters. The fourth part is devoted to applications of neutron imaging in various research fields. The last part of the course focuses on advanced neutron imaging methods like energy-selective imaging, phase contrast and dark field imaging, diffractive imaging, etc. The lectures are supplemented with practical exercises, which are partly carried out at the VR-1 reactor. The exercises are focused on practical demonstrations of neutron imaging experiments with various samples and processing of measured data.

Syllabus
Lectures: 1. Introduction to neutron imaging (1 lecture) 2. Neutron radiography (2 lectures) 3. Neutron tomography (2 lectures) 4. Instrumentation for neutron imaging (2 lectures) 5. Applications of neutron imaging (3 lectures) 6. Advanced neutron imaging methods (3 lectures) Exercises: 1. Introduction to neutron radiography measurements (2 exercises) (VR-1 reactor) 2. Neutron radiography data processing (2 exercises) (Lab) 3. Determination of SNR, resolution, and pixel size (2 exercises) (VR-1 reactor) 4. Quantification of the attenuation coefficient (1 exercise) (Lab) 5. Introduction to neutron tomography measurements (2 exercises) (VR-1 reactor) 6. Neutron tomography data processing (2 exercises) (Lab) 7. Applications of neutron imaging in multidisciplinary research (2 exercises) (VR-1 reactor)

This course will be dedicated to students focusing on neutron sciences, neutron applications, nuclear analytical techniques, or beam experiments. The Neutron Imaging course will be tested during the academic year 2023/2024. It could be later included in the regular education at the Czech Technical University in Prague, Department of Nuclear Reactors. The one-semester course (13 weeks) is intended to have a range 2+3, meaning 2 hours of weekly lectures and 3 hours of weekly exercises during the semester.

Examination of Cultural Heritage Objects

Even though the primary purpose of the newly developed neutron imaging facility at the Training reactor VR-1 is education and training, other possible applications were also tested. Testing the possibility of using neutron imaging on the reactor was carried out in the field of cultural heritage preservation. Other possible fields of applications, e.g., material science and engineering or energy research, will be tested in the future. In the field of cultural heritage research, neutron imaging measurements at the VR-1 reactor were performed with Buddhist or Bon votive statues from Central Asia. Asian votive statues are suitable samples for neutron imaging because empty metallic casts are usually filled with organic materials and ritually sealed and empowered. As a non-destructive technique, neutron imaging is an extremely important tool for the study of cultural heritage objects. Three Central Asia votive statues borrowed from a private collection were studied at the NIFFLER facility: A statue of Tsongkhapa from Ladakh in Northern India, a statue of Sherab Chamma from Tibet and a statue of Buddha Shakyamuni from China.

For neutron radiography, the Buddhist statue of Tsongkhapa from Ladakh in Northern India and the Bon statue of Sherab Chamma from Tibet were selected. The Tsongkhapa statue is 14.5 cm in height and was made at the end of the last millennium by a local Buddhist artist in Ladakh in the Northern Himalayas. The statue was filled and empowered in the Buddhist monastery in Diskit in Nubra Valley in Ladakh around 2000. The Chamma statue is 13.7 cm in height and was made at the beginning of the new millennium in Norther Himalaya (India or Nepal) and filled and empowered in the Bon monastery in Dolanji in Northern India in 2006. The results of neutron radiography of the Buddhist statue of Tsongkhapa and the Bon statue of Sherab Chamma are shown in Figure 1, respectively Figure 2 of [94], which are included in Annex A.3. For neutron tomography, a statue of Buddha Shakyamuni from China was selected. The Buddha Shakyamuni, in a mediation position, is 7 cm in height and was found in the local market in Chengdu, Sichuan Province, China, at the end of the last millennium; no other information about the origin is available. The results of neutron radiography and tomography are shown in Figure 5 and Figure 6 of [94], which are included in Annex A.3. The results of these experiments clearly showed the potential of the reactor or possibly other low-power research reactors in neutron imaging for multidisciplinary research, which can provide important data for anthropologists, archaeologists or experts in culture heritage preservation.

Neutron imaging measurements at the VR-1 reactor clearly showed the potential not only for the education of students to learn the basic principles of this technique and perform experiments but also for research in various disciplines. So far, the investigations of neutron imaging applications at the reactor have been focused on cultural heritage preservation. Further activities should now focus on testing other possible applications, such as material science and engineering, battery research or hydrogen storage research.

5.3   Knowledge Transfer to Other Research Reactors

The experience gained in the development of the neutron imaging facility at the VR-1 reactor was later used for the modification of two other facilities, mainly their detection systems. The detection system used at the VR-1 reactor is quite universal and can be used on almost any neutron imaging facility that does not have special requirements such as special shielding, lack of space, etc. Even so, the later version of the detection system based on 3D printed housing was designed to be easy to manufacture and adjust. The modifications of the detection box are significantly more straightforward, unlike the aluminium casing. The modular detector box can be easily modified for the specific requirements of a neutron source, a specific purpose, or a specific field of view. Tested variants were, for example, a special high-resolution setup and a long-distance periscope. A special high-resolution setup was built using a Heliflex lenses and camera with a small pixel size. This detector was designed by the Heinz Maier Leibnitz Zentrum (MLZ) of the Technical University of Munich and tested at the the TRIGA Mark-II reactor at the Vienna University of Technology. Heliflex lenses include a 90-degree mirror and focus their output image to infinity, i.e., they create a parallel beam. Therefore, in the first

approximation, there is no loss of intensity by spreading the light beam, and the detector camera can detect the light beam out of the Heliflex lenses with its own lens focused to infinity, i.e. a parallel beam, in varying distances without losing intensity. The magnification or demagnification depends on the ratio of the focal lengths of the Heliflex and the camera lens. Figure 7 of [89] shows the detector setup with a Heliflex lenses, and Figure 8 of [89] shows the results of neutron imaging of a gadolinium pattern from the TRIGA Mark-II reactor at the Vienna University of Technology with this setup, both figures are included in Annex A.4.

Moreover, the detector box can be modified, for example, for specific shielding requirements. This was the case with the detector box for the RA-6 reactor in San Carlos de Bariloche, Argentina. The detection system was designed in collaboration between CTU and MLZ and then built, commissioned, and tested as a part of the four-month PhD internship in Argentina. The original detection system at the RA-6 reactor was from 2009 and consisted of a CCD camera in combination with a ^{6}Li-based scintillator screen. The original system had several problems: The mirrors weren't fixed in position, which required precise alignment and orientation of the mirrors, otherwise causing spatially varying blurring of the images, or the scintillator screen was quite thick, which limited the spatial resolution. The new detection system had to meet the specific requirements of the shielding placed at the end of the beamline. Therefore, based on the original 3D-printed detector box, a 1.2-meter-long periscope was designed. The firmly connected parts of the detector system ensure the alignment of the two mirrors. The model of the periscope is shown in Figure 5 of [95]. The photos of the 3D printed periscope inside and outside of the shielding at the RA-6 reactor are shown in Figure 6 of [95], which is included in Annex A.5. Technical details of the detection system, the comparison of the old and the new detections systems and the results of neutron radiography measurements are given in [95] which is included in Annex A.5. As a part of an upgrade of the detection system for neutron imaging at reactor RA-6, a comparison of the resolution was performed. The resolution was measured using a gadolinium test pattern, i.e., Siemens star. While the original resolution was 500 µm, the resolution after the upgrade was 100 µm.

A simple neutron computed tomography setup was also installed at the RA-6 reactor as a part of the detection system upgrade. The setup was the same one used at the NIFFLER facility at the VR-1 reactor, consisting of an affordable translation and rotation stage, Raspberry Pi and Waveshare stepper motor controller. Same as at the VR-1 reactor, the tomography controller was later improved using a control system based on NICOS and TANGO. The results of the first neutron computed tomography with a new detection system and new tomography setup are shown in Figure 9. of [95], which is included in Annex A.5. After the development and commissioning of a new detection system for neutron imaging at the RA-6 reactor, measurements of various interesting samples were performed. For example, a new collaboration with the Paleontological Museum in Bariloche was established, and a few fossils were provided as samples.

The 3D-printed detector box was cheaply and easily adapted to the specific shielding requirements at the RA-6 reactor. By replacing the detector system, a significant increase in resolution was achieved using a modern CMOS camera in combination with a thinner scintillator screen. With better resolution and professional software for neutron tomography, neutron imaging at the RA-6 reactor can now be used not only for education and training but also in research in various disciplines like archaeology, palaeontology, material science and nuclear engineering. However, with the large number of fossils found in Argentina, palaeontology could potentially be a major research application.

The upgrade of the detection system at the RA-6 reactor was the first step in the field of knowledge transfer from the development of neutron imaging facility from the Training reactor VR-1 to other research reactors. Another activity which is currently underway is the development of a new neutron imaging facility at the LVR-15 reactor in Rez, near Prague. This development is under the leadership of the CTU neutron imaging group. The development of this facility is directly related to the development of the facility at the VR-1 reactor, but it will take place on a larger scale since the LVR-15 reactor has a reactor power of 10 MW. The development will include modifications of the beamline using filters, collimators and flight tubes, development of shielding and modifications of the detection system. The developed facility will be the first neutron imaging facility at a high-power research reactor in the Czech Republic and will provide user access to external users. As for other activities, other institutions operating low-power research reactors, for example, the TRIGA Mark II reactor operated by the University of Pavia, Italy or the LPRR reactor currently under construction in Riyadh, Saudi Arabia, have shown interest in building similar facilities for neutron imaging.

Discussion and conclusions

The dissertation thesis was prepared in the form of the commented set of five scientific papers that are integral part of the thesis and present the main part of the thesis, and they are supplemented by a unifying text. The PhD research, described in the thesis, was focused on the possibilities of using neutron imaging at very low-power research reactors. This was performed by the development of a neutron imaging facility NIFFLER at the Training reactor VR-1 with reactor power of 100 W.

The development of the neutron imaging facility at the VR-1 reactor was divided into several steps. First the individual components were designed. The crucial part of the design was dedicated to the radial beam adjustments. A radial beamline was chosen to develop the neutron imaging facility at the VR-1 reactor, but several modifications had to be performed to improve the quality of the beam. First, to improve the collimation ratio L/D, a pinhole was placed into the beamline. Different sizes of the pinhole were tested. Later, to adjust the neutron spectrum, an additional moderator was also placed into the beamline. Different materials and thicknesses of the moderator were tested. A series of calculations using the Monte Carlo code SERPENT was performed to determine the effect of the modifications of the radial beamline on the thermal neutron flux at the sample position. The results of these calculations and experiments showed that, in case of very low-power research reactors, parameters such as neutron flux at the sample position and the collimation ratio L/D have to be optimised. A proper balance between relatively high L/D and sufficient neutron flux at the sample position should be find. In case of the VR-1 reactor, the collimation ratio L/D is 50 and thermal neutron flux at the sample position is $5 \cdot 10^4$ neutrons/cm^{2}s.

The other parts of the design focused on the detection system, tomography setup, and shielding. An affordable detection system was designed to test the possibility of using neutron imaging at low-power neutron sources. The detection system was designed in collaboration with the Heinz Maier Leibnitz Zentrum of the Technical University of Munich. The detection system is a standard neutron imaging detection system based on the CMOS camera in combination with a scintillator screen. The system is placed in a compact, light-tight box with a few internal components, making the system transportable. Therefore, it was possible to test this system at

other research reactors, namely the TRIGA Mark II reactor at the Vienna University of Technology and the LVR-15 reactor at CVR near Prague. Even though the developed detection system is quite affordable, the results from the TRIGA Mark II reactor and the LVR-15 reactor showed its high quality and potential use even for high-power neutron sources/research reactors. Also, part of the design, the shielding around the radial beamline of the VR-1 reactor also had to be modified or the needs of neutron imaging. A wall of heavy concrete in combination with plates of borated polyethylene was built behind the whole setup; and a beam stopper from a combination of lead bricks and borated polyethylene blocks was added behind the detection system. And a setup for neutron computed tomography was also prepared as part of the design. At first, a simple setup, consisting of a rotation stage, linear stage, Raspberry Pi and a stepper motor controller, was built to test the possibility of performing neutron tomography at a reactor with such a low power. The tomography sequence was controlled by a Python script on the Raspberry Pi. Later, the controller for the tomography sequence was replaced by the professional control system NICOS. An essential step after the design was safety evaluation. The effect on safety, security, and safeguards had to be determined. After the safety evaluation, the individual parts of the facility were constructed, tested at the VR-1 reactor, and modified if necessary. The facility was then commissioned and put into permanent operation not only for neutron radiography but also for computed neutron tomography, which makes it the first neutron tomography facility operated at such a low power research reactor worldwide. This was highly appreciated by IAEA and the whole neutron imaging community worldwide.

After commissioning of the NIFFLER imaging facility, the research focused on testing different possibilities of using neutron imaging. The first step was to include neutron imaging into education at the Department of Nuclear Reactors. From 2022, neutron imaging experiments were included in two courses at the Czech Technical University in Prague, namely Advanced Experimental Neutron Physics and Research Reactors. A new detailed full-semester course on Neutron Imaging is being prepared, which will be introduced in the future for students at the Department of Nuclear Reactors. Although one of the goals of the thesis was to include neutron imaging in standard teaching at the VR-1 reactor, the results also showed the potential for multidisciplinary research, such as cultural heritage preservation. The possibility of using neutron imaging at very low-power research reactors was carried out in the field of cultural heritage preservation. The investigation of the internal structures of Buddhist or Bon votive statues from Central Asia was performed. Three Central Asia votive statues borrowed from a private collection were studied at the NIFFLER facility. Neutron imaging experiments of the statues revealed interesting internal contents made of organic materials inside metallic statues. This was the first step in collaboration with the National Gallery Prague which would like to perform similar experiments on their objects. These experiments showed that neutron imaging is a powerful tool for the investigation of cultural heritage objects, even at low-power neutron sources. However, cultural heritage preservation is one of the many applications of

neutron imaging. Other possible fields of applications of neutron imaging, for example, material science and engineering and energy research, will be tested at the VR-1 reactor in the future. More specifically, the investigations should focus on using low-power research reactors for battery and hydrogen economy research.

All results from the NIFFLER neutron imaging facility successfully confirmed the possibility of using very low-power research reactors, such as the Training reactor VR-1, for neutron imaging. The results not only demonstrated the feasibility of using neutron imaging at very low-power research reactors but also extended the range of applications of the VR-1 reactor. Neutron imaging is now routinely included in standard education at the Czech Technical University in Prague, and other activities are planned to provide this method to a broader spectrum of students. The results of neutron imaging experiments from the NIFFLER facility also showed the great potential of using neutron imaging at low-power research reactors not only for the education of students but also for multidisciplinary research, for example, in the field of cultural heritage preservation. The knowledge, experience and results from developing and testing the NIFFLER facility can provide insight and opportunity for other very low-power research reactors worldwide to build similar facilities for neutron imaging to benefit research reactors themselves and also user communities in various research disciplines using this excellent neutron application.

References

[1]   I. Anderson, R. McGreevy and H. Bilheux, Neutron imaging and applications: a reference for the imaging community, New York: Springer, 2008.

[2]   D. Hussey, M. Abir, J. Cook, D. Jacobson, J. LaManna, K. Kilaru, B. Ramsey and B. Khaykovich, "Design of a neutron microscope based on Wolter mirrors," *Nuclear Instruments and Methods in Physics Research Section A: Accelerators, Spectrometers, Detectors and Associated Equipment,* vol. 987, 2021.

[3]   P. Trtik, J. Hovind, C. Grünzweig, A. Bollhalder, V. Thominet, C. David, A. Kaestner and E. Lehmann, "Improving the Spatial Resolution of Neutron Imaging at Paul Scherrer Institut – The Neutron Microscope Project," *Physics Procedia,* vol. 69, pp. 169-176, 2015.

[4]   E. Lehmann, G. Frei, P. Vontobel, L. Josic, N. Kardjilov, A. Hilger, W. Kockelmann and A. Steuwer, "The energy-selective option in neutron imaging," *Nuclear Instruments and Methods in Physics Research Section A: Accelerators, Spectrometers, Detectors and Associated Equipment,* vol. 603, no. 3, pp. 429-438, 2009.

[5]   B. Schillinger, A. Beaudet, A. Fedrigo, F. Grazzi, O. Kullmer, M. Laaß, M. Makowska, I. Werneburg and C. Zanolli, "Neutron Imaging in Cultural Heritage Research at the FRM II Reactor of the Heinz Maier-Leibnitz Center," *Journal of Imaging,* vol. 4, no. 1, 2018.

[6]   C. Grünzweig, C. David, O. Bunk, M. Dierolf, G. Frei, G. Kühne, R. Schäfer, S. Pofahl, H. M. R. Rønnow and F. Pfeiffer, "Bulk magnetic domain structures visualized by neutron dark-field imaging," *Applied physics letters,* vol. 93, no. 11, 2008.

[7]   M. Strobl, A. Hilger, N. Kardjilov, O. Ebrahimi, S. Keil and I. Manke, "Differential phase contrast and dark field neutron imaging," *Nuclear Instruments and Methods in*

Physics Research Section A: Accelerators, Spectrometers, Detectors and Associated Equipment, vol. 605, no. 1-2, pp. 9-12, 2009.

[8]   R. Woracek, J. Santisteban, A. Fedrigo and M. Strobl, "Diffraction in neutron imaging—A review," *Nuclear Instruments and Methods in Physics Research Section A: Accelerators, Spectrometers, Detectors and Associated Equipment,* vol. 878, pp. 141-158, 2018.

[9]   C. Grünzweig, C. David, O. Bunk, J. Kohlbrecher, E. Lehmann, Y. W. Lai, R. Schäfer, S. Roth, P. Lejcek, J. Kopecek and F. Pfeiffer, "Visualizing the propagation of volume magnetization in bulk ferromagnetic materials by neutron grating interferometry," *Journal of Applied Physics,* vol. 107, no. 9, 2010.

[10]   N. Kardjilov, A. Hilger, I. Manke, M. Strobl and J. Banhart, "Imaging with Polarized Neutrons," *Journal of Imaging,* vol. 4, no. 1, 2017.

[11]   M. Schulz, P. Böni, C. Franz, A. Neubauer, E. Calzada, M. Mühlbauer, B. Schillinger, C. Pfleiderer, A. Hilger and N. Kardjilov, "Comparison of Polarizers for Neutron Radiography," *Journal of Physics Conference Series,* vol. 251, 2010.

[12]   IAEA, "Use of neutron beams for low and medium flux research reactors: radiography and materials characterization (IAEA-TECDOC-837)," International Atomic Energy Agency, Vienna, 1993.

[13]   IAEA, "Research Reactor Database," International Atomic Energy Agency, [Online]. Available: https://nucleus.iaea.org/RRDB/RR/ReactorSearch.aspx.. [Accessed November 2023].

[14]   INSR, "Neutron Imaging Facilities Survey," 2019. [Online]. Available: https://isnr.de/images/facilities/ni_facilities_database_v2019-02-04.pdf. [Accessed November 2023].

[15]   INSR, "Neutron Imaging Facilities," International Society for Neutron Radiography, 2023. [Online]. Available: https://isnr.de/index.php/ni-facilities. [Accessed November 2023].

[16]   A. Craft, D. Wachs, M. Okuniewski, D. Chichester, W. Williams, G. Papaioannou and A. Smolinski, "Neutron Radiography of Irradiated Nuclear Fuel at Idaho National Laboratory," *Physics Procedia,* vol. 69, pp. 483-490, 2015.

[17]   S. Koerner, B. Schillinger, P. Vontobel and H. Rauch, "A neutron tomography facility at a low power research reactor," *Nuclear Instruments and Methods in Physics Research Section A: Accelerators, Spectrometers, Detectors and Associated Equipment,* vol. 471, no. 1-2, pp. 69-74, 2001.

[18]   ANSTO, "Australian Centre for Neutron Scattering," ANSTO, [Online]. Available: https://www.ansto.gov.au/facilities/australian-centre-for-neutron-scattering. [Accessed November 2023].

[19]   ILL, "NEXT - Neutron and X-ray Tomography instrument," ILL, [Online]. Available: https://www.ill.eu/users/instruments/instruments-list/next/description/instrument-layout. [Accessed November 2023].

[20]   MLZ, "ANTARES - Cold neutron radiography and tomography facility," MLZ, [Online]. Available: https://mlz-garching.de/antares. [Accessed November 2023].

[21]   MLZ, "MEDAPP & NECTAR - Fission neutron facility for scientific, medical, and industrial applications," MLZ, [Online]. Available: https://mlz-garching.de/medapp-nectar. [Accessed November 2023].

[22]   BNC, "RAD – Static/dynamic white-beam-neutron and X-ray imaging station," BNC, [Online]. Available: https://www.bnc.hu/?q=rad. [Accessed November 2023].

[23]   BNC, "NORMA - Neutron Optics and Radiography for Material Analysis," BNC, [Online]. Available: https://www.bnc.hu/?q=norma. [Accessed November 2023].

[24]   JAEA, "Layout of JRR-3 Furnace Room and Beam Hall," JAEA, [Online]. Available: https://jrr3uo.jaea.go.jp/about/institution/tnrf.htm. [Accessed November 2023].

[25]   J-PARC, "BL22 RADEN Energy Resolved Neutron Imaging System," J-PARC, [Online]. Available: https://mlfinfo.jp/en/bl22/. [Accessed November 2023].

[26]   PSI, "Applied Materials Group - Neutron Imaging and Engineering Diffraction," PSI, [Online]. Available: https://www.psi.ch/en/niag. [Accessed November 2023].

[27]   LANSCE, "Energy Resolved Neutron Imaging (ERNI) at FP5," LANSCE, [Online]. Available: https://lansce.lanl.gov/facilities/lujan/instruments/fp-5/index.php. [Accessed November 2023].

[28]   ORNL, "Multimodal Advanced Radiography Station MARS, CG-1D, HFIR," ORNL, [Online]. Available: https://neutrons.ornl.gov/mars. [Accessed November 2023].

[29]   ORNL, "Spallation Neutrons and Pressure Diffractometer SNAP, BL-3, SNS," ORNL, [Online]. Available: https://neutrons.ornl.gov/snap. [Accessed November 2023].

[30]   NIST, "Neutron Imaging, an Essential Tool for the Hydrogen Economy," NIST, [Online]. Available: https://physics.nist.gov/MajResFac/NIF/. [Accessed November 2023].

[31]   NIST, "Cold Neutron Imaging Instrument," NIST, [Online]. Available:
         https://www.nist.gov/laboratories/tools-instruments/cold-neutron-imaging-
         instrument. [Accessed November 2023].

[32]   IAEA, "The applications of research reactors (IAEA-TECDOC-1234)," International
         Atomic Energy Agency, Vienna, 2001.

[33]   F. Ferreira, A. Silva and V. Crispim, "Electronic imaging system for neutron
         radiography at a low power research reactor," *Radiation Measurements,* vol. 45, no. 7,
         pp. 8006-809, 2010.

[34]   C. J. M. and K. M. H., "Performance Evaluation of Neutron Radiography Facility at
         Kyung Hee University Reactor, AGN-201K," in *Korean Nuclear Society Spring
         Meeting*, Jeju, 2012.

[35]   L. Bennetta, W. Lewisa and P. Hunglera, "The development of neutron radiography
         and tomography on a SLOWPOKE-2 Reactor," *Physics Procedia,* no. 43, pp. 21-33,
         2013.

[36]   C. Lange and N. Bernt, "Neutron imaging at the low flux training and research
         reactor AKR-2," *Nuclear Instruments and Methods in Physics Research Section A:
         Accelerators, Spectrometers, Detectors and Associated Equipment,* vol. 941, 2019.

[37]   L. Luiz, F. Ferreira and V. Crispim, "Visualization of crust in metallic piping through
         real-time neutron radiography obtained with low intensity thermal neutron flux,"
         Nuclear Engineering and Technology, vol. 49, no. 4, 2017.

[38]   C. Nares, Neutron Radiography, Non-Destructive Testing Methods and New
         Applications, London: InTech, 2012.

[39]   P. Reuss, Neutron Physics, EDP Sciences, 2008.

[40]   B. Schillinger and T. Bücherl , "Neutronen sehen, was Röntgenstrahlen verborgen
         bleibt," *ZfP-Zeitung 89,* no. 04, pp. 34-41, 2004.

[41]   PSI, "Neutron Physics," PSI, 2023. [Online]. Available:
         https://www.psi.ch/en/niag/neutron-physics. [Accessed November 2023].

[42]   E. Lehmann, D. Mannes, M. Strobl, B. Walfort, A. Losko, B. Schillinger, M. Schulz, .
         S. Vogel , D. Schaper, D. Gautier and D. Newmark, "Improvement in the spatial
         resolution for imaging with fast neutrons," *Nuclear Instruments and Methods in
         Physics Research Section A: Accelerators, Spectrometers, Detectors and Associated
         Equipment,* vol. 988, 2021.

[43]   IAEA, "Neutron Imaging: A Non-Destructive Tool for Materials Testing," IAEA, Vienna, 2008.

[44]   R. J. Holmes, "Gamma ray and neutron sources," IAEA, 1982.

[45]   B. Schillinger, "Intrumentation for Neutron Imaging," 2017. [Online]. Available: https://indico.frm2.tum.de/event/51/contributions/859/attachments/162/209/IAEA_ AUNIRA_Summer_School_Schillinger-Instrumentation_for_Neutron_Imaging.pdf. [Accessed December 2023].

[46]   N. Chankow , S. Punnachaiya and S. Wonglee , "Neutron radiography using Neutron Imaging Plate," *Applied Radiation and Radioisotopes,* vol. 68, no. 4, 2010.

[47]   A. Hewat, "Inexpensive Neutron Imaging Cameras Using CCDs for Astronomy," *Physics Procedia,* vol. 69, 2015.

[48]   B. Schillinger, "An Affordable Image Detector and a Low-Cost Evaluation System for Computed Tomography Using Neutrons, X-rays, or Visible Light," *Quantum Beam Science,* vol. 3(4), no. 21, 2019.

[49]   TELEDYNE FLIR, "Key differences between CCD and CMOS imaging sensors," Teledyne Flir, [Online]. Available: https://www.flir.eu/support-center/iis/machine-vision/knowledge-base/key-differences-between-ccd-and-cmos-imaging-sensors/. [Accessed November 2023].

[50]   RC TRITEC, "Scintillators for neutron imaging," RC TRITEC, [Online]. Available: https://www.rctritec.com/en/scintillators/products.html. [Accessed November 2023].

[51]   M. Makowska , B. Walfort , A. Zeller , C. Grünzweig and T. Bücherl , "Performance of the Commercial PP/ZnS:Cu and PP/ZnS:Ag Scintillation Screens for Fast Neutron Imaging," *Journal of Imaging,* vol. 3, no. 4, 2017.

[52]   A. C. Kak and M. Slaney, Principles of Computerized Tomographic Imaging, Society of Industrial and Applied Mathematics, 2001.

[53]   A. Kaestner and M. Schulz, "Processing Neutron Imaging Data – Quo Vadis?," *Physics Procedia,* vol. 69, pp. 336-342, 2015.

[54]   A. Kaestner, "Jupyter Notebooks - Introduction to Images," PSI, 2023. [Online]. Available: https://colab.research.google.com/github/ImagingELearning/ImageProcessing/blob/main/tutorials/02_WorkingWithImages/02_WorkingWithImages.ipynb. [Accessed November 2023].

[55] T. Neuwirt, S. Sebold and M. Schulz, "Neutron Imaging - AUNIRA 2021," 2021. [Online]. Available: file:///C:/Users/janic/Downloads/AUNIRA%20ANTARES_V2.pdf. [Accessed November 2023].

[56] A. Kaestner, "Jupyter Notebooks - Noise in neutron images," PSI, 2023. [Online]. Available: https://colab.research.google.com/github/ImagingELearning/ImageProcessing/blob/main/tutorials/03_Noise/NoiseInNeutronImages.ipynb. [Accessed November 2023].

[57] B. Schillinger and S. Saha, "The signal chain - how the removal of an image intensifier at the AERE reactor in Bangladesh improves neutron imaging," *Physics Procedia,* vol. 88, pp. 243-249, 2017.

[58] A. Kaestner, "Jupyter Notebooks - Introduction to resolution, pixels, and sampling," PSI, 2023. [Online]. Available: https://colab.research.google.com/github/ImagingELearning/resolution/blob/main/tutorials/01_Introduction/01_Resolution_Introduction.ipynb. [Accessed November 2023].

[59] A. Kaestner, Z. Kis, M. Radebe, D. Mannes, J. Hovind, C. Grunzweig, N. Kardjilov and E. Lehmann, "Samples to determine the resolution of neutron radiography and," *Physics Procedia,* vol. 00, 2016.

[60] PSI, "Neutron imaging: how neutrons create picture," Paul Scherrer Institute, Villigen, 2007.

[61] U. Garbe, Y. Ahuja, R. Ibrahim, H. Li, L. Aldridge, F. Salvemini and Z. Paradowska, "Industrial Application Experiments on the Neutron Imaging Instrument DINGO," *Physics Procedia,* vol. 88, pp. 13-18, 2017.

[62] S. Sasada, Y. Takahashi, K. Takeuchi, K. Hiroi, T. Shinohara, K. Watanabe and A. Uritani, "Strain distribution visualization of punched electrical steel sheets using neutron Bragg-edge transmission imaging," *Japanese Journal of Applied Physics,* vol. 61, no. 4, 2022.

[63] A. Jacob, A. Mehmanparast, J. Kelleher and G. Burca, "Neutron diffraction and neutron imaging residual strain measurements on offshore wind monopole weldments," *Procedia Structural Integrity,* vol. 13, pp. 517-522, 2018.

[64] K. Tran, R. Woracek, D. Penumadu, N. Kardjilov, A. Hilger , M. Boin, J. Banhart, J. Kelleher, A. Tremsin and I. Manke, "Phase and texture evaluation of transformation-

induced plasticity effect by neutron imaging," *Materials Today Communications* , vol. 35, 2023.

[65] M. Grosse, B. Schillinger and A. Kaestner, "In Situ Neutron Radiography Investigations of Hydrogen Related Processes in Zirconium Alloys," *Applied sciences,* vol. 11(13), 2021.

[66] A. Tengattini , N. Lenoir, E. Andò and G. Viggiani , "Neutron imaging for geomechanics: A review," *Geomechanics for Energy and the Environment,* vol. 27, 2021.

[67] R. Ziesche, N. Kardjilov, W. Kockelmann, D. Brett and P. Shearing, "Neutron imaging of lithium batteries," *Joule,* vol. 6, no. 1, pp. 35-52, 2022.

[68] F. Heubner, A. Hilger, N. Kardjilov, I. Manke, B. Kieback, L. Gondek, J. Banhart and L. Röntzsch, "In-operando stress measurement and neutron imaging of metal hydride composites for solid-state hydrogen storage," *Journal of Power Sources,* vol. 397, pp. 262-270, 2018.

[69] P. Boillat, E. Lehmann, P. Trtik and M. Cochet, "Neutron imaging of fuel cells – Recent trends and future prospects," *Current Opinion in Electrochemistry,* vol. 5, no. 1, pp. 3-10, 2017.

[70] K. Ryzewski, S. Herringer , H. Bilheux, L. Walker, B. Sheldon , S. Voisin, J.-C. Bilheux and V. Finocchiaro, "Neutron Imaging of Archaeological Bronzes at the Oak Ridge National Laboratory," *Physics Procedia,* vol. 43, pp. 343-351, 2013.

[71] E. Deschler-Erb, E. Lehmann and L. Pernet, "The complementary use of neutrons and X-rays for the non-destructive investigation of archaeological objects from Swiss collections," *Archaeometry,* 2004.

[72] C. Zanolli, B. Schillinger, A. Beaudet, O. Kullmer, R. Macchiarelli , L. Mancini, F. Schrenk, C. Tuniz and V. Vodopivec, "Exploring Hominin and Non-hominin Primate Dental Fossil Remains with Neutron Microtomography," *Physics Procedia,* vol. 88, pp. 109-115, 2017.

[73] M. Dawson, J. Francis and R. Carpenter, "New views of plant fossils from Antarctica: a comparison of X-ray and neutron imaging techniques," *Journal of Paleontology,* 2015.

[74] R. Metzke, H. Runck, C. Stahl, B. Schillinger, E. Calzada, M. Mühlbauer, M. Schulz, M. Schneider, H.-J. Priebe, W. Wall and J. Guttmann, "Neutron computed tomography of rat lungs," *Physics in Medicine and Biology,* vol. 56, no. 1, 2011.

[75]   G. Cai, C. Tötzke, A. Kaestner and M. Ahmed, "Quantification of root water uptake and redistribution using neutron imaging: a review and future directions," *Plant Journal*, 2022.

[76]   IAEA, "Neutron Imaging E-Learning Course," IAEA, 2020. [Online]. Available: https://elearning.iaea.org/m2/course/view.php?id=633. [Accessed November 2023].

[77]   IAEA, "AUNIRA 2023," IAEA, 2023. [Online]. Available: https://www.iaea.org/events/evt2205767. [Accessed November 2023].

[78]   L. Frybortova, J. Rataj, L. Sklenka, J. Frybort, F. Fejt and O. Novak, "The Training Reactor VR-1 - 30 Years of Operation," in *21st International Scientific Conference on Electric Power Engineering (EPE)*, 2020.

[79]   Czech Technical University in Prague, "Training Reactor," Czech Technical University in Prague, [Online]. Available: https://reaktor-vr1.cz/en/. [Accessed November 2023].

[80]   M. Stefanik, M. Cesnek, L. Sklenka, T. Kmjec and M. Miglierini, "Neutron activation analysis of meteorites at the VR-1 training reactor," *Radiation Physics and Chemistry*, vol. 171, 2020.

[81]   J. Crha, "Use of Research Reactors for Neutron Radiography and Tomography," FNSPE CTU, 2013.

[82]   J. Crha, "Neutron Imaging at Research Reactors in the Czech Republic," FNSPE CTU, 2015.

[83]   J. Crha, "Neutron Imaging at the Training Reactor VR-1," FNSPE CTU, 2016.

[84]   J. Crha, L. Sklenka and J. Soltes, "Neutron imaging on the VR-1 reactor," *Journal of Physics: Conference Series*, vol. 746, no. 1, 2016.

[85]   J. Leppanen, "Serpent - A Continuous-Energy Monte Carlo Reactor Physcis Burnup Calculation Code," VTT Technical Research Centre of Finland, Espoo, 2015.

[86]   M. Chadwick, "ENDF/B-VII.0: Next Generation Evaluated Nuclear Data Library for Nuclear Science and Technology," *Nuclear Data Sheets*, vol. 107.

[87]   J. Matouskova, B. Schillinger and L. Sklenka, "New Neutron Imaging Facility NIFFLER at Very Low Power Reactor VR-1," *Journal of Imaging*, vol. 9, no. 15, pp. 1-11, 2023.

[88]   J. Matouskova, B. Schillinger and L. Sklenka, "Development of a Neutron Imaging Facility at the Very Low Power Reactor VR-1," *Journal of Physics: Conference Series*, vol. 2605, 2023.

[89] B. Schillinger, N. Geerits, T. Juenger, J. Matouskova, T. Neuwirth, F. Oppermann, S. Sebold and S. Sponar, "Flexible camera detector box design using 3D printers," *Journal of Physics: Conference Series,* vol. 2605, 2023.

[90] "NICOS open-source scientific instrument control software," 2023. [Online]. Available: http://www.nicos-controls.org. [Accessed November 2023].

[91] B. Schillinger, A. Craft and J. Kruger, "The ANTARES instrument control system for neutron iamging with NICOS/TANGO/LiMA converted to a mobile system used at idaho national laboratory," in *11th World Conference on Neutron Radiography.*

[92] "TANGO base class specification," 2023. [Online]. Available: https://forge.frm2.tum.de/entagle/defs/entagle-master/. [Accessed November 2023].

[93] "TANGO controls," 2023. [Online]. Available: http://www.tango-controls.org. [Accessed November 2023].

[94] J. Matouskova, L. Sklenka and B. Schillinger, "Investigation of Buddhist and Bon Votive Statues at the Very Low Power Reactor VR-1," *Nuclear Instruments and Methods in Physics Research Section A: Accelerators, Spectrometers, Detectors and Associated Equipment,* vol. 1060, 2024.

[95] J. Matouskova, J. Marin, T. Juenger, F. Oppermann, F. Sanchez, S. Sebold, B. Schillinger and L. Sklenka, "New Detector Design os STORNI Neutron Imaging Facility at RA-6 Research Reactor," *Nuclear Instruments and Methods in Physics Research Section A: Accelerators, Spectrometers, Detectors and Associated Equipment,* vol. 1056, 2023.

List of Author Publications

Publications in Scientific Journals with Impact Factor

1. **J. Matoušková**, B. Schillinger, L. Sklenka: *New Neutron Imaging facility NIFFLER at Very Low Power Reactor VR-1*, JOURNAL OF IMAGING Vol. 9 (2023), ISSN 2313-433X, Impact factor: 3.2, year: 2023.

2. **J. Matoušková**, B. Schillinger, L. Sklenka: *Development of a Neutron Imaging Facility at the Very Low Power Reactor VR-1*, JOURNAL OF PHYSICS CONFERENCE SERIES, Vol. 2605 (2023), ISSN 1742-6596, Impact factor: 0.21, year: 2023.

3. B. Schillinger, N. Geerits, T. Juenger, **J. Matoušková**, T. Neuwirt, F. Oppermann, S. Sebold and S. Sponar: *Flexible camera detector box design using 3D printers*, JOURNAL OF PHYSICS CONFERENCE SERIES, Vol. 2605 (2023), ISSN 1742-6596, Impact factor: 0.21, year: 2023.

4. **J. Matoušková**, J. Marin, T. Juenger, F. Oppermann, F. Sanchez, S. Sebold, B. Schillinger, L. Sklenka: *New Detector Design of STORNI Neutron Imaging Facility at RA-6 Research Reactor*, NUCLEAR INSTRUMENTS AND METHODS IN PHYSICS RESEARCH SECTION A: ACCELERATORS, SPECTROMETERS, DETECTORS AND ASSOCIATED EQUIPMENT (2023), ISSN 1872-9576, Impact factor: 1.4, year: 2023.

5. **J. Matoušková**, L. Sklenka, B. Schillinger: *Investigation of Buddhist and Bon Votive Statues at the Very Low Power Reactor VR-1,* NUCLEAR INSTRUMENTS AND METHODS IN PHYSICS RESEARCH SECTION A: ACCELERATORS, SPECTROMETERS, DETECTORS AND ASSOCIATED EQUIPMENT (2023), ISSN 1872-9576, Impact factor: 1.4, year: 2024.

Other Publications

1. **J. Matouskova**, O. Huml: *Monte Carlo method for determining the uncertainty of the multiplication coefficient due to the uncertainty of the isotopic composition of spent nuclear fuel (in Czech),* 20. MIKULÁŠSKÉ SETKÁNÍ MLADÉ GENERACE ČESKÉ NUKLEÁRNÍ SPOLEČNOSTI, (2020).

2. **J. Matouskova:** *Neutron imaging at the VR-1 reactor (in Czech),* PRAŽSKÁ TECHNIKA, (1/2022) ISSN 1213-5348.

3. L. Sklenka, **J. Matouskova***: 65 years of nuclear education and research at the Nuclear Faculty (in Czech),* JADERNÁ ENERGIE, (4/2021) ISSN 2694-9024.

List of Author Presentations at Scientific Conferences

1. **J. Matouskova,** B. Schillinger, L. Sklenka: *Neutron Imaging at Low and Medium Flux Neutron Sources,* INTERNATIONAL CONFERENCE ON RESEARCH REACTORS: ACHIEVEMENTS, EXPERIENCE AND THE WAY TO A SUSTAINABLE FUTURE, Jordan (2023 - postponed to 2024). Invited speaker.

2. L. Sklenka, **J. Matouskova:** *Development of National Strategy for Decommissioning of Research Reactors in the Czech Republic,* INTERNATIONAL CONFERENCE ON RESEARCH REACTORS: ACHIEVEMENTS, EXPERIENCE AND THE WAY TO A SUSTAINABLE FUTURE, Jordan (2023 - postponed to 2024).

3. L. Sklenka, M. Stefanik, **J. Matouskova**: *The VR-1 Nuclear Experimental Hub – how a very low-power research reactor can serve the neutron science and applications community,* NEUTRONS4NA: CONSULTANCY MEETING ON THE DEVELOPMENT OF A NEW INITIATIVE ON USING NEUTRONS FOR NUCLEAR SCIENCES AND APPLICATIONS, Vienna (2023).

4. B. Schillinger, **J. Matouskova,** H. Ben-Abdelouahed, K. Kanaki, N. Skukan: *Neutron generators: From logical assumptions to totally different behaviour,* NEUWAVE-11: THE 11TH WORKSHOP ON NEUTRON WAVELENGTH DEPENDENT IMAGING, Tokyo (2023).

5. **J. Matouskova:** *NIFFLER – Facility for Neutron Imaging at Training Reactor VR-1,* FOURTH FRENCH-CZECH BARRANDE NUCLEAR RESEARCH WORKSHOP, Mont Saint Michel (2023). Invited speaker.

6. L. Sklenka, **J. Matouskova:** *Decommissioning of Research Reactor in Czech Republic,* NUSIM 2023, Czech Republic (2023).

7. **J. Matouskova**, B. Schillinger, L. Sklenka: *Development of Neutron Imaging Facility at Very Low Power Reactor VR-1,* ITMNR-9: THE 9TH INTERNATIONAL TOPICAL MEETING ON NEUTRON RADIOGRAPHY, Buenos Aires (2022).

8. B. Schillinger, N. Geerits, T. Jünger, **J. Matouskova**, T. Neuwirth, F. Oppermann, S. Sebold, S. Sponar: *Flexible camera detector box design using 3D printers*, ITMNR-9: The 9th International Topical Meeting on Neutron Radiography, Buenos Aires (2022).

9. **J. Matouskova**: *New Neutron Imaging Facility at Very Low Power Research Reactor VR-1*, Šimáně 2022: International Student Conference On Nuclear Engineering, Prague (2022).

10. **J. Matouskova**: *New Neutron Imaging System at the CTU Training Reactor VR-1*, AUNIRA 2021 – Training Workshop on the Advanced Use of Neutron Imaging for Research and Applications, online (2021). Invited speaker.

11. **J. Matouskova**: *Development of Neutron Imaging Facility at Training Reactor VR-1*, Šimáně 2021: International Student Conference On Nuclear Engineering, Prague (2021).

12. **J. Matouskova**: *Monte Carlo method for determining the uncertainty of the multiplication coefficient due to the uncertainty of the isotopic composition of spent nuclear fuel (in Czech)* Šimáně 2020: International Student Conference On Nuclear Engineering, Prague (2020).

13. **J. Matouskova**, O. Huml: *Monte Carlo method for determining the uncertainty of the multiplication coefficient due to the uncertainty of the isotopic composition of spent nuclear fuel, (in Czech)* 20. Mikulášské Setkání Mladé Generace České Nukleární Společnosti, online (2020).

Annexes

A.1.New Neutron Imaging Facility NIFFLER at Very Low Power Reactor VR-1

The undersigned co-authors of the paper *"New Neutron Imaging facility NIFFLER at Very Low Power Reactor VR-1"* confirm the essential contribution of Jana Matouskova to this work. At the same time, we agree that this paper will be included into her dissertation thesis.

Doc. Ing. Lubomir Sklenka, Ph.D.

Dr. rer. nat. Burkhard Schillinger

Article

New Neutron Imaging Facility NIFFLER at Very Low Power Reactor VR-1

Jana Matouskova [1,]*[ID], Burkhard Schillinger [2] and Lubomir Sklenka [1]

[1] Department of Nuclear Reactors, Faculty of Nuclear Sciences and Physical Engineering, Czech Technical University in Prague, V Holesovickach 2, 180 00 Prague, Czech Republic

[2] Heinz Maier-Leibnitz Zentrum (FRM II), Technische Universität München, 85748 Garching, Germany

* Correspondence: jana.matouskova@fjfi.cvut.cz

Abstract: The paper describes the construction of the neutron imaging facility at the very low-power research reactor VR-1. The training reactor VR-1 is operated by the Czech Technical University in Prague, Czech Republic. It is mainly used for the education of students in the field of nuclear engineering as well as for the training of professionals. Neutron imaging is the new field of VR-1 reactor utilisation currently under development. Extremely low reactor power at the level of 100 W brought many challenges that were necessary to overcome to build and commission a sustainable neutron radiography facility. The paper describes the reactor's neutron flux verification and the basic concept and design of the neutron imaging instrumentation. The first experimental results were mainly dedicated to testing the detection system for different radial beam port configurations, different L/D ratios, and different exposure times. Preliminary results of neutron radiography and tomography measurements at VR-1 clearly showed the potential of using neutron imaging in low-power reactors such as the VR-1 reactor.

Keywords: neutron radiography; neutron tomography; neutron imaging; very low power research reactor; training reactor VR-1

1. Introduction

Neutron imaging is most often performed on high-power neutron sources. However, in the last few years, the situation has slowly changed with the development of CCD and CMOS imaging systems. The reasonable price of these systems, together with suitable scintillator screens, has brought new chances for neutron imaging and low-flux neutron sources such as low-power research reactors. However, the low flux is the main but not the only challenge connected with neutron imaging at low-power research reactors. The second serious challenge is related to a specific mode of operation of low-power research reactors. High power reactors are constantly in operation during a cycle of several weeks, and activities can be performed simultaneously. On the other hand, a low-power reactor is usually operated on a one-shift daily basis and usually cannot be used for several activities simultaneously. Therefore, a special reactor time must be dedicated only to neutron imaging. There are several examples in the world of high-quality neutron imaging facilities at medium and low-power research reactors. For example, a highly successful neutron imaging system is a digital neutron computed tomography system at a 250 kW test reactor at the Idaho National Laboratory INL, Idaho Falls, ID, USA [1]. In this context, this study has two main objectives, to demonstrate the feasibility of neutron imaging at low-power reactors, such as the VR-1 reactor, and to extend the range of applications of the VR-1 reactor. Furthermore, as the reactor is now mainly used for education and training, we would like to include neutron radiography as another type of utilization, mainly for educational and demonstration purposes. However, if it is sufficiently improved, it could be possible to use it in research, for example, in the cultural heritage field, industry, etc.

2. Neutron Imaging Basic Principle

Neutron imaging is a non-destructive technique used to investigate internal structures and material compositions of optically opaque objects [2]. Other than in X-ray-imaging, where contrast depends on the position in the periodic system and thus the number of electrons in an atom, neutron imaging is also sensitive to many light elements, especially hydrogen, while most metals are penetrated easily. The transmitted neutron beam is detected by—mostly—a camera detector using a cooled scientific camera, a neutron sensitive scintillation screen and a mirror to take the camera out of the direct beam.

This creates a grayscale image or a shadowgraph that contains information about the thickness and material composition of the sample [3]. One of the fundamental quantities used in neutron radiography is the transmission T, which is defined by:

$$T = \frac{I}{I_0} \tag{1}$$

where I is the intensity of the neutrons that passed through the sample and I_0 is the intensity of neutrons on the sample [4]. The beam intensity is attenuated after passing through the object, and it can be described by the fundamental law of radiation attenuation in a matter (Lambert's law):

$$I(x) = I_0 \cdot e^{-\int \Sigma_{tot} d_x} \tag{2}$$

where I_0 is the intensity of neutrons incident on the sample, x is the path through the object, and Σ_{tot} is the total macroscopic cross-section [4]. Neutrons can interact with the matter and thereby be removed from the incident beam either by absorption or by a change in direction as they interact with the material in the beam (scattering) [3]. Absorption completely removes neutrons from the beam. Scattered neutrons are, in first approximation, assumed to be also removed from the direct beam, but they may still hit the detector in a place different from the original flight path, thus creating a background of scattered neutrons that produce background noise and blurring. An essential parameter of the neutron imaging facility, which affects the spatial resolution of the resulting image, is the L/D ratio, where L is the length between the smallest diameter of the collimator or diaphragm and the sample, and D is the smallest diameter of the collimator.

Raw data images obtained from camera software during the measurement need to be processed and analysed in the case the open-source software ImageJ was used. [5] The data processing process includes removing white spots caused by gamma radiation falling directly on the camera chip and normalisation with open beam and dark field images. First, to correct for camera offset and thermal noise, the dark image without a beam must be subtracted from both the projection and open beam images. An open beam image contains the intensity distribution of the beam, and by dividing the result of the dark field corrected projection by the result of the corrected open beam image, the image is normalised to the beam intensity distribution.

3. Neutron Imaging on Low Power Research Reactors

According to the International Atomic Energy Agency Research Reactor Database (RRDB), there are 223 [6] research reactors in operation around the world. Of these 223 reactors, 67 [6] research reactors declare the use of neutron imaging and two [6] research reactors that declare the use of neutron imaging are temporarily shut down. The range of potential applications of neutron imaging is primarily limited by reactor power. It is possible to use almost any research reactor with a collimated neutron beam. The main criterium for research reactors for neutron imaging is the intensity of the available neutron beam, which is related to reactor power. Different references present different requirements for neutron intensity/reactor power. The IAEA research reactor utilization matrix from the IAEA Applications of research reactors mentioned no capability for neutron imaging for thermal reactor power of 100 kW and less, and for reactors with a power of less than

1 MW, neutron imaging can be carried out in a limited way, and it is especially suitable for demonstration purposes [7].

Most reactors operating neutron imaging facilities are medium and high power research reactors with reactor power from kilowatts to tens of megawatts, for example, reactor FRM II [8] or high flux reactor at ILL [9]. However, according to IAEA RRDB, there are research reactors with less than 1 kW that declare the use of neutron imaging. These are the Brazilian Argonauta reactor [10], the Japanese UTR KINKI reactor [11] and the Korean AGN-201K reactor [12] (see Table 1.).

Table 1. Low power research reactors using neutron radiography according to RRDB [5].

Country	Facility/Type	Power (Watts)
Brazil	Argonauta/argonaut	200
Japan	UTR KINKI/argonaut	1
Korea	AGN-201K/homogeneous	10

Another low-power reactor which recently tested the possibility of using neutron imaging, although this reactor does not declare the use of neutron imaging according to the RRDB, is reactor AKR-2 in Germany [13]. The thermal power of the AKR-2 reactor is two watts [13], and to find a suitable location for the device, a study of L/D and neutron fluxes was performed in [13].

4. Training Reactor VR-1

The training reactor VR-1 is operated by the Czech Technical University in Prague (CTU). The VR-1 reactor is state-of-the-art experimental instrumentation for the education of students in the field of nuclear engineering from the Czech Republic and abroad. Research and development activities at the reactor are mainly focused on current challenges in nuclear energy development, particularly on the safe operation of nuclear installations, theoretical and experimental reactor physics, nuclear safety and nuclear fuel cycle [14]. Apart from traditional nuclear technology research, the VR-1 reactor is also active in using neutron applications in research, which enables various multidisciplinary research studies that puts together nuclear technology and natural sciences, social sciences and humanities. A photo of the VR-1 training reactor is shown in Figure 1 [14].

Figure 1. Research reactor VR-1.

The reactor is a pool-type, light water reactor based on low-enriched uranium (19.7% of U235) [14]. The reactor uses IRT-4M-type concentric fuel elements. The nominal thermal power of the reactor is 100 W, which can be increased up to 500 W up to 70 h annually [14]. The reactor is operated at atmospheric pressure at a temperature of about 20 °C. The

neutron moderator is demineralised light water, which is also used as a neutron reflector, biological shielding and as a coolant. The experimental equipment of the VR-1 reactor consists of several vertical irradiation tubes, one radial horizontal beam port, one tangential horizontal beam port, shutter and measuring boxes for experiments on a radial beam port, instrumentation for detection of delayed neutrons, instrumentation for bubble boiling simulation, instrumentation for the study of temperature reactivity effects, instrumentation for fast reactivity changes, etc.

5. Development of the Neutron Imaging Facility

5.1. Neutron Radiography at the VR-1 Reactor

The first step to developing neutron imaging at the training reactor VR-1 was experiments that took place from 2012 to 2016. These experiments were focused on the possibility of using neutron imaging at the VR-1 reactor [15]. It was the development of neutron imaging using photographic film detectors with a converter. Those activities showed the possibility of performing neutron imaging at low-power reactors such as the reactor VR-1. The results of experiments indicated the capability for neutron imaging at the VR-1 reactor even though it is very limited and should be intended primarily for educational and demonstration purposes.

5.2. Design and Construction of Experimental Set up

The experiments from 2013 to 2016 were followed by work in 2020 focusing on neutron imaging using digital imaging methods. In the beginning, a simple neutron radiography detection system was designed in cooperation with the Heinz Maier-Leibnitz Zentrum of the Technical University of Munich [16]. A new neutron imaging facility at the reactor VR-1 called NIFFLER—"Neutron Imaging Facility for Learning and Research"—is based on a cooled CMOS camera combined with a scintillator screen. The CMOS camera is placed inside the special camera box with a lens, additional cooling for the camera and lead shielding. The lead shielding is placed in the camera box to shield the camera from direct gammas that are created at the sample and cause white spots on the chip of the camera. The camera model is the cooled QHY 178 m with 14-bit digitization, 3027×2048 pixel array and 2.4 um pixel size [17]. Binning 2×2 was used for all measurements. The scintillator screen is made of ^{6}LiF/ZnS:Cu. Both 100 μm and 200 μm thickness were tried, but although the 100 μm screen theoretically delivers better resolution, the better detection efficiency and light output of the 200 μm screen provided better images in our low flux. The screen is placed on the scintillator box, which also contains a mirror positioned at an angle of $45°$. The mirror ensures that the camera is not placed directly in the beam but perpendicular to it. The field of view of the initial detector system is 6×6 cm^2, for tomography, we used a larger mirror box with 10×10 cm^2. The main parameters of the NIFFLER facility are given in Table 2. The detection system without the camera is shown in Figure 2.

Table 2. Main parameters of the NIFFLER neutron imaging facility.

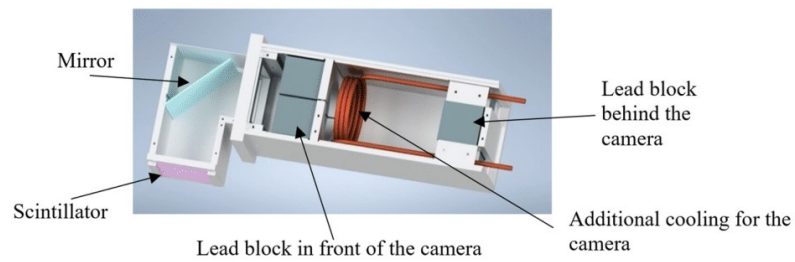|	
Camera type	CMOS (QHY 178 m cooled, 3072×2048 pixel)
Camera digitization	14-bit
Lens type	25 mm C mount
Scintillator screen	6LiF/ZnS:Cu
Field of view	6×6 cm^2 or 10×10 cm^2
Effective pixel size	39 μm or 65 μm (2×2 bin)

Figure 2. Model of the neutron imaging detection system without the camera.

A photo of a NIFFLER facility placed at the end of the radial beamline of the training reactor VR-1, with some additional shielding made of lead and borated PE, is shown in Figure 3.
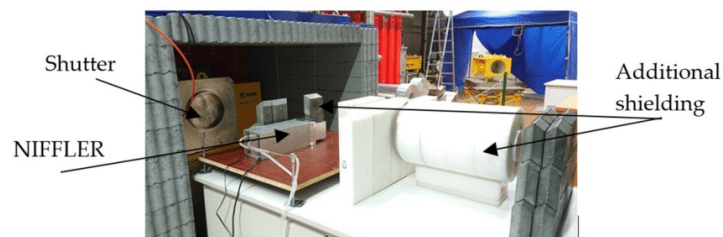

Figure 3. A photo of NIFFLER facility at the reactor VR-1.

The radial beamline of the reactor VR-1 had to be modified for the purposes of neutron imaging experiments. A hollow aluminum plug containing water with a central channel was first inserted into the radial beamline, limiting the beam from 25 cm to 9 cm (configuration 1). Then, a pinhole was placed at the end of this plug about 80 cm from the reactor core (configuration 2). The pinhole is made of 5 cm lead and 5 cm borated polyethylene, limiting the beam from 9 cm to 2 cm, and it serves to create a beam as parallel as possible and changes the collimation ratio L/D. Figure 4 shows a drawing of the radial beamline with modifications for neutron imaging (V2—cylindrical aluminum plug containing water with an inner diameter of 9 cm, pinhole with an inner diameter of 2 cm).
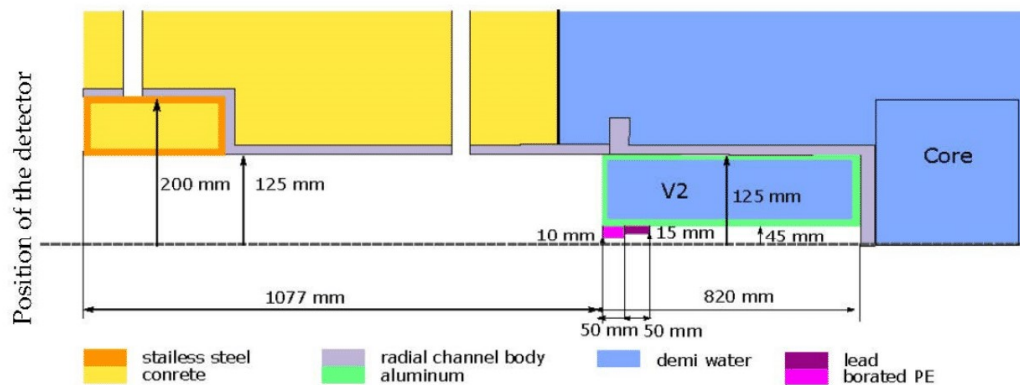
Figure 4. Drawing of the radial beamline with water plug (V2) and pinhole (Pb and PE).

5.3. Neutron Flux Verification

For verification of the thermal neutron flux in the radial beamline of the reactor VR-1, a simulation was performed. The calculation was achieved using the Monte Carlo calculation

code SERPENT in version 2.1.31 with a nuclear data library ENDF/B VII.0 [18]. The calculation of thermal neutron flux in the radial beamline was performed at the sample position (190 cm from the core) for two different configurations: Configuration 1—opened radial beamline with a cylindrical aluminum plug containing water (in Figure 4 defined as V2), reducing the beam to 90 mm; Configuration 2—opened radial beamline with a water plug and pinhole (in Figure 4, lead and borated PE).

For verification, the results of the calculation by the serpent calculation code were compared with the measurements with the help of neutron activation analysis (NAA). Neutron activation analysis was performed using gold foils and cadmium covers with Configuration 1 of radial beamline without the pinhole (L/D = 20). The deviation between the calculation in the Serpent calculation code and the neutron activation analysis measurements was around 10%. The results of thermal neutron flux in the radial beamline at the sample position (calculated with Serpent calculation code and measured with NAA) are shown in Table 3.

Table 3. Calculated and measured thermal neutron flux in different configurations of radial beamline.

Configuration	Verification	Thermal Flux ϕ_{th}(n/cm^{2}s)
Without the pinhole (L/D = 20)	SERPENT	2×10^5
With the pinhole (L/D = 50)		3.5×10^4
Without the pinhole (L/D = 20)	NAA	1.85×10^5

For both calculations and measurements, a thermal neutron spectrum was verified. With only 1 cm of water between the core and the beam tube nozzle, the neutron spectrum is mostly thermal, with a remaining share of epithermal and fast neutrons, to which the employed scintillation screen is not sensitive. Because of the thermal moderator in the reactor core, there are no cold neutrons in the beam beyond the tail of the Maxwell distribution.

6. Results

6.1. Neutron Radiography

The first set of neutron imaging measurements was performed to test the detection system with different radial beamline configurations, different L/D and different exposure times. The reactor power for all of these measurements was at the level of 100 Watts.

Configuration 1 was used as the first radial beamline configuration. The L/D ratio for this configuration of the radial beamline was 20. Exposure time was chosen step-by-step, and the first radiograph was created after an exposure time of 1 min. Furthermore, measurements were performed for further exposure times of 1–10 min. For the first measurements, a pocket watch was chosen as a sample (Figure 5). The pocket watch was chosen because it has an interesting internal structure and contains different materials. However, its disadvantage is that some parts are very small and therefore difficult to see. Figure 6 shows neutron radiographs of the pocket watch for different exposure times. The grayscales in the images are not identical, and they were stretched for optimum display. Although the 1 min and 3 min exposures look similar in this display, the 3 min exposure clearly has better statistics as can be seen on the sharpness of the central axle of the hands. The sample was placed in direct contact with the screen.
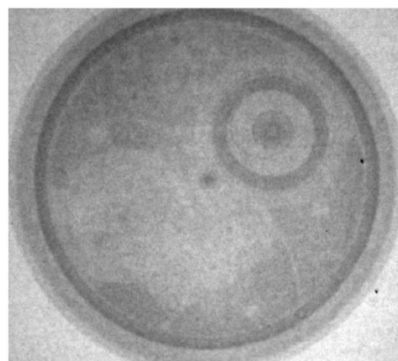
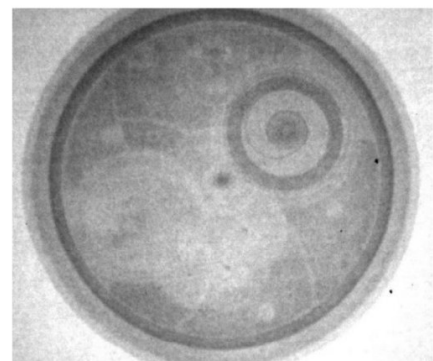1 cm

Figure 5. Photo of a pocket watch used as a sample.
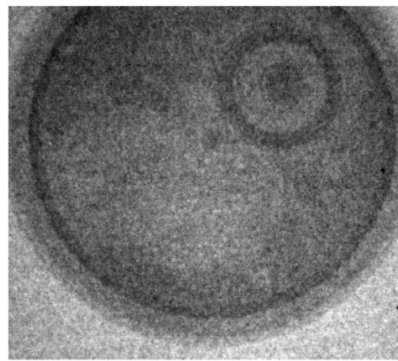
1 minute, average light output   1 cm
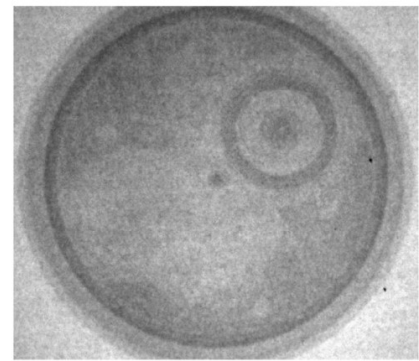
600 gray leves

3 minutes, average light output   1 cm

1 800 gray leves

5 minutes, average light output   1 cm

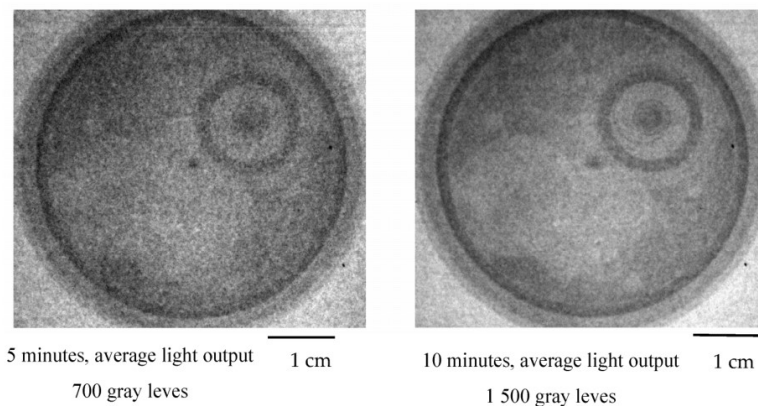3 000 gray leves

10 minutes, average light output   1 cm

6 000 gray levels

Figure 6. Neutron radiograph of a pocket watch at different exposure times (L/D = 20). Grayscales are stretched for optimal display.

The total fluence per sample for each measurement was also estimated using the SERPENT calculation code. Results of the total fluence are given in Table 4.

Table 4. The total fluence per sample for different exposure times (L/D = 20).

Exposure Time (Minutes)	Fluence (n/cm^2)
1	1.2×10^7
3	3.6×10^7
5	6×10^7
10	12×10^7

The radial beamline was later modified to Configuration 2. The L/D for this configuration of the radial beamline was 50. Figure 7 shows neutron radiographs of a pocket watch for different exposure times.

5 minutes, average light output   1 cm
700 gray leves

10 minutes, average light output   1 cm
1 500 gray leves

Figure 7. Neutron radiograph of a pocket watch at different exposure times (L/D = 50). Grayscales are stretched for optimal display, and are not the same as Figure 6.

The total fluence per sample for this configuration is given in Table 5.

Table 5. The total fluence per sample for different exposure times (L/D = 50).

Exposure Time (Minutes)	Fluence (n/cm^2)
5	1.05×10^7
10	2.1×10^7

Based on the rule that a higher collimation L/D gives a sharper image, the second set of measurements should bring sharper images. In this case, images suffer from insufficient neutron fluence. Although the L/D is very small for the first set of measurements, it gives a reasonably sharp image because the sample was very thin and placed directly on the scintillation screen.

6.2. Neutron Tomography

A simple and affordable setup was prepared to test the possibility of performing neutron tomography on a reactor with such low power. The setup is based on a simple rotation stage, translation/linear stage and a controller. This controller consisted of a Raspberry Pi and a GERTBOT motor controller [19], which has now been replaced by a Waveshare HAT controller [20] since the original board went out of production. The tomography sequence is composed of several steps, the first step is to take dark field images with a closed beam shutter, and the next step is to move the sample out of the field of

view and take open beam images. Both are necessary for image normalization, which is achieved by subtracting the dark field for camera offset and dark current, divided by the open beam to correct for beam profile. The last step of the tomography sequence is to move the sample back into the field of view and perform tomography measurements. This tomography sequence is controlled by a Python script on the Raspberry Pi [21]. A photo of the tomography setup is given in Figure 8.
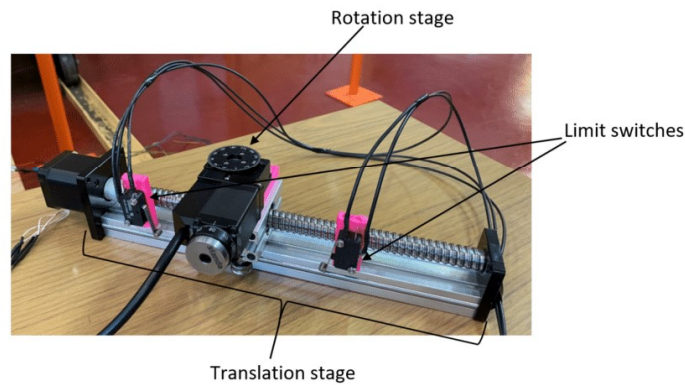

Figure 8. Neutron tomography setup.

Parameters for the neutron tomography test were chosen based on the neutron radiography results. The measurement was performed in the configuration 2 of the radial beamline with the L/D = 50. The power of the reactor was increased from 100 to 500 watts. Thus, the thermal neutron flux at the sample position was also five times higher than in the case of previous measurements, i.e., $1.75 \cdot \times 10^5$ n/cm^{2}s. The exposure time was chosen as 4 min per projection. The number of projections was primarily limited by the operating time of the reactor (the VR-1 reactor is operated in daily shifts and shut down overnight). Therefore, the longest time possible was used for the neutron tomography measurement, i.e., 12 h of reactor operation, which corresponded to 155 projections, five open beam images and five dark field images. An ancient Tibetan lock was chosen as a sample for the first test tomography, primarily for its interesting internal structure and the possible future use of neutron imaging on the VR-1 reactor to examine cultural heritage. The sample was placed about 5 cm from the scintillator screen. Figure 9 shows a photo of the ancient Tibetan lock. Due to the use of a larger sample, the field of view was also increased from the original 6×6 cm to 10×10 cm. For this purpose, only the scintillation/mirror box was replaced by a box with larger dimensions, and it was not necessary to change the entire detection system.

Figure 9. Ancient Tibetan lock used as a sample.

Two software programs were used to process the measured data: Octopus by Inside Matters [22] for reconstruction and VGStudio by Volume Graphics [23] for volume rendering. Figures 9 and 10 show the results of the first neutron computed tomography performed on a 500 W reactor. Due to bad neutron statistics, the tomographic reconstruction is noisy but sufficient to reconstruct the object.
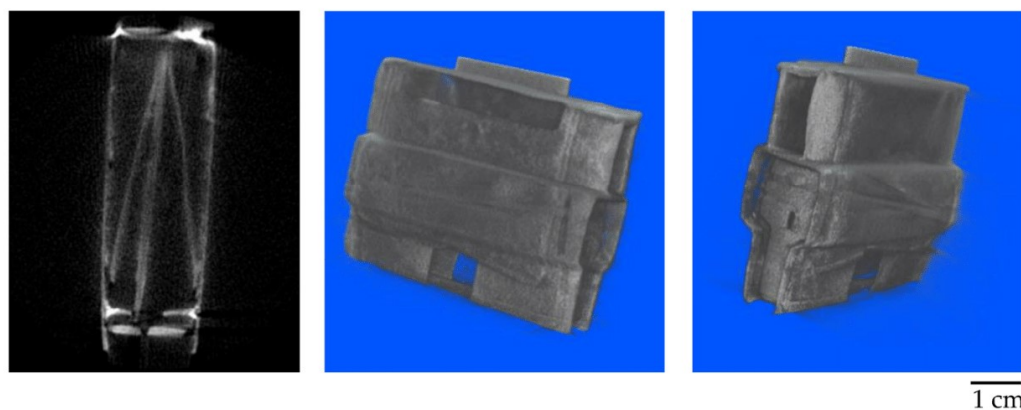

Figure 10. Results of first neutron computed tomography at 500 W, a tomographic slice and 3D views.

7. Discussion and Conclusions

This study focused on neutron imaging at the very low power reactor VR-1 using digital imaging techniques. A radial beamline of the reactor and a simple neutron imaging detection system designed in cooperation with Heinz Maier-Leibnitz Zentrum of the Technical University of Munich were used for these measurements. One task for the first neutron radiography measurements at the training reactor VR-1 was to determine the absolute thermal neutron flux at different positions in the radial beamline, especially at the sample position. Detailed flux verification was performed using the calculation code SERPENT. Finally, the calculation of neutron flux was compared to the results of the neutron activation analysis. The first set of neutron imaging measurements was performed to test the detection system for different radial beamline configurations, different L/D and different exposure times. Furthermore, the first neutron computed tomography was performed on a very low-power reactor at the level of 500 W.

Results of neutron imaging measurements at VR-1 showed the potential of performing neutron imaging at low-power reactors such as the VR-1 reactor. The two main objectives of this study were to demonstrate the feasibility of neutron imaging at low-power reactors, such as the VR-1 reactor, and to extend the range of application of the VR-1 reactor. The NIF-FLER neutron imaging facility at the VR-1 reactor will be further modified and improved to achieve the best possible results. Future work will primarily focus on modifications of the neutron spectrum and the modification of the beamline in order to optimise the L/D and the neutron flux at the sample position.

References

1. Craft, A.E.; Wachs, D.M.; Okuniewski, M.A.; Chichester, D.L.; Williams, W.J.; Papaioannou, G.C.; Smolinski, A.T. Neutron Radiography of Irradiated Nuclear Fuel at Idaho National Laboratory. *Phys. Procedia* **2015**, *69*, 483–490. [CrossRef]
2. Dawson, M.N. Applications of Neutron Radiography & Tomography. Ph.D. Thesis, School of Physics & Astronomy, the University of Leeds, Leeds, UK, May 2008.
3. Anderson, I.S.; McGreevy, R.L.; Bilheux, H.Z. *Neutron Imaging and Applications: A Reference for the Imaging Community*; Springer: New York, NY, USA, 2008.
4. Nares, C.H. *Neutron Radiography, Non-Destructive Testing Methods and New Applications*; Omar, M., Ed.; InTech: London, UK, 2012.
5. Available online: https://imagej.net/software/fiji/ (accessed on 5 December 2022).
6. IAEA. Research Reactor Database. 2021. Available online: https://nucleus.iaea.org/RRDB/RR/ReactorSearch.aspx (accessed on 29 November 2022).
7. IAEA. *The Applications of Research Reactors*; IAEA Nuclear Energy Series No. NP-T-5.3; IAEA: Vienna, Austria, 2014.
8. Schulz, M.; Schillinger, B. ANTARES: Cold neutron radiography and tomography facility. Journal of large-scale research facilities. *JLSRF* **2015**, *1*, A17. [CrossRef]
9. Tötzke, C.; Kardjilov, N.; Lenoir, N.; Manke, I.; Oswald, S.E.; Tengattini, A. What comes NeXT?—High-Speed Neutron Tomography at ILL. *Opt. Express* **2019**, *27*, 28640. [CrossRef] [PubMed]
10. Ferreira, F.J.O.; Silva, A.X.; Crispim, V.R. Electronic imaging system for neutron radiography at a low power research reactor. *Radiat. Meas.* **2010**, *45*, 806–809. [CrossRef]
11. Hohara, S.; Nohtomi, A. *Neutron Radiography*; Atomic Energy Research Institute, Kinki University: Osaka, Japan, 1895.
12. Choi, J.M.; Kim, M.H. Performance Evaluation of Neutron Radiography Facility at Kyung Hee University Reactor, AGN-201K. In Proceedings of the Transactions of the Korean Nuclear Society Spring Meeting, Jeju, Republic of Korea, 17–18 May 2012.
13. Lange, C.; Bernt, N. Neutron imaging at the low flux training and research reactor AKR-2. *Nucl. Instrum. Methods Phys. Res. Sect. A* **2019**, *941*, 162292. [CrossRef]
14. Frybortova, L.; Rataj, J.; Sklenka, L.; Frybort, J.; Fejt, F.; Novak, O. The Training Reactor VR-1-30 Years of Operation. In Proceedings of the 21st International Scientific Conference on Electric Power Engineering (EPE), Prague, Czech Republic, 19–21 October 2020.
15. Crha, J.; Sklenka, L.; Soltes, J. Neutron imaging on the VR-1 reactor. *J. Phys. Conf. Ser.* **2016**, *746*, 012034. [CrossRef]
16. Schillinger, B. An affordable Image Detector and a Low-Cost Evaluation System for Computed Tomography Using Neutrons, X-rays, or Visible Light. *Quantum Beam Sci.* **2019**, *3*, 21. [CrossRef]
17. Available online: https://www.qhyccd.com/ (accessed on 25 November 2022).
18. Leppänen, J. *Serpent—A Continuous-Energy Monte Carlo Reactor Physics Burnup Calculation Code*; VTT Technical Research Centre of Finland: Espoo, Finland, 2015.
19. Available online: https://www.gertbot.com/ (accessed on 29 November 2022).
20. Available online: https://www.waveshare.com/product/raspberry-pi/hats/motors-relays/stepper-motor-hat.htm (accessed on 5 December 2022).
21. Schillinger, B.; Craft, A. A Simple Controller for Neutron Computed Tomography that Interfaces Nearly Every Camera. Available online: https://www.isnr.de/index.php/tools (accessed on 25 November 2022).
22. Available online: https://octopusimaging.eu/ (accessed on 29 November 2022).
23. Available online: http://www.volumegraphics.com/ (accessed on 25 November 2022).

A.2. Development of a Neutron Imaging Facility at the Very Low Power Reactor VR-1

The undersigned co-authors of the paper "*Development of a Neutron Imaging Facility at the Very Low Power Reactor VR-1*" confirm the essential contribution of Jana Matouskova to this work. At the same time, we agree that this paper will be included into her dissertation thesis.

Doc. Ing. Lubomir Sklenka, Ph.D.

Dr. rer. nat. Burkhard Schillinger

Development of a Neutron Imaging Facility at the Very Low Power Reactor VR-1

J Matouskova[1], B Schillinger[2], L Sklenka[1]

[1] Department of Nuclear Reactors, Faculty of Nuclear Sciences and Physical Engineering, Czech Technical University in Prague, V Holesovickach 2, Prague, Czech Republic

[2] Heinz Maier-Leibnitz Zetrum (FRM II), Technische Universität München, 85748 Garching, Germany

Email: Jana.matouskova@fjfi.cvut.cz

Abstract. The paper describes the design and construction of a new neutron imaging facility at the very low-power research reactor VR-1. Neutron imaging has been under development at the VR-1 reactor as a new possible field of utilisation since 2020. The paper describes the main parts of the NIFFLER – "Neutron Imaging Facility for Learning and Research". The detector system was designed in collaboration with the Technical University of Munich. The radial beam line modifications include different collimation ratios L/D, additional moderator configurations and the basic concept and design of the instrumentation. The paper also includes calculations of thermal neutron flux at the detector position for different radial beamline configurations. The results achieved at the training reactor VR-1 showed the potential of using neutron imaging at other low and very-low-power research reactors worldwide.

1. Introduction

Neutron imaging was and still is mainly performed on high-power neutron sources, such as high-power research reactors or spallation sources. The official IAEA documents state that there is only some capability for neutron imaging, mainly for demonstration purposes, for research reactors with a power lower than 1 MW and no capability for research reactors with a power lower than 100 kW [1]. The situation started changing with the development of affordable detection systems with the use of astronomical CMOS cameras. These systems are ideal for testing of possibilities of neutron imaging on low-power neutron sources. An example of an affordable detection system was used to perform neutron imaging measurements at reactor VR-1 [2]. The neutron imaging system NIFFLER at reactor VR-1 was initially described in [3]. This publication is a follow-up that describes the beam modifications in more detail. The main focus was on the modifications of the radial beamline and the optimisation of beam parameters for neutron imaging. The results showed not only the capability for neutron imaging at very low power reactors but also the significance of beamline modifications, the collimation ratio L/D and modification of neutron spectrum, for example, with the use of additional moderators.

2. Experimental setup

2.1. Reactor VR-1

The reactor VR-1 is a very low-power training reactor operated by Czech Technical University in Prague (CTU). The nominal thermal power of the VR-1 reactor is 100 W, and the maximum thermal power is 500 W [4]. Thermal neutron flux in the core at the power of 100 W corresponds to $5.10^9 cm^{-2}s^{-1}$ [4]. It is a pool-type reactor that uses light water as a moderator, reflector and coolant. The pool-type arrangement assures simple access to the reactor core, easy insertion and extraction of various experimental samples and detectors, and simple and safe manipulation with fuel elements. The VR-1 reactor is equipped with several vertical irradiation tubes, one radial horizontal beamline and one tangential horizontal beamline [4].

2.2. Detection system

The standard neutron imaging detector consisting of a CMOS camera and scintillator screen was used at the radial beamline of the reactor VR-1. The CMOS camera is a cooled QHY 178m with 14-bit digitisation, a 3027 x 2048 pixel array and a 2.4 um pixel size [5]. The binning was set to 2x2, which corresponded to an effective pixel size of 39 μm or 65 μm, depending on the field of view. The scintillator is ^{6}LiF/ZnS:Cu type with 200 um thickness. The detection system is placed in a light-tight box with a 25 mm C mount lens, external cooling for the camera made out of a copper ring with an attached water-cooling pipe, and lead shielding in front of the camera. Part of the box is also a mirror placed at an angle of 45 degrees between the scintillator and the camera. The model of the detection system is shown in figure 1.
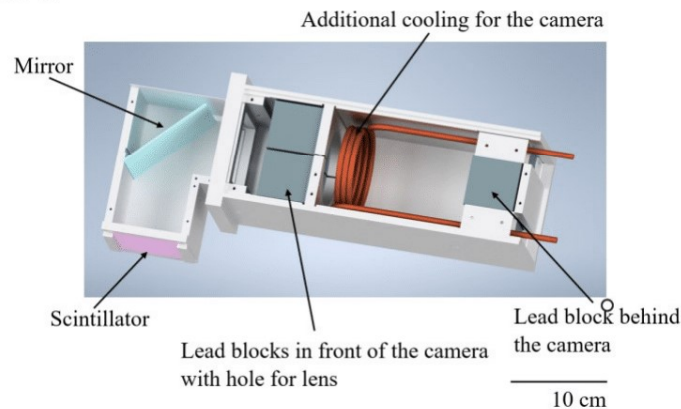

Figure 1: Design of the detector box without the camera

The system enables two different fields of view (FoV), 6x6 cm and 10x10 cm. Changing the field of view is possible because the detection system consists of two parts: the camera box and the scintillation/mirror box. Depending on the required field of view, the scintillation/mirror box can be replaced. A photo of the detection system is shown in figure 2.
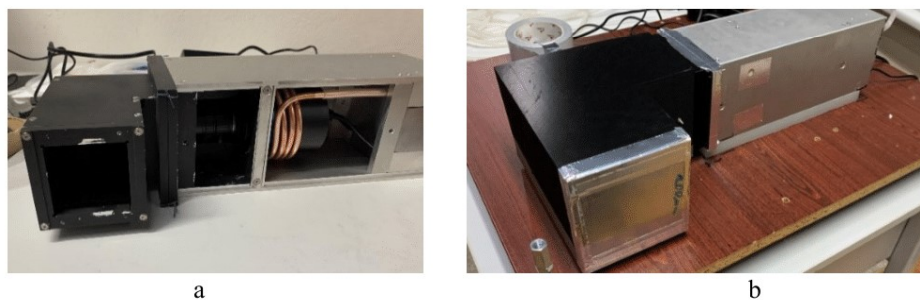

Figure 2: Detection system of NIFFLER facility (a – FoV 6x6 cm, b – FoV 10x10 cm)

The detector box has shielding only in the front of the camera around the lens to cut direct sight for gammas from the scintillation screen and sample. External shielding must be placed around the detector box to protect the camera chip from neutrons and gammas. Suitable materials are lead and borated PE.

2.3. Beamline modifications

The VR-1 reactor is equipped with two horizontal beamlines – radial and tangential. Due to the low power of the reactor and the easier access, the radial beamline was chosen for neutron imaging measurements. However, several changes had to be made. The radial beamline of the VR-1 reactor has the following parameters:

- Diameter = 25 cm
- Length = 200 cm
- Distance from the core = 1 cm

The first radial beamline modification was a modification of the L/D ratio, where L is the length between the smallest diameter of the collimator or diaphragm and the sample, and D is the smallest diameter of the collimator. [6]. With the original radial beamline parameters, L/D was around 10. In the first step, the L/D ratio was increased to 20, by reducing the diameter to 9 cm, by using a hollow aluminium plug containing water with a central channel. In the next step L/D ratio was further increased to 50, by reducing the diameter to 2 cm, by placing a pinhole made out of the lead and borated PE at the end of the aluminium plug about 80 cm from the reactor core. Figure 3 shows a model of the radial beamline at the reactor VR-1 with diameter modifications (a hollow aluminium plug containing water with a central channel and a pinhole).
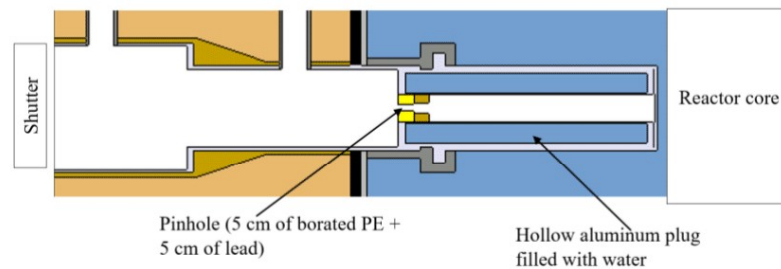

Figure 3: Model of the radial beamline with diameter modifications for neutron imaging.

Thermal neutron flux at the detector position for all configurations was calculated using the Monte Carlo calculation code Serpent in version 2.1.31 [7] with a nuclear data library ENDF/B VII.0 [8]. The results of thermal neutron flux calculations in the radial beamline at the detector position are shown in table 1. In addition, thermal neutron flux at the detector position was also measured using neutron activation analysis. Results of neutron activation analysis measurements and comparison with Monte Carlo calculation are described in [3].

Table 1. Calculated thermal neutron flux in different configurations of the radial beamline.

Configuration	Thermal Flux $\phi_{th}(n/cm^2 s)$
Original beamline (L/D = 10)	$6 \cdot 10^5$
First modification (L/D = 20)	$2 \cdot 10^5$
Second modification (L/D = 50)	$3.5 \cdot 10^4$

After the calculation, it was found that the energy spectrum of the neutron beam is very wide, a combination of all thermal, epithermal and fast neutrons. This is primarily because the radial beamline is located next to the reactor core. With only 1 cm of water, there is not enough moderator between the beginning of the radial beam tube and the core. For this purpose, another modification of the radial beamline was carried out, namely placing an additional moderator inside the radial beam tube next to

the reactor core. Several materials of different thicknesses were considered for this purpose: water, heavy water, PE and paraffin, with thicknesses of 1 cm, 2 cm, 3 cm, 4 cm, 5 cm and 6 cm. Another calculation was performed using the Monte Carlo calculation code Serpent in version 2.1.31 [7] with a nuclear data library ENDF/B VII.0 [8] for the effect of the additional moderator on the thermal neutron flux at the detector position. The results thermal neutron flux of selected configurations of radial beamline at the detector position is shown in table 2.

Table 2. Calculated thermal neutron flux of radial beamline with additional moderators.

Moderator material	Moderator thickness (cm)	Thermal Flux $\phi_{th}(n/cm^2 s)$
No moderator	-	$3.5 \cdot 10^4$
Paraffin	2	$3.7 \cdot 10^4$
PE	2	$4.2 \cdot 10^4$
Water	3	$4 \cdot 10^4$
Heavy water	3	$3.5 \cdot 10^4$
Paraffin	4	$5 \cdot 10^4$
PE	4	$4.8 \cdot 10^4$
Paraffin	5	$3.8 \cdot 10^4$

Paraffin, with a thickness of 4 cm, yielded the highest increase in thermal flux. The thermal neutron flux for the final configuration of the radial beamline, which is a beamline with a hollow aluminium plug containing water with a central channel with a pinhole and 4 cm of additional paraffin moderator, is $5.10^4 \ neutrons/cm^2 s^1$. Figure 4 shows a model of the radial beamline at the reactor VR-1 with diameter modifications and additional moderator modifications.
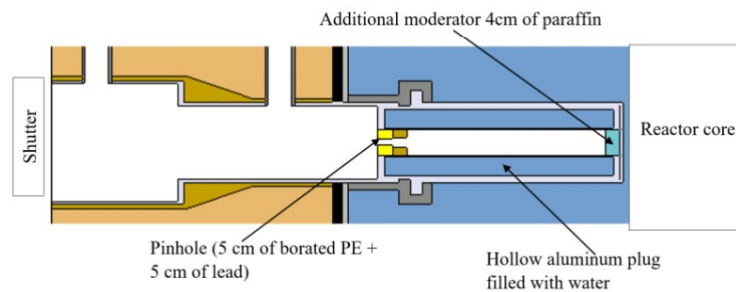

Figure 4: Model of the radial beamline with final modifications for neutron imaging

3. Results

Neutron imaging measurements were performed to compare the influence of the modifications of the radial beamline at the reactor VR-1. The reactor power was 100 W for all the measurements.

The first set of results shows the comparison of measurements with two different configurations of the radial beamline. The first measurement was performed after modification of the radial with L/D = 20. The second measurement was performed after adding a pinhole (figure 3) with L/D = 50. Samples were placed directly on the scintillator screen. Figure 5 shows the comparison of neutron radiographs of a ball-bearing with L/D = 20, respectively L/D = 50. Neutron fluence for each measurement was determined from values of neutron fluxes calculated with Monte Carlo code.
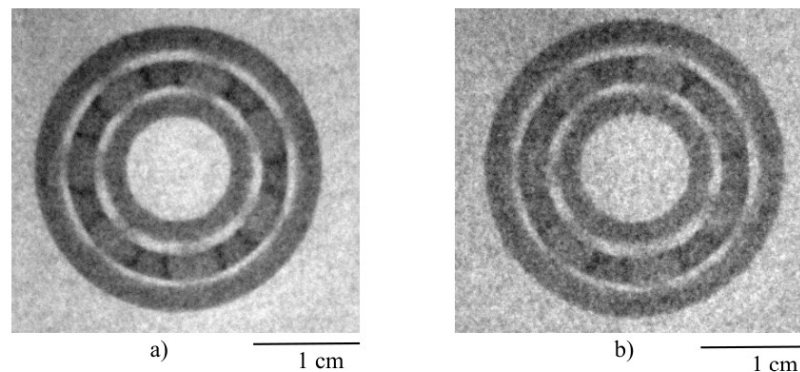
Figure 5: Neutron radiographs of a ball-bearing (a) L/D = 20, exp. time 5 minutes, total fluence $6 \cdot 10^7\ n/cm^2$, average light output 13 500 grey levels b) L/D = 50, exp. time 10 minutes, total fluence $2.1 \cdot 10^7\ n/cm^2$, average light output 3 300 grey levels).

In figure 5, based on the rule that a higher collimation ratio L/D gives a sharper image, image b) should be sharper than image a). But due to lower neutron flux, image b) is noisier, and the sharpness of both images is the same since the relatively thin sample was placed directly on the scintillator screen.

The next measurements focused on additional moderators' influence in the radial beamline. Based on the results of the calculations, several neutron radiography measurements were performed. First, an additional moderator in the form of 4 cm of paraffin was placed in the radial beamline. Figure 6 shows the comparison of neutron radiographs without and with the additional moderator. In both cases, L/D = 50. A 2.5" hard drive was used as a sample. The exposure time for both images is 10 minutes.
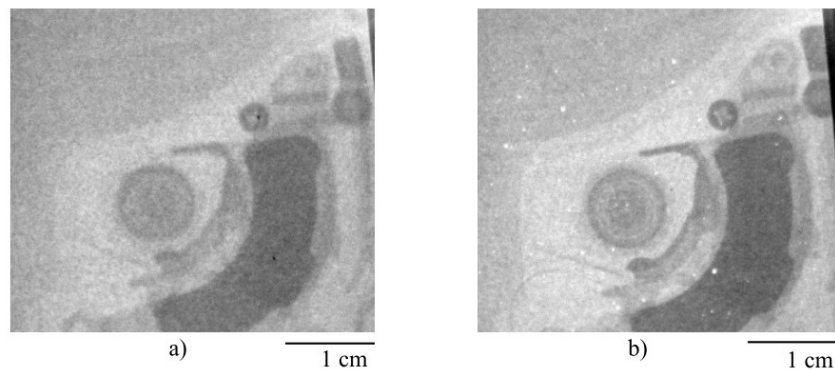

Figure 6: Neutron radiographs of a hard drive (a) no additional moderator, total fluence $2.1 \cdot 10^7\ n/cm^2$, average light output 19,000 grey levels, b) 4 cm of paraffin, total fluence $3 \cdot 10^7\ n/cm^2$, average light output 30,000 grey levels)

For the effect of additional moderators on the resulting neutron image, the effect on light output and the effect on the resolution was determined. For example, figure 6 shows the influence of an additional moderator in the form of 4 cm of paraffin improves both the light output and the resolution.

Other moderators were also tested, several combinations for which calculations were performed, and neutron imaging measurements confirmed the calculation results. The comparison of 2 cm, 4 cm and 6 cm paraffin is shown in figure 7. The exposure time for all three images is 10 minutes.
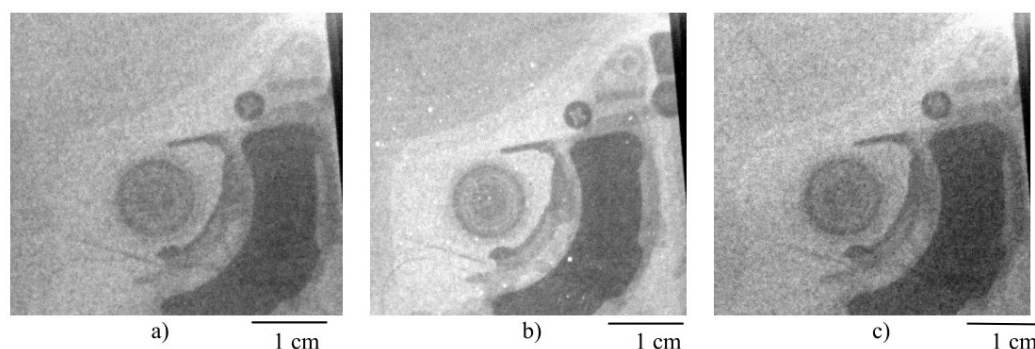
Figure 7: Neutron radiographs of a hard drive (a) 2 cm of paraffin, total fluence $2.2 \cdot 10^7 \, n/cm^2$, average light output 20,000 grey levels, b) 4 cm of paraffin, total fluence $3 \cdot 10^7 \, n/cm^2$, average light output 30,000 grey levels, c) 6 cm of paraffin, total fluence $2.3 \cdot 10^7 \, n/cm^2$, average light output 21,000 grey levels)

The best option was an additional moderator in the form of 4 cm of paraffin. For most of the moderators used, the light output was higher than in the case of a radial beamline without a moderator. The results of neutron imaging measurements confirmed that the neutron spectrum in the radial beamline was not sufficiently thermalised, and the adjustment of the beam with the help of an additional moderator led to an improvement in the results.

4. Summary and Conclusions

This paper focuses on designing and constructing a new neutron imaging facility at the very low-power research reactor VR-1. The main parts of this paper focus on detection system and beamline modifications. A radial beamline of the reactor VR-1 was used to perform the neutron imaging measurements. To improve the quality of the neutron beam, several modifications were made to the radial beamline of the reactor VR-1. First, a pinhole was placed in the radial beamline to improve the collimation ratio L/D. Later, an additional moderator was inserted into the radial beamline to adjust the neutron spectrum. A calculation using the Monte Carlo calculation code Serpent and neutron radiography measurements were performed to determine the effect of the modification of the radial beamline on the thermal neutron flux at the detector position. The results show that in the case of low-power reactors, the main parameters for neutron imaging, such as neutron flux at the detector position or L/D, have to be optimised to find the ideal balance between relatively high L/D and sufficient neutron flux. Additional moderators placed directly in the beamline can help to adjust the neutron spectrum. The results from the reactor VR-1 showed the potential for other low-power university reactors to use neutron imaging for educational purposes.

5. References

[1]   IAEA 2014 The applications of research reactors. *IAEA Nuclear Energy Series No.* **NP-T-5.3**.

[2]   Schillinger B 2019 An affordable Image Detector and a Low-Cost Evaluation System for Computed Tomography Using Neutrons, X-rays, or Visible Light, *Quantum Beam Sci.* **3** *21*.

[3]   Matouskova J, Schillinger B and Sklenka L 2023 New Neutron Imaging Facility NIFFLER at Very Low Power Reactor VR-1, *Journal of Imaging 9 15*.

[4]   Frýbortová L et al. 2020 The Training Reactor VR-1 - 30 Years of Operation, *21st International Scientific Conference on Electric Power Engineering, Prague.*

[5]   https://www.qhyccd.com/ (accessed on November 2022)

[6]   Anderson I S, McGreevy R L and Bilheux H Z 2008 Neutron imaging and applications: a reference for the imaging community, *Springer.*

[7]   Leppänen J 2015 Serpent – a Continuous-energy Monte Carlo Reactor Physics Burnup Calculation Code, *User's manual.*

[8]   Chadwick M B et al. 2006 ENDF/B-VII.0: Next Generation Evaluated Nuclear Data Library for Nuclear Science and Technology, *Nuclear Data Sheets, vol.* **107**.

A.3.Investigation of Buddhist and Bon Votive Statues at the Very Low Power Reactor VR-1

The undersigned co-authors of the paper *"Investigation of Buddhist and Bon Votive Statues at the Very Low Power Reactor VR-1"* confirm the essential contribution of Jana Matouskova to this work. At the same time, we agree that this paper will be included into her dissertation thesis.

Doc. Ing. Lubomir Sklenka, Ph.D.

Dr. rer. nat. Burkhard Schillinger

Full Length Article

Investigation of Buddhist and Bon votive statues at the Very low power reactor VR-1

Jana Matoušková [a],[*], Lubomir Sklenka [a], Burkhard Schillinger [b]

[a] *Czech Technical University in Prague, Department of Nuclear Reactors, V Holesovickach 2, Prague, 18000, Czech Republic*
[b] *Heinz Maier-Leibnitz Zentrum (FRM II) Technische Universität München, Lichtenbergstrasse 1, Garching, 85748, Germany*

ARTICLE INFO

ABSTRACT

The nuclear analytical techniques are excellent tools for the investigation in various research disciplines, i.e. cultural heritage preservation, archaeology or anthropology. Most of these radioanalytical techniques require sufficient sources of radiation. So far, neutron imaging has mostly been used at high-power neutron sources, i.e. high-power research reactors. On the other hand, small nuclear research reactors can provide more options for investigations in multidisciplinary research. Since the development of the NIFFLER neutron imaging facility in 2020, neutron imaging has been one of the nuclear analytical methods used at the very low-power research reactor VR-1 of the Czech Technical University in Prague. This paper deals with the investigation of the internal structures of Buddhist and Bon votive statues from Central Asia at the Training reactor VR-1. The experimental investigation was conducted to explore the possibilities of using neutron imaging for cultural heritage research at very low-power research reactors such as the VR-1 reactor. The results of these unique experiments clearly showed the potential of the VR-1 reactor or possibly other very low-power research reactors in neutron imaging for multidisciplinary research, which can provide important data for anthropologists, archaeologists or experts in cultural heritage preservation.

1. Introduction

Neutron imaging is a radioanalytical technique that has a wide variety of applications ranging from material science and engineering through energy research [1], cultural heritage preservation, archaeology [2] and palaeontology [3], to biomedical and biological engineering. The range of potential applications of neutron imaging is primarily limited by the intensity of the neutron beam, which is proportional to the power of the neutron source. For this reason, neutron imaging is most often performed on high-power neutron sources, such as high-power research reactors or spallation sources. However, modern detection systems have brought new possibilities for neutron imaging at low-power neutron sources, such as very low-power research reactors.

As neutron imaging is a non-destructive technique, it makes it an extremely important tool for the study of cultural heritage objects, i.e. ancient or unique historical objects like statues, mediaeval weapons or fossils. This paper deals with the possibility of using neutron imaging in cultural heritage preservation, in this case specifically to investigate the internal structures of votive statues from Central Asia at the Training reactor VR-1. The analysis includes three Buddhist and Bon statues from a private collection. The goal of this study was to analyse and demonstrate the possible use of neutron imaging for cultural heritage research at very low-power research reactors.

1.1. Neutron imaging

Neutron imaging is a powerful technique used to investigate internal structures and material compositions of optically opaque objects [4]. Other imaging methods are, for example, X-ray imaging, gamma imaging, proton imaging, etc. These methods use various types of radiation, from particles such as electrons or protons to electromagnetic waves such as X-rays and gamma rays. The imaging principle is similar for all methods, the radiation intensity is attenuated by passing through the investigated object by an amount that depends on the thickness of the object and its material composition [4]. However, the difference is in the way of interaction of the incident particle with the matter. X-rays interact only by electromagnetic interaction with the electron shell (photo effect, Compton scattering, production of electron-positron pairs). Therefore, the probability of X-ray interaction with the material depends on the number of protons of the elements (and thus on their atomic number) of which the object is composed, but the probability of neutron interaction can vary not only for elements with similar atomic numbers but also for isotopes of one element [4]. In contrast, neutrons interact and thereby are removed from the incident beam mainly by strong interaction with atomic nuclei (absorption, single-particle

scattering, or coherent scattering on lattices) or react to the magnetic moment [5]. The ideal attenuation process for neutron imaging is absorption because it completely removes neutrons from the beam. The scattering also causes an attenuation process, but scattered neutrons do not have to be removed from the beam. They may still hit the detector in a place different from the original path, thus creating a background of scattered neutrons that produce background noise and blurring. [4]. The beam attenuation is described by Lambert's law, the basic law of radiation attenuation in a matter (1):

$$I(x) = I_0 \cdot e^{-\int \Sigma_{\text{tot}} \, dx} \tag{1}$$

Neutron imaging usually uses thermal or cold neutrons. The beam intensity is attenuated after passing through the imaged object. This creates a grayscale image or a shadowgraph that contains all the information about the thickness and material composition of the sample. [4]. Simple neutron radiography produces a two-dimensional (2D) attenuation map of neutron radiation that has penetrated a three-dimensional (3D) object. Neutron computed tomography uses a large number of 2D neutron radiographs recorded under different angles to reconstruct a 3D image [6].

1.2. Use of neutron imaging at very low power research reactors

Although neutron imaging is mainly performed at high-power neutron sources, with the most well-known being the reactor FRM-II at MLZ [7], the high flux reactor at ILL [8], and the neutron spallation source SINQ at PSI [9], there are a few very low-power neutron sources that use this method. With the focus on research reactors with reactor power under 100 kW, there are six reactors that either tested the possibility of using neutron imaging or declared the use of neutron imaging according to the International Atomic Energy Agency Research Reactor Database [10] - the Brazilian Argonauta reactor (200 W) [11], the Japanese UTR KINKI reactor (1 W), the Korean AGN-201K reactor (10 W) [12], the Canadian SLOWPOKE-2 at Royal Military College (20 kW) [13], the reactor AKR-2 in Germany (2 W) [14], the Iranian MNSR reactor (30 kW) [15] and the Czech Training reactor VR-1 (100 W) [16]. All of these reactors use their neutron imaging facilities mainly for demonstration experiments for students. Some of these reactors tested the possibility of using neutron imaging in various research disciplines. Unfortunately, none of these very low-power research reactors, except now the VR-1 reactor, focused on research in cultural heritage preservation.

2. Neutron imaging at the VR-1 reactor

The Czech Technical University in Prague, as a key national nuclear academic institution, understands that "nuclear" is not only nuclear power technology. For example, neutron applications and nuclear analytical techniques such as neutron imaging, neutron activation analysis or x-ray fluorescence spectrometry can bring additional benefits to society. That is why CTU's nuclear physicists or chemists provide multidisciplinary research and education in collaboration with various natural sciences, life sciences, social sciences and humanities experts, such as environmental monitoring, biology, medicine, chemistry, forensics, archaeology, anthropology, or cultural heritage preservation.

The Training reactor VR-1, operated by the Czech Technical University in Prague, is a near-zero power nuclear reactor. The nominal thermal power of the VR-1 reactor is 100 W, and the maximal thermal power is 500 W [17]. The maximal reactor power is limited to 80 h per year. The VR-1 reactor is equipped with several experimental facilities, i.e. vertical irradiation tubes, one radial horizontal beamline and one tangential horizontal beamline [17]. The reactor is a state-of-the-art facility used mainly for the education of students and the training of professionals. The research and development activities focus on experimental neutron physics, nuclear safety and neutron applications, for example, neutron activation analysis [18].

2.1. The NIFFLER neutron imaging facility

The NIFFLER - "Neutron Imaging Facility for Learning and Research" was developed, built, and commissioned at the VR-1 reactor in the last two years [16]. The detection system of the NIFFLER facility, based on [19], consists of a CMOS camera in combination with a ^{6}LiF/ZnS:Cu scintillator screen. The camera is a cooled QHY178 m type with a 25 mm C-mount lens. The field of view of the detection system is 10×10 cm^2. A detailed description of the detection system is provided in [16]. The NIFFLER facility uses a standard pinhole-detector configuration. The 10 cm long conical pinhole consists of lead with an inner diameter of 3 cm and borated polyethylene with an inner diameter of 2 cm. A detailed description of the radial beam line for the needs of neutron imaging is provided in [20]. The collimation ratio L/D = 50 was achieved by installing an appropriate diaphragm in the beamline. This collimation ratio is relatively low, but in the case of very low-power reactors, it is necessary to find the optimum between a sufficient L/D and a sufficient neutron flux at the sample position, in contrast to high-power reactors, where the L/D should be as high as possible (at least 100). The thermal neutron flux at the sample position at reactor power 100 W is $5 \cdot 10^4$ neutrons/cm^2 s. The resolution of the NIFFLER neutron imaging facility was determined from the modulation transfer function with the measurement of a gadolinium edge as 350 μm [21].

3. Neutron imaging in cultural heritage research

Neutron imaging is widely used in research in cultural heritage preservation worldwide [22,23]. The use of neutron imaging for cultural heritage is one of the main applications of this method. Many museums and scientific centres use X-ray imaging to study cultural heritage objects. However, X-rays have a lower penetration at high atomic numbers, while neutrons do not penetrate thick layers of organic materials. For this reason, neutron imaging has been established as an alternative in the non-destructive investigation of cultural heritage objects [3]. Examples of the applications of neutron imaging in cultural heritage preservation are neutron imaging of archaeological bronzes [24], Roman bronze sculptures and other metallic samples and metallurgic examinations on mediaeval swords [2], neutron computed tomography with thermal and cold neutrons of fossils embedded in rock [3], exploring hominin and non-hominin primate dental fossil remains with neutron microtomography [25], etc.

The first neutron imaging experiments at the VR-1 reactor aimed to explore the research capabilities of the NIFFLER neutron imaging facility in the field of cultural heritage preservation. The first research activities at the VR-1 reactor were focused on studies of internal parts of Buddhist or Bon votive statues from Central Asia. Three Central Asia votive statues were studied at the VR-1 reactor: a statue of Tsongkhapa from Ladakh in Northern India, a statue of Sherab Chamma from Tibet and a statue of Buddha Shakyamuni from China. The conversion process from empty painted or unpainted metallic cast to votive statues as objects of worship is the same for all statues, even from different religions and cultures (Tibetan Bon and Buddhism, Chinese Buddhism). All three statues were made in local workshops as empty metallic casts and offered to worshippers in local shops. Believers brought the empty statue to a monastery where monks ritually filled it with the wooden stick (which represents Mt. Meru, the axis mundi) and some other organic votive objects such as protective votive pills, fragments of cloth, etc., sealed it and empowered it by particular rituals. Only after finishing this process can statues be ritual votive objects. All of the statues were borrowed from a private collection for investigation of internal structures using neutron imaging measurements.

Fig. 1. Photo and neutron radiography of the Buddhist statue of Tsongkhapa from Ladakh in Northern India.

Fig. 2. Photo and neutron radiography of the Bon statue of Sherab Chamma from Tibet.

3.1. Neutron radiography

For neutron radiography, the Buddhist statue of Tsongkhapa from Ladakh in Northern India and the Bon statue of Sherab Chamma from Tibet were selected.

The Tsongkhapa (*tsong kha pa*, also Je Tsongkhapa or Je Rinpoche) was one of the most important monks and spiritual leaders (1357–1419) in Tibetan history. As the principal reformer of Tibetan Buddhism at the beginning of the 15th century, he founded the Gelug tradition (Gelug school) of Tibetan Buddhism. The Yellow hat reformed Gelug tradition has dominated Tibetan Buddhism last five hundred years [26–28]. The Tsongkhapa statue can be found at all monasteries or almost any shrines which belong to the Gelug tradition. The investigated statue of Tsongkhapa (14.5 cm in height) was made at the end of the last millennium by a local Buddhist artist in Ladakh in the Northern Himalayas. The statue was filled and empowered in the Buddhist monastery in Diskit in Nubra Valley in Ladakh around 2000.

The reactor power for neutron radiography of Tsongkhapa statues was set to 100 W, which corresponds to thermal neutron flux at the sample position to $5 \cdot 10^4$ neutrons/cm^2 s. The collimation ratio was L/D = 50, and the exposure time was set to 10 min. The sample was placed close to the scintillator screen. Fig. 1 shows the photo and the neutron radiography of the Tsongkhapa statue.

The neutron radiography of Tsongkhapa clearly shows the metal cast, which is mostly likely made of bronze and has a thickness of a few millimetres. This material is relatively transparent to neutrons and can be easily measured. Some parts, such as hands and decorative pieces, are made of solid material. Due to the same contrast, it looks like these parts are made from the same material as the cast. Inside the statue is the thick, plain wooden stick representing axis mundi, which originates at the bottom of the lotus throne and ends in the upper part of the shoulders. Other organic votive objects can be seen in the bottom part of the Tsongkhapa statue. Due to the organic nature of these materials, they are not too transparent for neutrons, and for their accurate determination, a higher resolution or neutron tomography measurement would be needed. However, it is evident that the filling inside the lotus throne is quite homogeneous and may be one kind of material.

The second statue chosen for neutron radiography was the Bon statue of Sherab Chamma from Tibet. Sherab Chamma (*shes rabs byams ma*) is one of the leading female protectors of Tibetans in the ancient Bon religion [29,30]. Sherab Chamma is Bon parallel of much well-known Buddhist female protector Dolma (*sgrol ma*), particularly to one

Dolma manifestation - Dolma jang (also known as Green Tara). The Chamma statue can be found at all almost Bon monasteries or Bon shrines. The investigated statue of Chamma (13.7 cm in height) was made at the beginning of the new millennium in Northern Himalaya (India or Nepal) and filled and empowered in the Bon monastery in Dolanji in Northern India in 2006.

The same parameters, as for the Tsongkhapa statue, were also used for neutron radiography of the Chamma statue, the reactor power 100 W, which corresponds to thermal neutron flux at the sample position to $5 \cdot 10^4$ neutrons/cm^2 s, the collimation ratio was L/D = 50, and the exposure time 10 min. The sample was placed close to the scintillator screen. Fig. 2 shows the neutron radiography of the Chamma statue.

The neutron radiography of Sherab Chamma clearly shows the metal cast, which is mostly likely made of bronze and has a thickness of a few millimetres. Same as for the Tsongkhapa statue, the material is relatively transparent to neutrons and can be easily measured. Some parts, such as hands and decorative pieces, are made of solid material. Again, due to the same contrast, it looks like these parts are made from the same material as the cast. Inside the statue is the thick, plain wooden stick representing axis mundi, which originates at the bottom of the lotus throne and ends in the lower part of the deity's head. Contrary to most wooden axes mundi in Tibetan Buddhist or Bon status, which are simple sticks (as in the Tsonkhapa case), the Chamma's axis mundi is a contoured stupa (in Tibetan chorten). This extraordinary shape of the axis mundi can be one of the topics of research for Tibetologists who deal with Buddhist and Bon iconography. Similarly to the Tsongkhapa statue, Sherab Chamma is filled with other organic votive objects, which can be seen in the bottom part of the statue. Due to the organic nature of these materials, they are not too transparent for neutrons, and for their accurate determination, a higher resolution or neutron tomography measurement would be needed. Unlike the Tsongkhapa statue, the filling inside the lotus throne is not homogeneous and may be made of several kinds of materials.

Raw data from both neutron radiography measurements obtained from the camera software were processed and analysed using the open-source software ImageJ [31]. The data processing included image filtering, i.e. removing white spots caused by gamma radiation falling directly on the camera chip, etc. and also image normalization. Normalization is a data correction process for beam inhomogeneity, thermal noise, and offset. For image normalization, two extra images must be taken. An open beam image (ob), an image without a sample, is taken because the neutron beam and the detection system are not homogeneous. A dark image (di), an image with a closed beam shutter, contains

Fig. 3. Photos of Buddha Shakyamuni statue.

thermal noise and offset of the camera. Then, the normalization (T) is:

$$T = \frac{\text{data-di}}{\text{ob-di}} \qquad (2)$$

3.2. Neutron tomography

For neutron tomography, a small statue of Buddha Shakyamuni from China was selected. The Buddha Shakyamuni in a mediation position [27,28] (7 cm height) was found in the local market in Chengdu, Sichuan Province, China, at the end of the last millennium; no other information about the origin is available. Fig. 3 shows photos of the Buddha Shakyamuni statue, and Fig. 4 shows neutron radiography and a tomographic slice of the Buddha Shakyamuni statue.

The parameters for neutron computed tomography were based on the experience from the measurements of the first neutron tomography at very low-power research reactors described in [16]. While neutron radiography measurements were performed at the reactor power of 100 W, for neutron tomography, the reactor power was increased to 500 W to improve the signal-to-noise ratio, which corresponds to $2 \cdot 10^5$ neutrons/cm^2 s. The collimation ratio L/D = 50, and due to the increase in reactor power, the exposure time was reduced to 3 min per projection. For neutron tomography, a data set of 300 projections at half rotation, five open beam images and five dark current images were taken. The sample was placed around 5 cm from the scintillator screen.

Fig. 5 shows 3D reconstruction and several cuts through the 3D reconstruction of the Buddha Shakyamuni statue. Raw data images obtained from camera software were processed and analysed with the open-source software ImageJ [31]. To process the measured data, three softwares were used: MuhRec by PSI [32] for reconstruction, KipTool by PSI [33] for data filtering and VGStudio MAX by Volume

Graphics [34] for volume rendering. Due to low neutron flux at the sample position (insufficient neutron statistics), the tomographic reconstruction is noisy, but the data are sufficient to reconstruct the object and to see internal structures. Neutron tomography measurements are usually performed at research reactors with significantly higher reactor power. Currently, the VR-1 reactor is the only research reactor with reactor power under 1 kW to perform neutron computed tomography experiments worldwide.

The neutron tomography of Buddha Shakyamuni shows the metal cast, which is mostly likely made of bronze and has a thickness of a few millimetres. It is evident from the tomography reconstruction that the thickness of the cast is not the same everywhere; for example, the cast is thinner in the leg area and thicker in the shoulders area. In this case, not only the hands and decorative pieces but also the head is made of solid material. Again, due to the same contrast, it looks like these parts are made from the same material as the cast. Inside the statue is a plain wooden stick with variable thickness representing the axis mundi. Due to the different contrast of the cast material and the material of the stick, it is obvious that these are two different materials. The position and slope of the axis mundi are surprisingly different from what was expected - a slope instead of vertical and location in the top deeply inserted to the head. This interesting shape of the axis mundi can also be potentially a topic of research for Tibetologists who deal with Buddhist iconography. There is no obvious presence of other filling materials inside the examined Buddha statue. Even though the internal structure of the Sherab Chamma is slightly more interesting, the Buddha statue was selected for neutron tomography mainly due to its smaller size to fit into the field of view of the detection system (10 × 10 cm^2).

4. Conclusions

The non-destructive investigation of the internal structures of Buddhist and Bon statues using both neutron radiography and neutron computed tomography was successfully performed at the Training reactor VR-1. This type of challenging samples had not been previously analysed by neutron imaging at the VR-1 reactor or any other low-power research reactor. Neutron imaging experiments of three votive statues revealed interesting internal contents made of organic materials inside metallic statues. In this case, it was mainly wooden sticks representing the axis mundi, whose appearance is distinguished by the type of statue and the religion (Buddhist or Bon).

The investigations have shown that neutron imaging is a powerful tool that can be used to reveal internal structures and materials of cultural heritage objects. The unique experimental results presented here clearly show that, even though it is challenging, low-power neutron sources like the VR-1 reactor can be successfully used for multidisciplinary research. It is evident that neutron imaging, even at low-power neutron sources, can be a useful research tool for experts in cultural
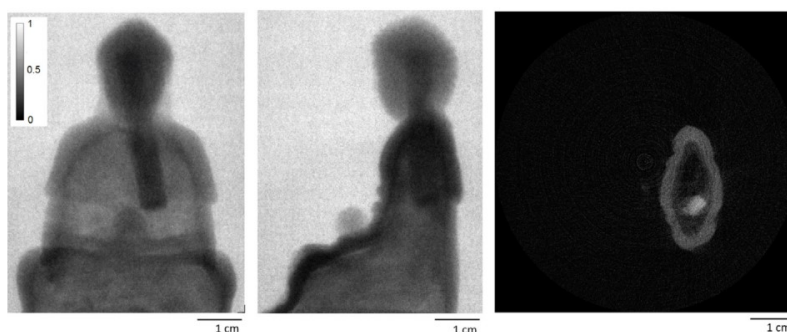

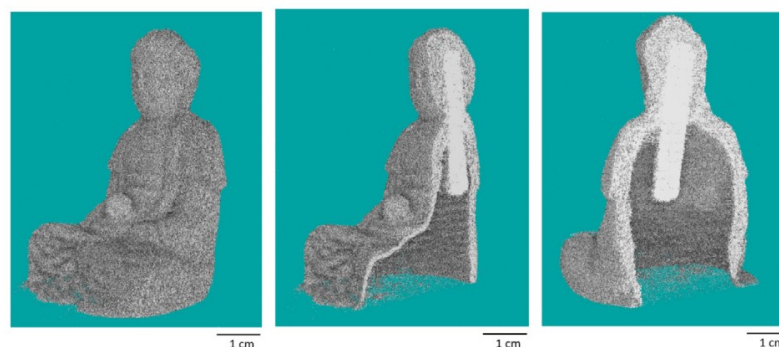Fig. 4. Neutron radiography (0° and 90°) and a tomographic slice of Buddha statue.

Fig. 5. 3D reconstruction of Buddha statue and two cuts through the 3D reconstruction from different angles.

heritage preservation as it can provide additional information about historical objects.

The Training reactor VR-1 is currently the only research reactor with reactor power under 1 kW that provides both neutron radiography and neutron computed tomography experiments. Further activities at the VR-1 reactor will now focus on testing some other possible cultural heritage samples such as fossils etc., and also on testing other applications of neutron imaging, for example, battery research or hydrogen storage research.

CRediT authorship contribution statement

Jana Matoušková: Data curation, Formal analysis, Investigation, Methodology, Software, Validation, Visualization, Writing – original draft, Writing – review & editing. **Lubomir Sklenka:** Conceptualization, Funding acquisition, Project administration, Resources, Supervision, Writing – original draft, Writing – review & editing. **Burkhard Schillinger:** Conceptualization, Supervision, Writing – review & editing.

Declaration of competing interest

The authors declare that they have no known competing financial interests or personal relationships that could have appeared to influence the work reported in this paper.

Data availability

Data will be made available on request.

References

[1] R. Ziesche, N. Kardjilov, et al., Neutron imaging of lithium batteries, Joule 6 (2022) http://dx.doi.org/10.1016/j.joule.2021.12.007.
[2] E. Deschler-Erb, E. Lehmann, L. Pernet, The complementary use of neutrons and X-rays for the non-destructive investigation of archaeological objects from swiss collections, Archaeometry (2004).
[3] B. Schillinger, A. Beaudet, A. Fedrigo, F. Grazzi, O. Kullmer, M. Laass, M. Makowska, I. Werneburg, C. Zanolli, Neutron imaging in cultural heritage research at the FRM II reactor of the Heinz Maier-Leibnitz center, J. Imaging 4 (1) (2018) http://dx.doi.org/10.3390/jimaging4010022.
[4] I. Anderson, R. McGreevy, H. Bilheux, Neutron Imaging and Applications: A Reference for the Imaging Community, in: Neutron Scattering Applications and Techniques, Springer, New York, USA, ISBN: 978-0-387-78692-6, 2009.
[5] D.A. Garrett, H. Berger, Technological development of neutron radiography, At. Energy Rev. 15 (2) (1997) 125–142, International Atomic Energy Agency.
[6] A. Kak, M. Slaney, Principles of Computerized Tomographic Imaging, Society of Industrial and Applied Mathematics, 2001, 9780898714944.
[7] M. Schulz, B. Schillinger, ANTARES: Cold neutron radiography and tomography facility, J. Large-Scale Res. Facil. JLSRF 1 (20) (2015) http://dx.doi.org/10.17815/jlsrf-1-42.
[8] C. Totzke, N. Kardjilov, N. Lenoir, I. Manke, S.E. Oswald, A. Tengattini, What comes neXT? High-speed neutron tomography at ILL, Opt. Express 27 (20) (2019) 28640–28648, http://dx.doi.org/10.1364/OE.27.028640.
[9] A.P. Kaestner, S. Hartmann, G. Kuehne, G. Frei, C. Grunzweig, L. Josic, F. Schmid, E.H. Lehmann, The ICON beamline – A facility for cold neutron imaging at SINQ, Nucl. Instrum. Methods Phys. Res. A 659 (1) (2011) 387–393, http://dx.doi.org/10.1016/j.nima.2011.08.022.
[10] Research reactor database, 2023, URL https://nucleus.iaea.org/RRDB/RR/ReactorSearch.
[11] L.C. Luiz, F.J.O. Ferreira, V.R. Crispim, Visualization of crust in metallic piping through real-time neutron radiography obtained with low intensity thermal neutron flux, Nucl. Eng. Technol. 49 (4) (2017) 781–786, http://dx.doi.org/10.1016/j.net.2016.12.018.
[12] M.-H. Choi, Performance evaluation of neutron radiography facility at Kyung Hee University reactor, AGN-201K, in: Transactions of the Korean Nuclear Society Spring Meeting, Jeju, Korea, May 17-18, 2012, 2012.
[13] L.G.I. Bennett, W.J. Lewis, P.C. Hungler, The development of neutron radiography and tomography on a SLOWPOKE-2 reactor, Physics Procedia 43 (2013) 21–33, http://dx.doi.org/10.1016/j.phpro.2013.03.003, The 7th International Topical Meeting on Neutron Radiography (ITMNR-7).
[14] C. Lange, N. Bernt, Neutron imaging at the low flux training and research reactor AKR-2, Nucl. Instrum. Methods Phys. Res. A 941 (2019) 162292, http://dx.doi.org/10.1016/j.nima.2019.06.033.
[15] M. Choopan Dastjerdi, J. Mokhtari, A. Asgari, E. Ghahremani, A neutron radiography beamline relying on the Isfahan miniature neutron source reactor, Nucl. Instrum. Methods Phys. Res. A 928 (2019).
[16] J. Matouskova, B. Schillinger, L. Sklenka, New neutron imaging facility NIFFLER at very low power reactor VR-1, J. Imaging 9 (1) (2023) http://dx.doi.org/10.3390/jimaging9010015.
[17] L. Frybortova, J. Rataj, L. Sklenka, J. Frybort, F. Fejt, O. Novak, The training reactor VR-1 - 30 years of operation, in: 2020 21st International Scientific Conference on Electric Power Engineering, EPE, 2020, pp. 1–7, http://dx.doi.org/10.1109/EPE51172.2020.9269254.
[18] M. Stefanik, M. Cesnek, L. Sklenka, T. Kmjec, M. Miglierini, Neutron activation analysis of meteorites at the VR-1 training reactor, Radiat. Phys. Chem. 171 (2020) http://dx.doi.org/10.1016/j.radphyschem.2019.108675.
[19] B. Schillinger, An affordable image detector and a low-cost evaluation system for computed tomography using neutrons, X-rays, or visible light, Quantum Beam Sci. 21 (3) (2019).
[20] J. Matouskova, B. Schillinger, L. Sklenka, Development of a neutron imaging facility at the very low power reactor VR-1, J. Phys. Conf. Ser. 2605 (2023) http://dx.doi.org/10.1088/1742-6596/2605/1/012003.
[21] A.P. Kaestner, Z. Kis, M.J. Radebe, D. Mannes, J. Hovind, C. Grünzweig, N. Kardjilov, E.H. Lehmann, Samples to determine the resolution of neutron radiography and tomography, Physics Procedia 88 (2017) 258–265, http://dx.doi.org/10.1016/j.phpro.2017.06.036.
[22] N. Kardjilov, G. Festa (Eds.), Neutron Methods for Archaeology and Cultural Heritage, Springer, Cham, Switzerland, ISBN: 978-3-319-33161-4, 2017.

5

[23] Nuclear Techniques for Cultural Heritage Research, IAEA Radiation Technology Series No. 2, International Atomic Energy Agency, Vienna, Austria, ISBN: 0-906026-35-0, 2011.

[24] K. Ryzewski, S. Herringer, et al., Neutron imaging of archaeological bronzes at the Oak Ridge National Laboratory, Physics Procedia 43 (2013) http://dx.doi.org/10.1016/j.phpro.2013.03.041.

[25] C. Zanolli, B. Schillinger, et al., Exploring hominin and non-Hominin primate dental fossil remains with neutron microtomography, Physics Procedia 88 (2017) http://dx.doi.org/10.1016/j.phpro.2017.06.014.

[26] T. Shakabpa, Tibet: A Political History, Potala Publications, New York, USA, ISBN: 0-9611474-1-5, 1984.

[27] L. Chandra, Buddhist Iconography: Compact Edition, Aditya Prakashan, New Delhi, India, ISBN: 81-85179-71-9, 1999.

[28] F. Louis, Buddhism (Flammarion Iconographic Guides), Flammarion, Paris, France, ISBN: 2-08013-558-9, 1995.

[29] P. Kvaerne, The Bon Religion of Tibet: The Iconography of a Living Tradition, Serindia Publications, London, U.K., ISBN: 0-906026-35-0, 2001.

[30] C. Baumer, Tibet's Ancient Religion Bon, Weatherhill, Trumbull, USA, ISBN: 0-8348-0517-0, 2013.

[31] Fiji image processing package, 2023, URL https://imagej.net/software/fiji/.

[32] A.P. Kaestner, MuhRec - A new tomography reconstructor, Nucl. Instrum. Methods Phys. Res. A 651 (1) (2011) 156–160, http://dx.doi.org/10.1016/j.nima.2011.01.129.

[33] C. Carminati, M. Strobl, A. Kaestner, KipTool, a general purpose processing tool for neutron imaging data, SoftwareX 10 (2019).

[34] VGStudio MAX, 2023, URL https://www.volumegraphics.com/.

A.4.Flexible Camera Detector Box Design Using 3D Printers

The undersigned leading academic staff of the research team confirm a contribution of Jana Matouskova to the paper "*Flexible camera detector box design using 3D printers*". At the same time, I agree that this paper will be included into her dissertation thesis.

Dr. rer. nat. Burkhard Schillinger

Flexible camera detector box design using 3D printers

B Schillinger[1], N Geerits[2], T Jünger[1], J Matoušková[3], T Neuwirth[1], F Oppermann[1], S Sebold[1] and S Sponar[2]

[1]Heinz Maier-Leibnitz Zentrum, Technische Universität München, Lichtenbergstr.1, 85748 Garching, Germany
[2]Atominstitut, Technische Universität Wien, Stadionallee 2, 1020 Vienna, Austria
[3]Czech Technical University Prague, V Holešovičkách 2, Prague 8, 180 00, Czech Republic

Burkhard.Schillinger@frm2.tum.de

Abstract. In the early days of electronic neutron imaging, the best available and most expensive components were used to build detectors. Experience has shown that only few parameters are truly important, so we have built a whole new line of specialized neutron imaging detectors based on astronomy cameras and 3D printed housings with external shielding. As an additional benefit, 3D printed housings produce no gammas on neutron capture, and provide nearly spot-free images. Plans and print files for 3D printed detectors are available for free on request.

1. Introduction

Typical neutron imaging detectors employ a cooled scientific camera, a neutron sensitive scintillation screen, and a mirror to take the camera out of the direct neutron beam. Gamma photons generated on neutron capture in the sample, in the detector walls or in the beam catcher may hit the camera chip directly, and generate local charge clouds appearing as spots or streaks (figure 1). Permanent damage to the chip is also possible for high-energy gammas. Lead shielding around the camera makes the setup bulky and inflexible. The image on the left shows our first camera detector in 1996, still without lead shielding, a later model around 2007 is on the right, shown with walls made from standard lead bricks. The setup was not very stable, and difficult to operate for different fields of view.
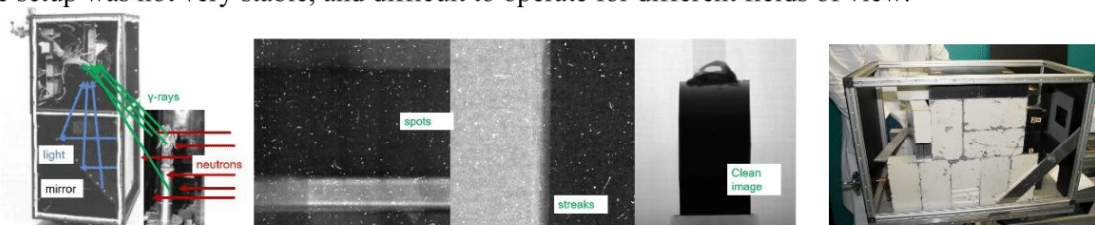

Figure 1. First camera box in 1996, a neutron radiography with spots and streaks, a radiography, and a later detector with shielding stacked inside the camera box.

2. First compact camera box with external shielding

Our new designs rely on a very compact camera box with exchangeable mirror and neutron screen box with external shielding, plus one lead brick directly at the front of the camera. Low-cost cooled astronomy cameras easily match expensive scientific cameras for this application.

The use of smaller C-Mount lenses with shorter focal length for these cameras instead of DSLR lenses (which are much bigger and need a larger focal length due to their size) for large-chip cameras allows for a very compact design; set up close to the neutron sensitive screen, C-mount lenses cover about the same solid angle and collect about the same amount of light as DSLR lenses in a greater distance.

The first box [1] consisted of aluminium, and was successfully tested at the FRM II reactor. Figure 2 shows the design of the camera box, a setup at the ANTARES imaging facility and enclosure in lead bricks. Since the enclosure hampers air flow for the air cooling of the cameras, we added a water cooling ring on the camera body in the area of the heat sink for the air cooling, which provides even more efficient cooling. Image quality is excellent, as can be seen in figure 3, which shows a photo and a neutron computed tomography of a dried hornet, with 9 µm effective pixel size. The box with the camera and the box holding the mirror and the neutron scintillation screen are separate parts that are connected with a flange. This allows to turn the mirror box around to reverse viewing direction, or exchange for a bigger size for a larger field of view. Quantitative evaluation of a single detector model is not subject of this publication.
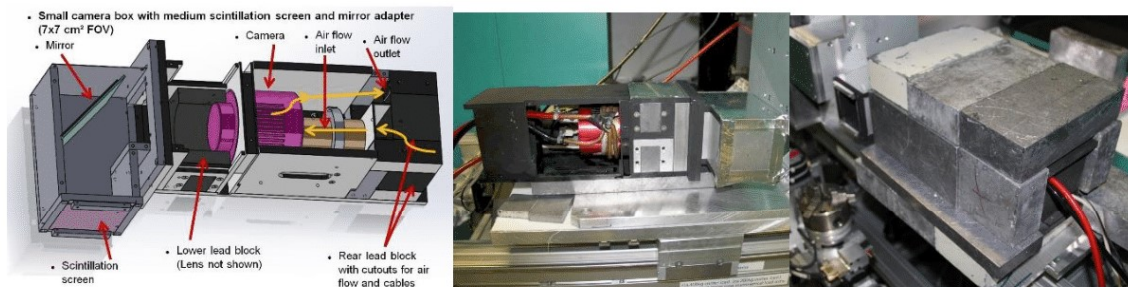

Figure 2. Compact camera box design and setup at beamline without and with external lead shielding. [1]

Figure 3. Photo and neutron computed tomography of a dried hornet, with 9 µm effective pixel size. [1]

3. New cameras and 3D printing

Our first high-end CCD camera Andor ikon-L cost us 65,000 €. It can expose up to 4 hours at -100 C, with 16 bit resolution at 2k x 2k pixel. New astronomy cameras have two to six times the resolution at 14 or 16 bit for exposures of up to 10 minutes or more, for 1600 to 3000 €, providing much higher resolution at lower cost and insignificant noise level. Figure 4 shows a table that compares the ikon-L CCD camera with a 14 bit (ASI94) and 16 bit (ASI600) CMOS camera. With this low cost, the camera is no longer the most expensive part of the setup that can be afforded only once, and must be used for all specific applications. Instead, it makes sense to build several specialized detectors for e.g. high resolution, large field of view or large distance.

Lens selection must be done for a detector box design according to the required field of view, and to the chip size of the camera. While the large chip of the ikon-L requires a DSLR lens, the two CMOS cameras cited here can use DSLR lenses or C-Mount lenses with an illuminated area of 1" or 4/3 " size that covers the respective chip. For short distances to the screen, additional distance rings between the camera and the lens must be used.

Our new basic camera box is 3D-printed from standard PLA filament, and again, the box holding mirror and screen is a separate item that can be exchanged for different sizes. Figure 5 shows the compact design with few parts for both camera box and mirror box. The mirror is inserted into grooves and held with a rubber cord which is pressed into the groove on the backside of the mirror to press it against the front side of the groove. This simple solution provides surprising accuracy in adjustment in the mirror. Not shown in the images is the lead brick in two halves with a center cutout for the lens, which is inserted in front of the camera and around the lens to protect the camera against direct gammas from the sample position. All other shielding must be stacked externally around the box. Since our FRM II reactor at Heinz Maier-Leibnitz Center of Technische Universität München was down, figure 6 shows our setup at the TRIGA reactor of Atominstitut Vienna [2], and a test neutron radiography of a printed circuit board with a CPU socket. For the relatively low intensity beam, a few lead bricks in front of the detector box were sufficient to shield the camera, together with a sheet of borated rubber, which is not shown here. To our positive surprise, practically no gamma spots were visible in the images, as the plastic housing does not produce capture gammas like aluminium, and no scattered neutrons seemed to reach the camera either. Further tests will have to be performed with a beam of higher intensity.

	CCD ikon-L	CMOS ASI 294	CMOS ASI2600
Resolution	2048 x 2048	4144 x 2822	6248 x 4176
Temperature	-100°C	-15…-20°C	-15…-20°C
Exposure time	4 hours	~ 5 -10 min	~ 5 -10 min
Digitization	16 bit	14 bit	16 bit
Pixel size	12.5 µm	4.63 µm	3.76 µm
Lens type	DSLR	DSLR or 1" C-Mount	DSLR or 4/3" C-Mount
Price	~ 65,000 €	~ 1600 €	~ 3000 €

Figure 4. Comparison of ikon-L 16 bit scientific CCD camera to two scientific CMOS cameras with 14/16 bit.

Figure 5. 3D-printed parts of the camera box and the mirror box. The mirror is held by rubber cords pressed into the holding groove.
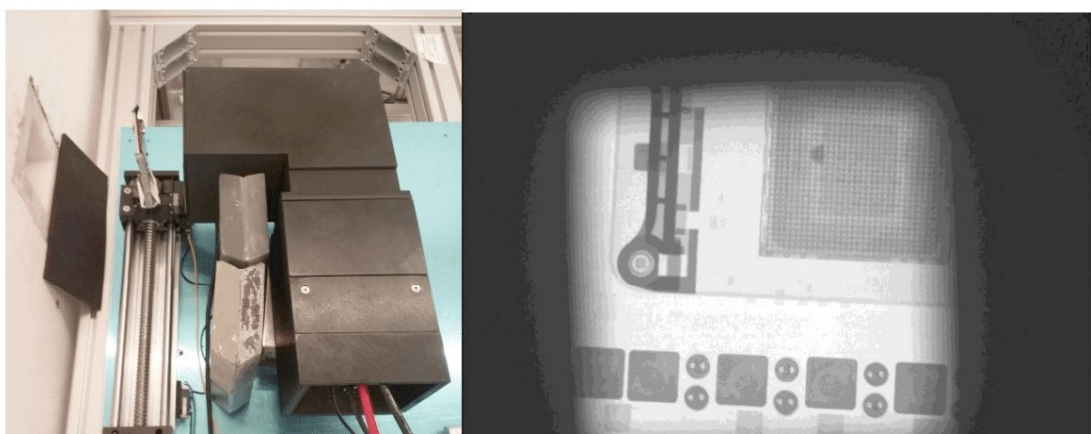

Figure 6. Setup at the TRIGA reactor of Atominstitut Vienna, and test neutron radiography of a printed circuit board with a CPU socket. Field of view is approximately 10 x 6.7 cm².

4. Specialized detectors: High resolution, and long distance periscope

A special high-resolution setup was built using a heliflex lens, and a camera with only 2.4 μm pixel size. Rodenstock Heliflex lenses were originally built for electro-optical medical X-ray intensifiers for radioscopy where a camera had to view a one-inch output of the intensifier in 90 degrees in order to get out of the direct beam. Heliflex lenses include a 90 degree mirror, and focus their output image to infinity, i.e. they create parallel beam. In consequence, in first approximation, the distance of the camera with a second lens has nearly no influence on the image size and sharpness, as the parallel optical beam does not widen, and coves a nearly constant solid angle. The projection ratio is given by the ratio of the focal lengths of the camera lens and the Heliflex lens, which were, in our case, 50 mm and 87 mm, so effective pixel size was 4.1 μm. Figure 7 shows our camera detector setup with a Heliflex lens. The holder for the lens replaces the mirror box. Screens are mounted on the round screen holder at the left side. This setup was also tested at the Atominstitut Vienna, both with a printed paper sheet for optical test as well as with a standard RC Tritec 100 μm ^{6}LiF+ZnS neutron scintillation screen. The optical image in figure 8 left shows paper fibers, while the gadolinium test pattern on the neutron screen in figure 8 right also shows the structure of the scintillation screen, which was produced with a printing

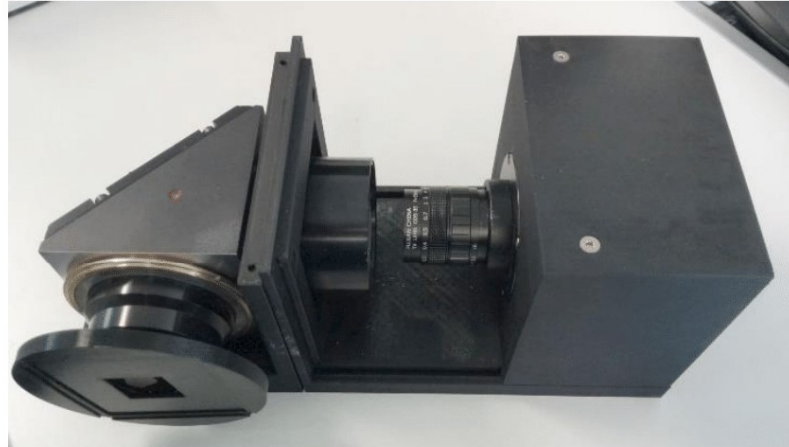technique. Full quantitative evaluation was not possible in the short beam time, and is not subject of this paper.

Figure 7. Camera detector setup with a Heliflex lens. Screens are mounted on the round screen holder at the left side.
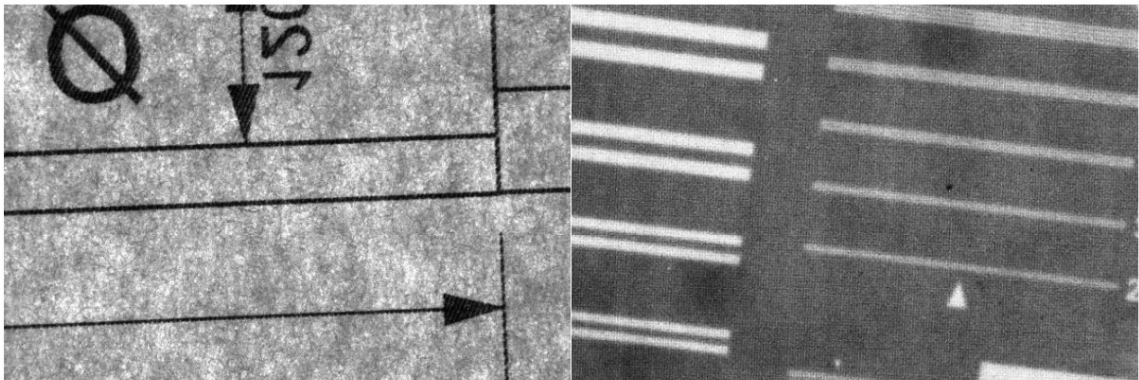

Figure 8. Optical test image showing paper fibers (left), and neutron image of a gadolinium pattern (right), also showing the printed structure of the neutron scintillation screen. With 3096x2080 pixels of effectively 4.1μm the field of view is 12.7 x 8.5 mm².

Another special detector was built for the RA-6 reactor in Bariloche, Argentina [3]. The beam tube for neutron imaging that is mounted outside the reactor wall consists of steel and is mounted on a radial beam tube, which causes such a high gamma dose inside that a camera cannot be placed sideways of the beam with just a single mirror, as it would suffer severe damage from the gamma radiation. We therefore built a 1.2 meter long periscope to go through a 6 cm opening in the beam channel, using a 100 mm lens. The setup (figure 9 left) produces high-resolution images (figure 9 right), but requires long exposure times, as the lens in such a large distance does not collect a lot of light, and incoming neutrons are severely undersampled, with the solid angle covered by the lens capturing less than one photon per detected neutron reaching the camera. In spite of the high quality images, this remains a non-ideal solution for a case where major changes in the beamline would be required for a more efficient collection of neutrons. The whole setup including tomography will soon be described in a separate publication.

Figure 9. Periscope detector setup (left) for the RA-6 reactor and high resolution radiography (right).

5. General benefits of 3D printed detectors

With 3D printing, cost and workshop times are drastically reduced, and modular detector housings allow for a quick adaptation of the detector for a specific purpose and field of view. In addition, the light-weight detector housing allows to pack a whole computed tomography setup in a suitcase for travelling. The plastic housing avoids gamma spots originating from neutron capture in an aluminium detector housing. Damages from neutrons scattered in the plastic housing were not observed in a low-intensity beam, but this still has to be verified with high intensity.

6. Summary and Outlook

In the past, with only one very expensive camera available, we tried to build one multi-purpose detector box with integrated shielding. Now with 3D printing and low-cost high-quality cameras, e.g. by ASI [4] or QHYCCD [5], it makes much more sense to build customized detector boxes for specific applications, and rely on external shielding. Any design must take into account the specific chip size of a specific camera to calculate the field of view. With their low price, the new cameras can also be treated as expendables, and be replaced if they suffer damage on an experiment. C-mount lenses on short distances collect about the same amount of light as DSLR lenses far away.

A complete portable neutron CT controller system based on the ANTARES facility controls at the FRM II reactor is described in [6]. 3D print files, schematics and software images are available for free download [7].

7. References

[1] Schillinger B 2019 An affordable image detector and a low-cost
 evaluation system for computed tomography using neutrons, X-rays or visible light, *Quantum Beam Sci. 3 21,* https://www.mdpi.com/2412-382X/3/4/21
[2] Mach W, Jericha E, Bacak M, Hainz D, Musilek A, Villa M and Abele H 2017, Installation of a Thermal White Neutron Beam Facility at the TRIGA reactor in Vienna, *NENE 2017 conf. proc.*

[3] Marin J and Sanchez F A 2012, Redesign, construction and characterization of the new neutron radiography facility of the RA-6, *XXXIX Annual meeting of the Argentine Assoc. of Nucl.* Techn. (AATN 2012)

[4] https://astronomy-imaging-camera.com

[5] https://qhyccd.com

[6] Schillinger B and Krüger J 2023, A freely distributable professional computed tomography system using NICOS*, this issue*

[7] https://forge.frm2.tum.de/wiki/projects:mobile_tomography:index

A.5. New Detector Design of STORNI Neutron Imaging Facility at RA-6 Research Reactor

The undersigned leading academic staff of the research confirm the essential contribution of Jana Matouskova to the paper "*New detector design of STORNI neutron imaging facility at RA-6 research reactor*". At the same time, we agree that this paper will be included into her dissertation thesis.

Ing. Julio H. Marin

Doc. Ing. Lubomir Sklenka, Ph.D.

Dr. rer. nat. Burkhard Schillinger

Full Length Article

New detector design of STORNI neutron imaging facility at RA-6 research reactor

Jana Matoušková [a],[*], Julio Marin [b],[c], Tobias Juenger [d], Fynn Oppermann [d], Fernando Sanchez [b], Simon Sebold [d], Burkhard Schillinger [d], Lubomir Sklenka [a]

[a] Czech Technical University in Prague, Department of Nuclear Reactors, V Holesovickach 2, Prague, 18000, Czech Republic
[b] Centro Atómico Bariloche, Comisión Nacional de Energía Atómica, Av. Exequiel Bustillo 9500, San Carlos de Bariloche, Argentina
[c] Instituto Balseiro, Av. Exequiel Bustillo 9500, San Carlos de Bariloche, Argentina
[d] Heinz Maier-Leibnitz Zentrum (FRM II) Technische Universität München, Lichtenbergstrasse 1, Garching, 85748, Germany

ARTICLE INFO

ABSTRACT

The paper describes an upgrade of the neutron imaging facility at the RA-6 research reactor in Argentina. The RA-6 reactor is mainly used for education and training. Still, it is also equipped with several research facilities such as a neutron boron capture therapy facility, neutron activation analysis facility and neutron imaging facility. In 2022, the detection system of the neutron imaging facility was upgraded with the use of an astronomical CMOS camera and a 3D-printed housing. The upgrade was focused on improvements to the optical components resulting in better image quality and spatial resolution.

1. Introduction

Since the 80s, neutron imaging has been used at the RA-6 research reactor in Bariloche Atomic Centre, Argentina. The neutron imaging facility at RA-6 underwent a significant upgrade in 2009, in which the collimator of the beamline and shielding were improved. Since its development, neutron imaging at the RA-6 reactor has been mainly used for the education of students and training of young professionals from the Balseiro Institute and Bariloche Atomic Centre. But it is also used for research activities in physics, engineering and multi-disciplinary research such as archaeology, palaeontology and cultural heritage [1]. Although the facility used digital imaging methods, the design from 2009 no longer reflected the development in the field of detection systems for neutron imaging over the last few years. In 2022 collaborative efforts of Czech Technical University in Prague, Technical University in Munich and Bariloche Atomic Centre led to an upgrade of the neutron imaging facility to improve the quality of the results and extend the possibilities of use of neutron imaging in Argentina. The facility newly called STORNI – "Smart TOmography and Radiography Neutron Instrument" – honours Alfonsina Storni, an Argentine poet and playwright.

2. Upgrade of STORNI facility

2.1. RA-6 research reactor

RA-6 reactor is operated by Bariloche Atomic Centre (CAB), National Atomic Energy Commission (CNEA), Argentina. The reactor was

commissioned in 1982, and it was designed as state-of-the-art instrumentation for the education and training of students from the Balseiro Institute and young professionals from the whole of Argentina in the field of nuclear engineering, nuclear energy, safe operation etc [2]. Apart from education and training, the RA-6 reactor is also active in using neutron applications in research and development. The reactor is equipped with a neutron imaging facility, boron neutron capture therapy facility, prompt gamma neutron activation analysis facility, neutron activation analysis laboratory, and beamline for time-of-flight experiments.

The RA-6 reactor is an open pool-type reactor cooled and moderated by light water. The reactor uses an MTR-type fuel with low-enriched uranium. The nominal power of the reactor is 500 kW, and the maximal power is 1 MW. The reactor has five horizontal radial beamlines, several irradiation facilities, in-core irradiation positions and a thermal column [2].

2.2. Neutron imaging beamline

The STORNI neutron imaging facility is located at beamline number 1 of the RA-6 research reactor, next to its biological shielding. The beamline consists of an aluminium tube in which the beam is adjusted with a conical collimator made out of the lead, borated polyethylene and cadmium to define its divergence. The length of the beamline (L) is 4 m, and the smallest diameter (D) of the beamline, effectively acting as
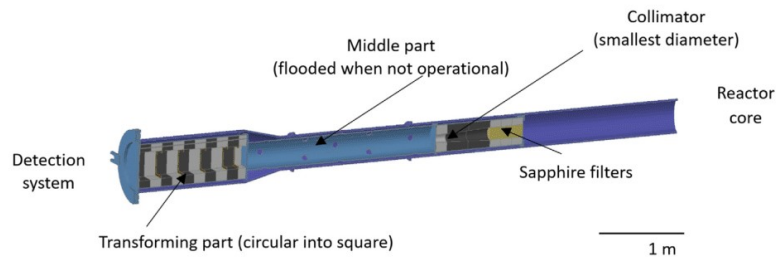
Fig. 1. Parts of the beamline of the STORNI neutron imaging facility.

Fig. 2. Shielding of STORNI neutron imaging facility.

a pinhole collimator, is 4 cm which results in an L/D ratio of 100. The beam is also filtered by three sapphire monocrystals, ensuring a thermal neutron spectrum. The last part of the beamline transforms the circular beam into a square to minimise shielding requirements. The middle part of the beam tube can be flooded with water to block the beam when the facility is not operational. At the sample position, the beam is a square of 25×25 cm^2. A model of the beamline with the collimator and other parts is shown in Fig. 1.

2.3. Shielding

At the end of the beamline, there is an external shielding. The shielding consists of two main parts, the first contains the detection system, while the second part is a beam stopper. The first part of the shielding consists of a carbon steel structure filled with borated paraffin and externally coated with lead. Inside the shielding is a space for part of the detection system and for placing the samples with dimensions of up to $40 \times 40 \times 40$ cm^3. The shielding has a pyramid hole for the detection system. The smallest diameter of the hole is 6.6×6.6 cm^2 on the surface of the shielding block. The shielding also has three access ways, the biggest being 40×40 cm^2 and the others 20×20 cm^2. The beam stopper is placed behind the first part of the shielding. It has a cylindrical shape with 90 cm in diameter and 130 cm in length. It is filled with heavy concrete and has a cavity filled with borated paraffin. Fig. 2 shows a photo of the shielding at STORNI.

2.4. Detection system

The upgrade was focused on the improvement of the detection system of the STORNI neutron imaging facility. The beamline and the shielding remained from the previous design of the facility. As a part of the upgrade of the detection system of the STORNI neutron

imaging facility, the neutron flux at the sample position was measured using neutron activation analysis. At the reactor power of 500 kW, the thermal neutron flux at the sample position is $2.54 \cdot 10^6$ n/cm^{2}s, and the epithermal neutron flux at the sample position is $2.93 \cdot 10^4$ n/cm^{2}s. The schematic picture of the whole facility is shown in Fig. 3.

2.4.1. Old detection system

The old detection system from 2009 was used until its upgrade in 2022. The original system consisted of a 500 μm 6LiF/ZnS(Ag) scintillator screen, CCD camera and condensing lens (f = 0.95, 25 mm). The camera type was a Penguin 600 CLM from Pixera Corporation with 10-bit true digitisation (blown up to 16-bit, i.e. internal multiplication by 32, with 32 as the minimal greyscale step) and a 1040×1392 pixel array. The field of view was 20×20 cm^2. The setup also included two surface mirrors to protect the camera from radiation. However, the system had several limitations. The mirrors were not fixed in position, which required precise alignment and orientation of the mirrors, otherwise causing spatially varying blurring of the image. The dead time for transmitting the images was very long (as long as exposure time), and the camera was not capable of being digitally triggered by other than the original software. The scintillation screen used was 500 μm thick, which limits the spatial resolution due to the blurring of the light spot generated by the captured neutron [3]. Fig. 4 shows the schematic image of the detection system.

2.4.2. New detection system

The detection system upgrade in 2022 was created in cooperation with the Czech Technical University in Prague (CTU) and the Technical University of Munich (TUM). The design of the upgrade was based on results from the very low-power training reactor VR-1 [4,5] and results from the FRM-II research reactor [6]. The detector design had to meet the specific requirements of the shielding placed at the end of
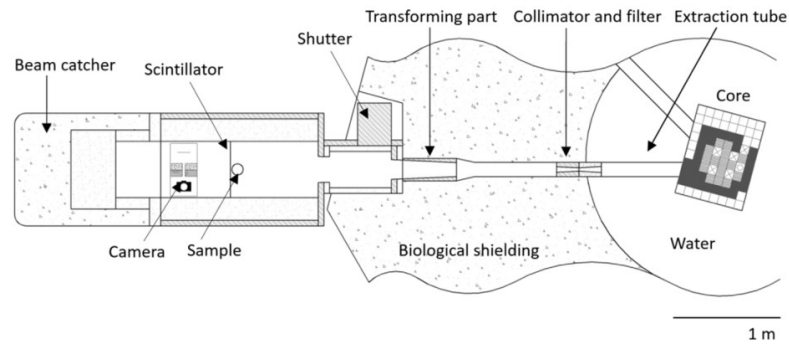
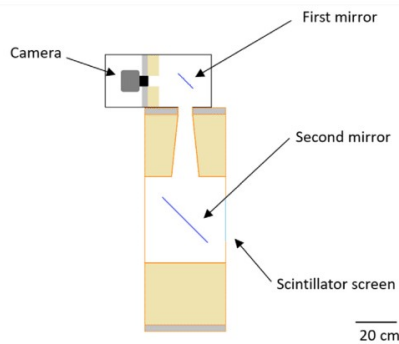**Fig. 3.** Schematic picture of main parts of STORNI neutron imaging facility.

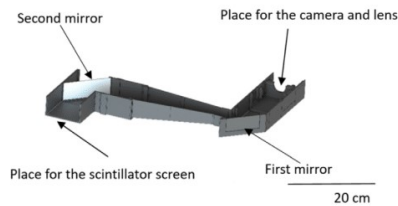**Fig. 4.** Schematic image of the old detection system.

Fig. 5. Cut through the model of the periscope.

Table 1
Comparison of main parameters of the detection systems.

	Old detection system	New detection system
Camera	Penguin 600 CLM	ASI 294MM
Camera type	CCD	CMOS
Digitisation	10-bit	14-bit
Lens type	Xenon 0.95/25 Schneider Kreuznach, C-Mount	100 mm C Series Fixed Focal Length Lens f/2.8 Techspec
Scintillator screen	500 μm ^{6}LiF/ZnS (Ag)	200 μm ^{6}LiF/ZnS (Ag)
Field of view	20 × 20 cm^2	12 × 12 cm^2
Resolution	1040 × 1392	4144 × 2822
Pixel size	4.65 μm	4.64 μm
Effective pixel size	192 μm	42.5 μm

an air fan, but an external water cooling ring that works perfectly for keeping the camera at a constant temperature of −15 °C was added. Fig. 6 shows the photo of the periscope outside and inside the shielding.

3. Comparison with the old facility

The upgrade of the STORNI neutron imaging facility at the RA-6 reactor was mainly focused on improving the detection system. As a result, the detection system was designed to consist of several parts firmly connected so that both mirrors are in precisely given positions. Thanks to this, there is no blurring of the image due to misalignment of the mirrors, as was the case with the previous system version. Table 1 shows the comparison of the main parameters of the detection system before and after the upgrade.

3.1. Neutron radiography

Neutron radiography measurements were performed using a gadolinium test pattern to compare the resolution of the detection system before and after the upgrade. The comparison of neutron radiography results of a gadolinium test pattern [9] is shown in Fig. 7.

The original resolution was 500 μm, while the resolution after the upgrade was 100 μm. The resolution was determined by the visibility of details of the gadolinium test pattern [10]. Even though the setup produces high-resolution images, it requires long exposure times, in the order of minutes. This is because the distance between the scintillator screen and the lens is large, and therefore, the lens covers only a small solid angle and thus does not collect much light, and neutrons are undersampled with the solid angle covered by the lens, capturing less than one photon per detected neutron reaching the camera. Significant changes in the beamline and the shielding would be required to solve the problem of a more efficient collection of neutrons, for example, introducing a larger opening in the first part of the shielding or reduction of the gamma dose inside the shielding next to the beam so a camera can be placed inside — omitting the upper mirror for a direct vertical

the beamline. Therefore, a 1.2-meter-long periscope was designed to go through a beam tube in the shielding. The whole detector setup was 3D printed with standard PLA filament. [7] Fig. 5 shows cut through the periscope model.

The system uses a 200 μm ^{6}LiF+ZnS neutron scintillation screen from RC Tritec, a CMOS camera from ASI and a 100 mm C-mount lens. The 200 μm scintillator screen was used because it was already available at the facility. The camera type is an ASI 294MM Pro with 14-bit digitisation, a 4144 × 2822 pixel array and a 4.64 μm pixel size [8]. Few cooled cameras meet the requirements of affordable price and at least 14-bit digitisation. The employed camera is nearly the only one fitting the criteria. Its chip size fits with the lens bought for long-distance imaging and the resulting field of view. The field of view is limited to 12 × 12 cm^2 due to the small dimension of the beam tube (6 × 6 cm^2 at the smallest part). The setup also includes two surface mirrors, lead shielding in front of the camera (in the form of two lead bricks with a centre cutout for the lens), and additional cooling for the camera. The camera is two-stage Peltier cooled, originally only with

Fig. 6. 3D printed periscope (a) outside the shielding (b) part of the periscope inside the shielding — scintillator box with the first mirror (the scintillator is missing in the photo) (c) part of the periscope outside the shielding — camera box with the second mirror.
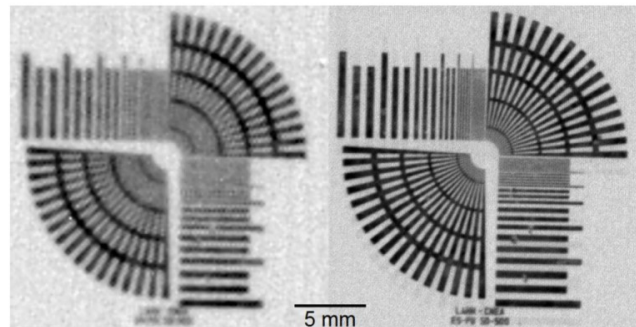

Fig. 7. Neutron radiography of a gadolinium test pattern (a) before the upgrade, (b) after the upgrade.

mount of the camera is not possible due to a high gamma dose emitted from the beam tube through the hole that would damage the camera.

3.2. Neutron tomography

A simple neutron computed tomography (CT) setup was installed as part of the upgrade. The setup consists of affordable translation and rotation stages and a controller [11]. The controller includes Raspberry Pi and Waveshare HAT stepper motor controller [12]. The tomography sequence, which consists of tomography measurements and measurements of the open beam and dark field images, is controlled by Python script. First, dark images are recorded, then with the help of the translation stage, the sample is moved out of the field of view, and the open beam images are recorded. Finally, the sample is returned, and a tomographic sequence is performed according to the required number of projections. A photo of the tomography setup is shown in Fig. 8.

Later the controller was improved. Instead of using Python script on the Raspberry Pi, the new control system is based on the Networked Instrument COntrol System (NICOS) developed at MLZ and used to control the full instrument suite at FRM-II as well as at other large-scale facilities [13–15]. Communication to the hardware was implemented using Entangle [16], an implementation of TANGO [17] developed at MLZ. This enables the state-of-the-art, user-friendly control of the instrument, including scripting of measurement procedures and a graphical user interface.

The first complete CT at STORNI with the new detection system and new tomography setup was an old alarm clock. Due to the long exposure time caused by the large distance between the scintillator and the lens and the limited operational time of the RA-6 research reactor, only a reduced data set of 300 images at 90 s of exposure time was measured for a half rotation. Fig. 9 shows a photo, a radiograph and a 3D reconstruction of the object. To process the measured data, two
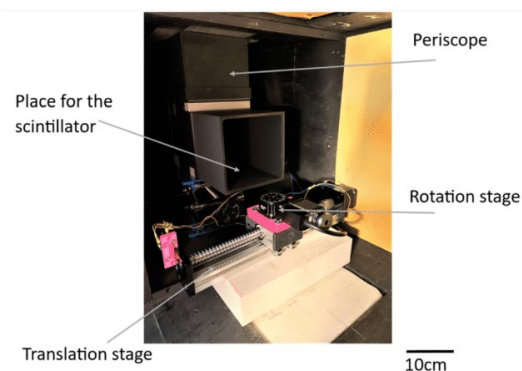

Fig. 8. Neutron tomography setup at the STORNI neutron imaging facility.

software were used: MuhRec by PSI [18] for reconstruction and Amira by Thermo Scientific [19] for volume rendering.

4. Conclusions

By replacing the existing detector system of STORNI with a new and improved system, a significant increase in resolution was achieved by using a modern astronomical CMOS camera with better resolution and higher digitisation, thinner scintillator screen and 3D printed housing, cheap and easily adapted to the unique geometric constraints at STORNI, that ensures alignment of the two-mirror system. The beamline and the shielding remain from the previous system. The
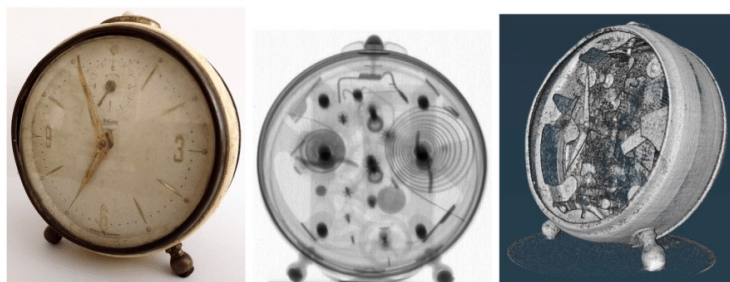
Fig. 9. First CT with the new set-up: (a) photo, (b) radiograph and (c) 3D reconstruction of an old alarm clock.

detection system was designed in collaboration with the Czech Technical University in Prague, the Technical University of Munich and the Bariloche Atomic Centre. A special two-mirror system consisting of a 1.2-meter-long periscope was designed to fulfil the requirements of special shielding placed at the end of the beamline. By performing an upgrade of the detection system of the STORNI neutron imaging facility, the resolution of the system improved from 500 μm to 100 μm. The setup for computed neutron tomography was also upgraded with a control system based on TANGO/NICOS. Even though the primary purpose of the facility is the education of students and training of young professionals from the Balseiro Institute and Bariloche Atomic Centre, with better resolution and professional software for CT, the STORNI neutron imaging facility will also serve for research in various fields such as archaeology, palaeontology and cultural heritage, engineering, and nuclear physics. Given the large number of fossils found in Argentina, palaeontology should be a major research application.

Declaration of competing interest

The authors declare that they have no known competing financial interests or personal relationships that could have appeared to influence the work reported in this paper.

Data availability

Data will be made available on request.

Acknowledgements

References

[1] A. Tartaglione, et al., Present and future activities on neutron imaging in Argentina, Physics Procedia 29 (2015) 124–129.

[2] H. Blaumann, et al., RA-6 reactor conversion and neutronic tests of the new silicides fuel core, in: Proceedings of the 31st International Meeting on Reduced Enrichment for Research and Test Reactors.

[3] W.C. Chuirazzi, A.E. Craft, Measuring thickness-dependent relative light yield and detection efficiency of scintillator screens, J. Imaging 6 (7) (2020) http://dx.doi.org/10.3390/jimaging6070056.

[4] J. Matouskova, B. Schillinger, L. Sklenka, New neutron imaging facility NIFFLER at very low power reactor VR-1, J. Imaging 9 (1) (2023) http://dx.doi.org/10.3390/jimaging9010015.

[5] J. Matouskova, B. Schillinger, L. Sklenka, Development of a neutron imaging facility at the very low power reactor VR-1, J. Phys. Conf. Ser. (2023) (forthcoming).

[6] B. Schillinger, et al., Flexible camera detector box design using 3D printers, J. Phys. Conf. Ser. (2023) (forthcoming).

[7] B. Schillinger, An affordable image detector and a low-cost evaluation system for computed tomography using neutrons, X-rays, or visible light, Quantum Beam Science 3 (4) (2019) http://dx.doi.org/10.3390/qubs3040021.

[8] Astronomican camera ASI294MM Pro, ZWO Company, URL https://astronomy-imaging-camera.com/product/asi294mm-pro/.

[9] C.E. Callisaya Choque, Design, fabrication, characterisation and application of devices with high neutronic contrast for their implementation in neutron radiography and tomography instruments of LAHN, 2020, Instituto Sábato, Buenos Aires, (In Spanish), available online: https://www.cnea.gob.ar/nuclea/handle/10665/1568.

[10] A.P. Kaestner, et al., Samples to determine the resolution of neutron radiography and tomography, Physics Procedia 88 (2017) 258–269, http://dx.doi.org/10.1016/j.phpro.2015.07.018.

[11] B. Schillinger, A.A. Craft, Simple controller for neutron computed tomography that interfaces nearly every camera, 2023, URL https://www.isnr.de/index.php/tools.

[12] Stepper motor HAT for Raspberry pi, drives two stepper motors, 2023, Waveshare, https://www.waveshare.com/product/raspberry-pi/hats/motors-relays/stepper-motor-hat.htm.

[13] NICOS open-source scientific instrument control software, 2023, NICOS - Networked Instrument Control system community, URL http://www.nicos-controls.org.

[14] B. Schillinger, A. Craft, J. Kruger, The ANTARES instrument control system for neutron imaging with NICOS/TANGO/LiMA converted to a mobile system used at idaho national laboratory, in: Neutron Radiography, 11th World Conference on Neutron Radiography, WCNR-11.

[15] B. Schillinger, J. Kruger, A freely distributable professional computed tomography system using NICOS, J. Phys. Conf. Ser. (2023) (forthcoming).

[16] TANGO base class specification, 2023, Heinz Maier-Leibnitz Zentrum (FRM II) Technische Universität München, URL https://forge.frm2.tum.de/entangle/defs/entangle-master/.

[17] Tango controls, 2023, Tango controls, URL http://www.tango-controls.org.

[18] A.P. Kaestner, MuhRec - A new tomography reconstructor, Nucl. Instrum. Methods Phys. Res. A 651 (1) (2011) 156–160.

[19] Amira software, 2023, Thermo Fisher Scientific, https://www.thermofisher.com/cz/en/home/electron-microscopy/products/software-em-3d-vis/amira-software.html.